

# **A COCERVATE-BASED PLATFORM FOR GROWTH FACTOR DELIVERY**

by

**Hunghao Chu**

Bachelor of Science, National Taiwan University, 2003

Master of Science, National Tsing Hua University, 2005

Submitted to the Graduate Faculty of  
Swanson School of Engineering in partial fulfillment  
of the requirements for the degree of  
Doctor of Philosophy

University of Pittsburgh

2011

UNIVERSITY OF PITTSBURGH  
SWANSON SCHOOL OF ENGINEERING

This dissertation was presented

by

Hunghao Chu

It was defended on

November 23rd, 2011

and approved by

Johnny Huard, Ph.D., Professor,  
Bioengineering Department

Steven Little, Ph.D., Assistant Professor,  
Chemical and Petroleum Engineering Department

Sanjeev Shroff, Ph.D., Professor,  
Bioengineering Department

Dissertation Director: Yadong Wang, Ph.D., Associate Professor,  
Bioengineering Department

Copyright © by Hunghao Chu

2011

## A COACERVATE-BASED PLATFORM FOR GROWTH FACTOR DELIVERY

Hunghao Chu, Ph.D.

University of Pittsburgh, 2011

Growth factors participating in a variety of biological processes have great potential in regenerative medicine. However, unprotected growth factors degrade quickly and have little efficacy at tissue repair. Delivery of growth factors with different vehicles has been examined to prolong the half-lives of growth factors and therefore increase its therapeutic efficacy. After decades of research, controlled delivery of growth factor still faces some significant limitations, and none has reached clinical translation.

Heparin, a highly sulfated macromolecule, is used as an anticoagulant clinically. In addition, it has high affinity to a large number of biomolecules, including many growth factors. The interaction between heparin and heparin-binding growth factors is known to adjust their conformation, protect them from proteolytic degradation and regulate their activities. Incorporation of heparin in growth factor delivery is consequently a strategy to potentiate the bioactivity of growth factors. Currently, most approaches used to immobilize heparin on the delivery vehicles rely on covalent modification of heparin that may alter its inherent properties. To maximize the efficacy of heparin, we developed a coacervate-based delivery platform in which heparin is utilized to complex with a polycation without any modification. The polycation neutralizes the negative charges of heparin and precipitates it out of solution. This approach allows spatiotemporal control of the release of heparin-binding growth factors. This dissertation covers the design, production, characterization and application of heparin-based coacervate in controlled release of growth factors.

## TABLE OF CONTENTS

<b>PREFACE</b>	<b>XI</b>
<b>1.0 BACKGROUND</b>	<b>1</b>
<b>1.1 CARDIOVASCULAR DISEASE</b>	<b>1</b>
<b>1.2 THERAPEUTIC ANGIOGENESIS</b>	<b>4</b>
<b>2.0 SPECIFIC AIMS</b>	<b>14</b>
<b>3.0 DESIGN OF A PLATFORM FOR GROWTH FACTOR DELIVERY</b>	<b>17</b>
<b>3.1 SYNTHESIS OF A BIOCOMPATIBLE POLYCATION</b>	<b>19</b>
<b>3.1.1 Introduction</b>	<b>19</b>
<b>3.1.2 Experimental section</b>	<b>20</b>
<b>3.1.3 Results and discussion</b>	<b>25</b>
<b>3.1.4 Summary</b>	<b>39</b>
<b>3.2 CHARACTERIZATION OF [PEAD:HEPARIN] COACERVATE</b>	<b>40</b>
<b>3.2.1 Introduction</b>	<b>41</b>
<b>3.2.2 Experimental section</b>	<b>42</b>
<b>3.2.3 Results</b>	<b>46</b>
<b>3.2.4 Discussion</b>	<b>57</b>
<b>3.2.5 Summary</b>	<b>60</b>
<b>4.0 THERAPEUTIC ANGIOGENESIS VIA FGF2 COACERVATE</b>	<b>61</b>
<b>4.1 IN VIVO ANGIOGENIC ACTIVITY OF FGF2 COACERVATE</b>	<b>62</b>
<b>4.1.1 Introduction</b>	<b>62</b>

4.1.2 Experimental section	64
4.1.3 Results	69
4.1.4 Discussion	87
4.1.5 Summary	89
4.2 POST-MYOCARDIAL INFARCTION ANGIOGENESIS BY FGF2 CERVATE	90
4.2.1 Introduction	91
4.2.2 Experimental section	92
4.2.3 Results and discussion	93
4.2.4 Summary	104
5.0 CONCLUSION	105
REFERENCES	107

## LIST OF TABLES

1. Current treatment of CVD.....	3
2. VEGF family and function.....	12
3. FGF family and function.....	13

## LIST OF FIGURES

1. Design of a coacervate-based delivery platform.....	18
2. Synthesis of PEAD.....	26
3. <sup>1</sup> HNMR and GPC analysis of PEAD.....	27
4. IR spectra of PED and PEAD.....	28
5. Degradation of PEAD.....	29
6. In vitro biocompatibility of PEAD.....	31
7. In vivo biocompatibility of PEAD and PEI.....	33
8. In vivo biocompatibility of PEAD and PEI.....	34
9. Zeta potential measurement of [PEAD:DNA] and [PEAD:HA].....	36
10. SEM micrographs of [PEAD:DNA] and [PEAD:HA].....	38
11. Macroscopic pictures of [PEAD:heparin].....	47
12. Zeta potential measurement of [PEAD:heparin].....	48
13. DMB binding assay.....	49
14. SEM micrographs of [PEAD:heparin].....	50
15. Release profiles of FGF2 coacervate and NGF coacervate.....	52
16. HAEC proliferation.....	54
17. PC-12 neurite growth.....	56
18. Macroscopic pictures of FGF2 coacervate.....	70
19. SEM micrographs of FGF2 coacervate.....	70

20. FGF2 loading efficiency of [PEAD:heparin] coacervate.....	71
21. FGF2 digestion by trypsin.....	72
22. Encapsulation of FGF2 in fibrin gel.....	73
23. HUVEC tube formation by FGF2.....	73
24. Pericyte chemotaxis by FGF2.....	74
25. Subcutaneous injection of FGF2 coacervate.....	75
26. Macroscopic pictures of the animal injected with FGF2 coacervate.....	76
27. H&E staining of subcutaneous tissue.....	76
28. Comparison of hemoglonbin concentration.....	78
29. Comparison of hemoglobin at injeciton and contralateral sites.....	78
30. DAPI/ $\alpha$ -SMA/CD31 staining of subcutaneous tissue.....	80
31. DAPI/ $\alpha$ -SMA/CD31 staining of subcutaneous tissue (high magnification).....	80
32. Quantification of $\alpha$ -SMA andCD31 positive cells.....	82
33. Comparison of blood vessel number.....	83
34. PDGFR- $\beta$ /CD31 staining of subcutaneous tissue.....	84
35. VWF/CD31 staining of subcutaneous tissue.....	85
36. $\alpha$ -SMA/desmin staining of subcutaneous tissue.....	86
37. $\alpha$ -SMA/calponin staining of subcutaneous tissue.....	87
38. Acute myocardial infarction model.....	91
39. ESA, EDA and FAC.....	95
40. H&E staining of heart tissue (2 wk) .....	97
41. DAPI/actinin staining of heart tissue (2 wk) .....	98
42. H&E staining of heart tissue (2 wk) .....	99
43. DAPI/actinin staining of heart tissue (2 wk) .....	100
44. Masson's trichrome staining of heart tissue (6 wk) .....	101
45. H&E staining of heart tissue (6 wk) .....	102

46. VWF/CD31 staining of heart tissue (6 wk) .....103  
47.  $\alpha$ -SMA/CD31 staining of heart tissue (6 wk).....104

## PREFACE

I would like to express my sincere gratitude to my advisor, Dr. Yadong Wang, for providing me an excellent project and a great environment to conduct my Ph.D. research. Besides, I would like to thank my thesis committee: Drs. Johnny Huard, Steven Little and Sanjeev Shroff for their insightful comments and valuable suggestions for my thesis.

Moreover, I also appreciate so many friends and mentors in the US and Taiwan who have ever assisted and inspired me in any respect during my doctoral study. Without them, I would not get through difficult times easily.

Last, my deepest gratitude goes to my family especially my parents, my parents-in-law and my wife, Chun-Wan Yen, for their continuous support and encouragement all through my life. To them, I dedicate this thesis.

## 1.0 BACKGROUND

### 1.1 CARDIOVASCULAR DISEASE

Despite decades of efforts on prevention and treatment, cardiovascular diseases (CVD) are still the leading cause of death in the US and other developed countries. The latest statistics from the American Heart Association highlights the morbidity and mortality of CVD [1]:

- An estimated 82,600,000 American adults ( $\geq 20$  years old) have 1 or more types of CVD.
- CVD caused 813,804 of all 2,243,712 deaths (33.6%) or 1 of every 2.9 death in 2007. Each day, more than 2200 Americans died from CVD. The death rate of CVD patients was 251.2 per 100,000 (0.251%).
- Coronary heart disease caused  $\approx 1$  of every 6 deaths in 2007. It was estimated that 785,000 Americans had a new heart attack, 470,000 had a recurrent attack. Totally, 16,300,000 Americans had coronary heart disease including 7,900,000 had heart and 9,000,000 had chest pain.
- Stroke caused  $\approx 1$  of every 18 death in 2007. It was estimated that 610,000 Americans had a new stroke and 185,000 had a recurrent stroke. Totally, 5,700,000 Americans had stroke.
- 5,700,000 Americans had heart failure.
- 650,000 to 1,300,000 Americans had congenital cardiovascular defect.

The risk factors of CVD including hypertension, smoking, high cholesterol, diabetes and obesity are still prevalent in the US:

- 76,400,000 (33.5%) of US adults have hypertension (systolic pressure  $\geq 140$  mmHg and/or diastolic pressure  $\geq 90$  mmHg).
- Among Americans  $\geq 18$  years old, 23.1% of men and 18.3% of women are smokers.
- 33,600,000 of US adults have high serum cholesterol ( $\geq 240$  mg/dL).
- 18,300,000 Americans had been diagnosed diabetes.
- 149,300,000 Americans are overweight and obese.

The cost of health care and treatment for CVD patients is extremely high:

- The total number of cardiovascular operations and procedures rose from 5,382,000 in 1997 to 6,846,000 in 2007 (27% increase).
- The direct and indirect cost of CVD was estimated to be 286 billion dollars in 2007. The amount is higher than the 228 billion dollars spent on cancer and benign neoplasms.

Current diagnosis for CVD relies mostly on physical examination, electrocardiogram (EKG), echocardiography (ECG) and blood test. Treatment depending on severity of the disease includes medication and surgery ([Table 1](#)) [2].

**Table 1.** Current treatment of CVD

<b>Cardiovascular disease</b>	<b>Treatment</b>
Heart valve problems	Medication Heart valve surgery
Arrhythmia	Medication Pacemaker Cardiac defibrillation
Heart attack	Medications-clotbusters (should be administered as soon as possible for certain types of heart attacks) Coronary angioplasty Coronary artery bypass graft surgery
Stroke	Medications-clotbusters (must be administered within 3 hours from onset of stroke symptoms for certain types of strokes) Carotid endarterectomy

## 1.2 THERAPEUTIC ANGIOGENESIS

There are two processes that lead to new blood vessel formation, vasculogenesis and angiogenesis. Blood vessel formation in early development is termed vasculogenesis, initiated by mesodermal stem cells which differentiate *in situ* to angioblasts and then to endothelial cells. Angiogenesis is a highly coordinated process that requires many associated cells and signals to complete. Insufficient vascularization leads to ischemic conditions which inhibit tissue growth or survival whereas abnormal angiogenesis can promote tumor progression or other diseases such as macular degeneration. Following vasculogenesis, angiogenesis is a process which includes sprouting and intussusceptive growth of pre-existing blood vessels and subsequent remodeling and maturation to form new vasculature [3]. Developing vasculature requires signals to induce vessel stabilization to prevent nascent vessels from becoming leaky or nonfunctional and subsequent regression back to their original state. Unlike vasculogenesis which happens primarily during the embryonic stage, angiogenesis occurs frequently during adulthood. As long as there are active vessels, new vasculature can be generated following biophysical and physiological cues in the environment, of which the most highly studied are angiogenic factors. Notable angiogenic factors include vascular endothelial growth factor (VEGF), angiopoietin, transforming growth factor, fibroblast growth factor (FGF), hepatocyte growth factor, and platelet-derived growth factor, although dozens of other proteins are also known to participate in blood vessel formation. The importance of several angiogenic factors has been revealed by gene knockout resulting in embryonic lethality [4,5].

Under normal physical conditions, most secretory growth factors are associated with components of the extracellular matrix (ECM) including heparan sulfate proteoglycan and fibronectin [6]. Physiological fluctuations such as insufficient nutrients and low oxygen concentration (hypoxia) induce the release of proangiogenic factors via cleavage of ECM by hydrolytic enzymes. A chemical gradient is created as released factors diffuse away in the surrounding tissue. Several downstream angiogenic processes are driven by this gradient including activation of additional angiogenic genes, proteolytic degradation of the ECM, proliferation and migration of endothelial cells to form tubes, and recruitment of mural cells that stabilize the nascent vessels.

Jeffery M. Isner pioneered the concept of therapeutic angiogenesis decades ago led by [7]. His seminal work observing revascularization in response to VEGF injection in a hindlimb ischemia model demonstrated that single factor administration can be adequate to generate functional blood vessels. Subsequently, several other angiogenic factors have also been utilized alone or combined to promote angiogenesis. Contrary to cancer treatment where drugs are selected to inhibit blood vessel growth, angiogenic therapy aims to develop neovasculature through various strategies. Therapeutic angiogenesis has been widely examined for treatment of many human diseases. Treatment of cardiovascular disorders, which incur high mortality and morbidity in developed countries, could be significantly improved with successful therapeutic angiogenesis. Other processes such as wound healing and organ repair and regeneration also depend on a sufficient blood supply. Unfortunately, there is no FDA-approved drug or device that can induce angiogenesis efficiently.

Therapeutic angiogenesis includes gene delivery, protein delivery and cell delivery. Gene delivery has the advantage of high protein production efficiency, essentially providing a sustained source of protein release. Furthermore, genes carried by viral vectors such as adeno-associated virus, lentivirus and retrovirus are integrated into the host chromosome, resulting in expression of angiogenic genes even after cell division. However, this is not always desirable,

as over-production of a certain angiogenic factor could inhibit blood vessel formation which requires a precise balance between different signals. One prior study revealed that unregulated over-production of VEGF in the myocardium caused heart failure and vascular tumor formation [8]. Viral vectors, which are the most effective vehicle to transfer genes, can also trigger immune responses against viral components [9]. Other gene transfer methods using non-viral vectors such as ultrasound and electric field are less efficient and require much investigation [10,11]. Several Phase-III clinical trials of angiogenic gene delivery to treat human cardiovascular diseases have been conducted but the results are mostly discouraging [12].

Protein delivery is the most straightforward strategy for therapeutic angiogenesis. Blood vessel formation is induced by simple injection of angiogenic proteins, with the extent of angiogenesis being controlled by dosage and duration of release. Compared to gene- and cell-based therapies, protein delivery is thought of as an “off-the-shelf” treatment. Protein can be manufactured and shipped in lyophilized form, reconstituted in buffer and applied immediately. Production and purification of angiogenic proteins is well established, and the cost is relatively low. All of these factors contribute to the advantages of angiogenic protein therapy. Nevertheless, maintaining angiogenic activity at a specific site of interest is a significant challenge. Angiogenic protein, like viral vectors or cells, can be delivered either systematically or locally. Systematic administration, such as intravenous or intraperitoneal injection, is performed easily but is inefficient at targeting a desired tissue and most of injected protein is rapidly cleared by the mononuclear phagocyte system [13]. Only a small fraction reaches the desired region, so high dosage and repeated injection of angiogenic factors is required [14]. Local administration such as intracoronary, intramyocardial or intracerebral injection can better confine the distribution of the protein but usually requires a special device or highly invasive surgery [15].

Cell-based therapy is another active field that is drawing a lot of attention. Compared to single factor therapies, therapeutic angiogenesis via cell therapy is believed to have a more

comprehensive and extensive effect. Cell selection is based on the capability of the candidate cells to differentiate into blood vessel-associated cells or secrete proangiogenic factors. Several stem/progenitor cells such as bone marrow cells and endothelial progenitor cells had been identified, isolated and applied in clinical trials with myocardial infarction patients [16]. The results indicate multiple benefits highlighted by improved blood perfusion and cardiac function. However, acquiring enough cells, on the order of millions per patient, is a significant challenge and their in vivo viability is usually very low. Most cells fail to integrate with the host tissue and die soon after delivery. In recent years, induced pluripotent stem cells (iPS), generated by activating key transcriptional factors, provide an attractive avenue for cell therapy [17]. The beauty of this technique is that terminally differentiated cells can be reprogrammed back to an embryonic-like state and then differentiated to a desired cell type under specific culture conditions [18]. Autologous cells are used which avoids many difficulties such as limited cell sources and immune rejection. However, the most effective way to achieve pluripotency is based on viral vectors that carry similar safety concerns to gene therapy. As a very young technology, iPS therapy still requires significant investigation followed by validation in clinical trials before its potential can be accurately evaluated [19].

In many cases delivery of angiogenic factors targets ischemic tissue that is intrinsically different from normal tissue [20,21]. For example, ischemia causes hypoxic conditions that shift glucose metabolism from aerobic to anaerobic. Hence, the production of lactic acid is greatly increased and results in acidosis which reduces pH value down to approximate 6.5, significantly lower than the normal value of approximate 7.4 [22]. In addition, ischemia is often accompanied by intense inflammatory responses including infiltration of neutrophils and macrophages and secretion of reactive oxygen species and hydrolytic enzymes to the local region [23]. Lysosomal enzymes released from the necrotic tissue could degrade surrounding proteins. Furthermore, a new study found that the rapid development of microvasculature accompanying inflammation is not necessarily favorable and could trigger a refractory mechanism to clear angiogenic factors

[24]. All of these elements constitute a harsh environment that makes the bioactivity of delivered angiogenic factors difficult to maintain.

Among all angiogenic factors, VEGF is believed to be the most important modulator involved in all steps of vasculature formation [25]. The human VEGF family is comprised of 5 members including VEGF (VEGF-A, vascular permeability factor), VEGF-B, VEGF-C, VEGF-D and placenta growth factor. Generated by alternative splicing, VEGF-A has 5 isoforms, amongst which VEGF<sub>121</sub> and VEGF<sub>165</sub> are predominant. All isoforms except VEGF<sub>121</sub> contain heparan sulfate binding domains; their bioactivity is therefore localized and reliant on the presence of heparan sulfate [26, 27]. All VEGF isoforms bind to VEGF receptor-1 (VEGFR-1, a.k.a Flt-1) and VEGF receptor-2 (VEGFR-2, a.k.a Flk-1 and KDR), which are receptor tyrosine kinases (Table 2) [28]. The activation of VEGFR results in phosphorylation and dimerization of the receptor. Downstream signaling is diverse and includes MAPK, PI3K and PLC- $\gamma$  pathways. VEGF<sub>165</sub> and other high molecular weight isoforms also bind to neuropilin-1, which serves as a co-receptor that enhances VEGF-VEGFR interaction and alters VEGF signaling [29,30]. Endothelium is the major tissue that expresses both VEGFR-1 and VEGFR-2 and consequently processes such as proliferation and survival of endothelium is highly regulated by VEGF. For therapeutic purposes, local VEGF levels have been upregulated by gene, protein, and cell therapy. Thus far, *vegf* gene delivery has comprised the majority of clinical trials [31]. In some trials, significant neovasculature formation and increased blood perfusion were observed [32,33]. On the other hand, several studies concluded that VEGF expression has to be very tightly regulated in order to avoid side effects [34,35]. Animal studies have further confirmed that stable and functional vessel growth requires a high degree of control over VEGF production [36]. Future efforts in VEGF gene or protein therapeutic strategies will be required to achieve this goal.

Another potent and widely employed angiogenic factor is FGF. FGFs are expressed in diverse organisms from nematodes to vertebrates. In vertebrates, 22 FGFs with 30-70% amino

acid sequence homology, bind selectively to 4 major receptors: FGFR1b/c, FGFR2b/c, FGFR3b/c and FGFR4 [37,38]. Direct comparison of amino acid sequences suggests that FGFs share conserved sequences in the primary FGFR binding site but differ in the secondary site, resulting in the selectivity between FGFRs [39]. FGFR is also a receptor tyrosine kinase and its activation induces phosphorylation and dimerization. Similar to VEGF, downstream signaling pathways include MAPK, PI3K and PLC- $\gamma$  which control both genotype and phenotype. It is worth noting that heparan sulfate binds to all FGF-FGFR complexes and potentiates the FGF signal transduction. The FGF pathway participates in many biological processes including embryonic development [40], wound healing [41], angiogenesis [42] and tumorigenesis and is thus regarded as one of the most pleiotrophic factors. Specifically in angiogenesis, it is well known that the effects of FGFs include migration [43], proliferation [44,45], differentiation and survival of blood vessel-associated cells. Recent studies also show that the integrity of the vasculature is highly regulated by FGF signaling. When FGF signaling is inhibited, endothelial junctions become compromised resulting in increased vessel permeability [46]. FGF signaling is also capable of controlling other angiogenic factor pathways, especially VEGF. This is evident because sustained stimulation by FGF is required to maintain VEGFR expression in the endothelium [47].

Among all FGF members, FGF2 is the most extensively studied and most often utilized in therapeutic angiogenesis. Multiple animal studies have demonstrated the potential of controlled delivery of FGF2 alone or combined with other factors in treating ischemic diseases [48,49]. So far, a few FGF2 phase-I human trials have been conducted in myocardial infarction patients. No obvious toxicity was observed when high dosage of FGF2 was administered by intracoronary delivery, verifying that these levels of FGF2 are safe in humans [50,51]. However, long-term benefit was not observed, possibly due to insufficient activity of FGF2 in the human body [52,53].

Besides FGF2, other FGF members also can initiate angiogenesis and may be successful therapeutics. For example, *fgf4* and *fgf5* are two angiogenic genes that have been delivered via adenovirus at the embryonic stage for treating coronary heart diseases [54,55]. FGF9, in contrast to FGF2 that affects both endothelium and mesenchyme, is known to primarily target mesenchyme. Developmental studies suggest that FGF9 induces *vegfa* expression in lung mesenchyme and is necessary for capillary formation [56]. Another study elucidates the upregulation of FGF9 during the maturation of the smooth muscle layer which controls the survival and physiological response of the vasculature [57]. Superior to FGF2 alone, co-delivery of FGF2 and FGF9 in growth factor-depleted matrigel generates blood vessels of larger diameter and with thicker smooth muscle layers.

Although FGF members share conserved amino acid sequences, the expression pattern and functions of each are still distinctive. Current knowledge of FGFs was mainly accumulated by gene knockout studies which are not able to detect events at molecular level (Table 3). Consequently, the biological roles of many FGFs require further investigation to decipher. It is highly possible that more FGFs or FGF combinations will possibly be utilized in future therapeutics.

Besides VEGF and FGF, other angiogenic factors have also been intensely investigated. Angiopoietin-1, which binds to the Tie2 receptor, is able to balance the effects of VEGF and enhance vasculature stability and its efficacy has been demonstrated in animal studies [58,59]. Hepatocyte growth factor, which stimulates endothelial cell proliferation, can potentiate the mitogenic activity of VEGF and increase VEGF production [60]. It has also been shown to promote secretion of proteases that are involved in ECM degradation and cell migration [61]. Granulocyte colony-stimulating factor acts primarily as a cytokine to mobilize progenitor cells from the bone marrow and has been demonstrated to recruit CD34-positive cells to the infarct area and improve ventricular function in a clinical study [62]. However, its overall effect is still

debated [63]. Other angiogenic factors such as insulin-like growth factor, erythropoietin and stem cell factor have also been investigated in clinical trials [64].

Another group of proteins drawing significant attention in therapeutic angiogenesis are morphogens such as Sonic hedgehog[65] , Notch [66] and Wnt [67]. The effects of morphogens are thought to be more comprehensive because they can regulate transcriptional upregulation of myriad pathways. However, their mechanisms in blood vessel development have to be better understood before clinical trials can be justified.

Blood vessels that carry oxygen, nutrients and signals are critical in both developmental and adult physiology. Induction of neovasculature has the potential to treat many human diseases. No matter which approach is used, angiogenic activity has to be maintained and precisely controlled in order to achieve stable vascularization. In addition to further understanding of angiogenic factors, improvements in delivery strategies will be critical for the success of therapeutic angiogenesis.

**Table 2.** VEGF family and function

	<b>Major receptor</b>	<b>Function</b>
<b>VEGF</b>	VEGFR-1; VEGFR-2 ; neuropilin	Vasculogenesis; Angiogenesis
<b>VEGF-B</b>	VEGFR-1	Vasculogenesis; Angiogenesis
<b>VEGF-C</b>	VEGFR-3 (Flk-4)	Lymphangiogenesis
<b>VEGF-D</b>	VEGFR-3	Lymphangiogenesis
<b>Placenta growth factor</b>	VEGFR-1	Angiogenesis

**Table 3.** FGF family and function

	<b>Phenotype of knockout mouse</b>	<b>Physiological role</b>
<b>FGF1</b>	Normal	Not established
<b>FGF2</b>	Loss of vascular tone; Slight loss of cortex neurons	Not established
<b>FGF3</b>	Inner ear agenesis in humans	Inner ear development
<b>FGF4</b>	Embryonic lethal	Cardiac valve leaflet formation; Limb development
<b>FGF5</b>	Abnormally long hair	Hair growth cycle regulation
<b>FGF6</b>	Defective muscle regeneration	Myogenesis
<b>FGF7</b>	Matted hair; Reduced nephron branching in kidney	Branching morphogenesis
<b>FGF8</b>	Embryonic lethal	Brain, eye, ear and limb development
<b>FGF9</b>	Postnatal death; Gender reversal; Lung hypoplasia	Gonadal development; Organogenesis
<b>FGF10</b>	Failed limb and lung development	Branching morphogenesis
<b>FGF16</b>	Embryonic lethal	Heart development
<b>FGF17</b>	Abnormal brain development	Cerebral and cerebellar development
<b>FGF18</b>	Delayed long-bone ossification	Bone development
<b>FGF19</b>	Increased bile acid pool	Bile acid homeostasis; Lipolysis; Gall bladder filling
<b>FGF20</b>	No knockout model	Neurotrophic factor
<b>FGF21</b>	No knockout model	Fasting response; Glucose homeostasis; Lipolysis and lipogenesis
<b>FGF22</b>	No knockout model	Presynaptic neural organizer
<b>FGF23</b>	Hyperphosphataemia; Hypoglycaemia; Immature sexual organs	Phosphate homeostasis; Vitamin D homeostasis

## 2.0 SPECIFIC AIMS

Growth factors participating in a variety of biological processes have great potential to be applied in regenerative medicine. However, unless protected, free growth factors are degraded quickly by proteases and therefore have little efficacy at tissue repair. Delivery of growth factors with different vehicles has been examined to prolong the half-lives of growth factors and therefore potentiate the bioactivity of growth factors. Even after decades of effort, existing vehicles for growth factor delivery still have some limitations that need to be overcome.

Heparin, a highly sulfated macromolecule, is used as an anticoagulant in clinical treatment. In addition, it has high affinity to a large number of biomolecules including many growth factors. The interaction between heparin and heparin-binding growth factors is known to adjust their conformation, protect them from proteolytic degradation and regulate their activities. Incorporation of heparin in growth factor delivery is consequently a strategy to potentiate the bioactivity of growth factors. Currently, most approaches used to immobilize heparin on the delivery vehicles rely on the covalent modification of heparin that may alter its inherent properties. To maximize the efficacy of heparin, we have developed a coacervate-based delivery platform in which heparin is utilized to complex with a polycation without any modification. The polycation neutralizes the negative charges of heparin and precipitates it out of solution. The spatiotemporal properties of heparin and heparin-binding growth factors are expected to be controlled through this approach. To give a comprehensive evaluation of this delivery platform in translational medicine, this thesis covers the below aspects from the invention to its application:

### Specific aim 1: Development of a coacervate-based platform for growth factor delivery

We introduced a coacervate-based platform containing heparin and a novel polycation, poly(ethylene argininylaspartate diglyceride) (PEAD). PEAD, composed of arginine, aspartate, and diglyceride moieties was synthesized through a polycondensation reaction followed by a coupling reaction. The backbone of this polycation contained ester bonds and was therefore expected to be hydrolyzable. The biocompatibility of PEAD was evaluated via in vitro and in vivo assays and compared with a widely used polycation, polyethyleneimine. The characterization of the [PEAD:heparin] coacervate includes several physical methods. Its potential to be applied as a delivery vehicle was evaluated by determining the load efficiency and release profiles of heparin-binding growth factors. Lastly, the bioactivity of the delivered growth factors was compared with the free-form growth factors using cell-based assays.

### Specific aim 2: Therapeutic angiogenesis via FGF2 coacervate

Therapeutic angiogenesis via growth factor delivery has potential in treatment of many human diseases, especially cardiovascular-related. However, due to the insufficient bioactivity of the delivered factors, the nascent blood vessels do not have sufficient stability and regress over time. I evaluated the ability of [PEAD:heparin] coacervates to deliver an angiogenic factor and examine the responses in vivo by two approaches.

#### Sub-aim 2.1: In vivo angiogenic activity of [PEAD:heparin:FGF2].

In a rodent model, we subcutaneously injected fibroblast growth factor-2 (FGF2) containing coacervate and observed long term angiogenesis. FGF2, a potent angiogenic factor, has the ability to induce the proliferation of endothelial cells, similar to vascular endothelial growth factor. In addition, FGF2 has ability to stimulate mural cells to associate and stabilize the endothelial tubes. I anticipated that if the bioactivity of FGF2 was well preserved, mature blood vessels will be generated even at low dosage of applied FGF2. For comparison, the hemoglobin concentration at the injection site will be measured. The expression of associated markers will

be evaluated to determine the maturity of neovasculature. I expected that the [PEAD:heparin] coacervate effectively enhance the bioactivity of FGF2.

Sub-aim 2.2: Post-myocardial infarction recovery promoted by [PEAD:heparin:FGF2].

Ischemia induced by myocardial infarction (MI) causes short blood supply locally and compromises contractile function. Further examining this coacervate-based delivery platform to promote angiogenesis, I determined its efficacy in a MI model. Successful angiogenesis imparts functional recovery that was assessed by echocardiography. In addition, histological staining was used for observation of gross appearance and fibrosis. Immunohistochemistry was utilized to study angiogenesis, the integrity of myocardium and the inflammatory responses.

### 3.0 DESIGN OF A PLATFORM FOR GROWTH FACTOR DELIVERY

The FGF family is well known for its high affinity to heparin which modulates the interaction between FGFs and their receptors. As revealed by the crystal structure (Fig. 1 left), the heavily anionic heparin brings the cationic sequences on FGF and its receptor closely together and stabilizes the ternary complex largely through polyvalent ionic interactions [68]. In order to mimic the interactions between these three components, a synthetic polycation was applied to substitute the heparin-binding sequence of the FGF receptor and form a ternary complex containing the polycation, heparin and FGF (Fig. 1 right). The addition of a polycation neutralized the excess negative charge of heparin and immediately induced formation of [polycation:heparin:heparin-FGF] coacervates. This approach was expected to anchor the heparin-binding factor and enabled its controlled release. Charge interaction between the polycation and heparin was utilized instead of covalent modification of heparin in an effort to minimize the perturbation of the functions of heparin.

Most existing polycations have low biocompatibility. A novel polycation, poly(ethylene argininylaspartate diglyceride) (PEAD), was consequently designed and used to form [PEAD:heparin] coacervate. PEAD, composed of arginine, aspartate, and diglyceride moieties was synthesized through a polycondensation reaction followed by a coupling reaction. The backbone of this polycation contained ester bonds and was therefore expected to be hydrolyzable. The biocompatibility of PEAD was evaluated via in vitro and in vivo assays and compared with a widely used polycation, polyethyleneimine. The characterization of the [PEAD:heparin] coacervate included several physical methods. Its potential to be applied as a

delivery vehicle was evaluated by determining the load efficiency and release profiles of heparin-binding growth factors. Lastly, the bioactivity of the delivered growth factors was compared with the free-form growth factors using cell-based assays.

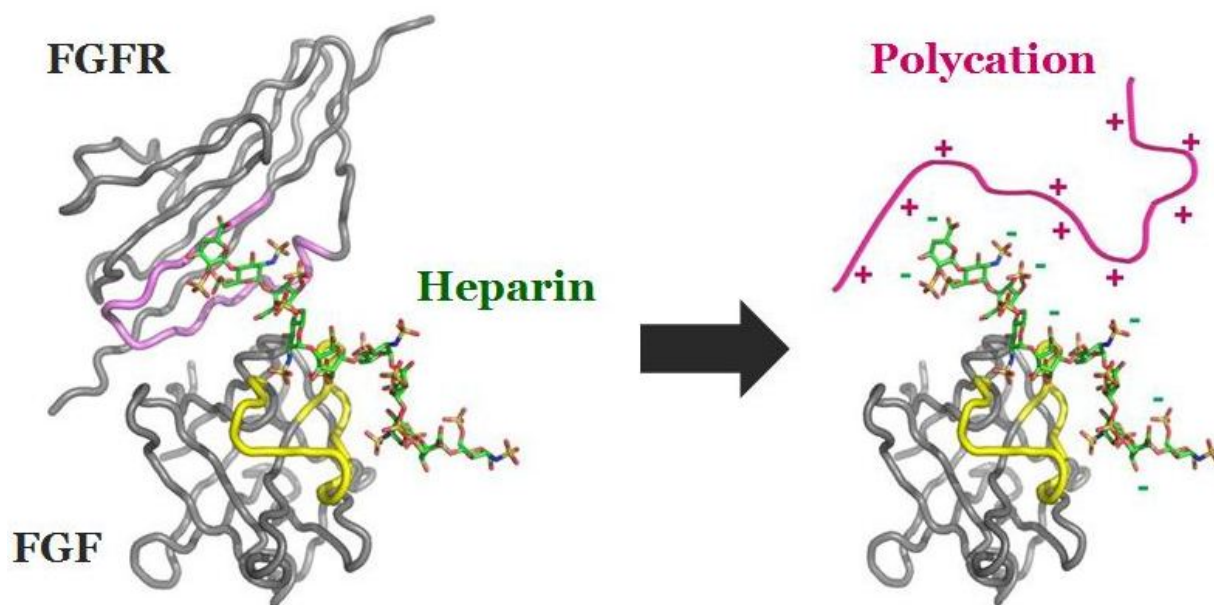


**Figure 1.** Design of a coacervate delivery matrix. The crystal structure of [FGF:heparin:FGFR] complex indicates that heparin actively participate in the interaction of FGF and its receptor whose heparin-binding domains are labeled yellow and pink, respectively (left). The top right scheme represents the design of the coacervate where a synthetic polycation replaces the heparin-binding domain of FGFR and forms a complex with heparin and FGF.

### **3.1 SYNTHESIS OF A BIOCOMPATIBLE POLYCATION**

Polycations are very useful in biotechnology. However, most existing polycations have high toxicity that significantly limits their clinical translation. Our laboratory designed poly(ethylene argininylaspartate diglyceride) (PEAD) that is based on arginine, aspartic acid, glycerol, and ethylene glycol. A set of in vitro assays demonstrated that PEAD exhibited no cytotoxicity at 1 mg/ml, which is at least 100 times higher than the widely used polycation-polyethylenimine (PEI). Subcutaneous injection of 1 mg PEAD in rats did not cause an adverse response acutely or after 4 weeks. Zeta potential measurements revealed that PEAD has high affinity to biological polyanions such as DNA and hyaluronic acid (HA). This polycation represents a new platform of biocompatible polycations that may lead to clinical innovations in gene therapy, controlled release, tissue engineering, biosensors, and medical devices.

#### **3.1.1 Introduction**

Self-assembly of polycations and polyanions can generate complexes with distinct physical and chemical properties. It is a highly active field of research in recent years

[69,70,71]. Polycations such as poly-L lysine (PLL), polyethylenimine (PEI) and chitosan have strong interactions with biological polyanions. This interaction can be used to form a nonviral vector for gene therapy [72] a drug delivery vehicle with controlled-release capability [73,74], and layer-by-layer assembly of thin films with unique properties [75,76]. Furthermore, polycations have been used as coatings to enhance cell attachment [77], tools to separate membrane proteins [78,79,80] and reagents to eradicate microbes [81,82,83]. Despite this diverse range of applications, high toxicity to mammalian cells hinders further biomedical development of polycations [84,85,86,87,88,89,90]. Consequently, there is significant interest in improving the biocompatibility of polycations [91,92,93,94].

Our laboratory has previously reported a polycation, poly(L-argininate glyceryl succinate) with high biocompatibility and utility in controlled release of heparin-binding growth factors [95,96]. However, the synthesis of poly(L-argininate glyceryl succinate) is time consuming. This may compromise its potential adoption in translational research. Thus, a new polycation was designed with the same design principle but the production was simplified. Poly(ethylene argininylaspartate diglyceride) (PEAD) was made from commercially available starting materials in 2 steps. In vitro and in vivo tests demonstrated that PEAD had much higher biocompatibility than PEI. PEAD has high affinity to biological polyanions, which makes it potentially very useful in biomedical applications.

### **3.1.2 Experimental section**

#### **Materials**

$N_{\alpha}$ -Boc-L-aspartic acid (t-BOC aspartic acid),  $N_{\alpha}$ -Boc-L-arginine (t-BOC arginine) (EMD Chemicals, Gibbstown, NJ), ethylene glycol diglycidyl ether (EGDE), trifluoroacetic acid (TFA)

(TCI America, Portland, OR), anhydrous 1,4-dioxane, dimethylformamide (DMF) and tetra-*n*-butylammonium bromide (TBAB) (Acros organics, Geel, Belgium), dicyclohexylcarbodiimide (DCC, stored in N<sub>2</sub> glovebox), N-hydroxysuccinimide (NHS) (Alfa Aesar, Ward Hill, MA) and 4-dimethylaminopyridine (DMAP) (Avocado Research Chemicals Ltd, Lancaster, UK) were used without further purification. Polyethyleneimine (PEI) MW ~ 25,000 (Polysciences, Warrington, PA), Potassium hyaluronate (EMD Chemicals, Gibbstown, NJ) and plasmid pEYFP-N1 (4.7Kb) (Clontech, Mountain View, CA) were used as received.

### Synthesis of PEAD

The polymerization of EGDE and t-BOC aspartic acid was performed as previously reported [97,98,99]. Briefly, EGDE (1.306 g, 7.5 mmol) was mixed with t-BOC aspartic acid (1.749 g, 7.5 mmol) and TBAB (5 mg, 0.016 mmol). 2 ml of 1,4-dioxane or DMF were added to the mixture and the reaction mixture was heated to 100 °C and maintained under N<sub>2</sub> for 48 h. The solvent was evaporated at reduced pressure followed by extraction of TBAB using deionized water and precipitation of the product in excess diethyl ether. The precipitation was repeated twice until no impurity peaks were observed in the <sup>1</sup>H NMR spectrum. The t-BOC protective group on the aspartate was removed with 1:4 TFA:dichloromethane solution (20 ml) for 2 h at room temperature to obtain the intermediate, poly(ethylene aspartate diglyceride) (PED).

Conjugation of t-BOC arginine to PED was performed by DCC/NHS coupling. Briefly, t-BOC arginine (625 mg, 2.28 mmol), DCC (611 mg, 2.96 mmol), NHS (262 mg, 2.28 mmol) and DMAP (5 mg, 0.041 mmol) were dissolved in DMF and reacted for 10 min followed by the addition of PED (700 mg, 2.28 mmol). The mixture was stirred under N<sub>2</sub> for 24 h. The insoluble dicyclohexylurea was removed by filtration. After most DMF was removed by evaporation at reduced pressure, the solution was added dropwise into 15 ml of TFA and stirred for 90 min at

ambient temperature to remove the t-BOC group on arginine. TFA was removed by evaporation at reduced pressure and the product was precipitated in ethyl acetate followed by hexanes. The precipitation was repeated at least twice until no impurity or solvent peaks were observed in the  $^1\text{H}$  NMR spectrum.

### **Characterization of PEAD**

$^1\text{H}$  NMR and FTIR spectra were recorded on a Mercury 400 NMR (Varian, Palo Alto, CA) and a Nicolet IR-100 spectrometer (Thermo, Waltham, MA), respectively. The molecular weight of the polymers was determined by a PL-GPC 50 Plus-RI equipped with a PD 2020 Light Scattering Detector and a PL-BV 400RT Viscometer (Varian, Palo Alto, CA). Two MesoPore 300x7.5 mm columns and DMF containing 0.1 % LiBr were used as stationary and mobile phases, respectively. Polylatide-poly(ethylene oxide) (PL-PEO) standards were used for calibration and molecular weight calculation.

The degradation of PEAD was monitored by the variation of light scattering. Briefly, 10 mg/ml of PEAD in PBS containing 0.5% of FBS was incubated at 37 °C under gentle agitation. At day 0, 7, 14, and 30, aliquots were collected for analysis. A Viscotek VE2100 GPC (Malvern, Westborough, MA) equipped with a Suprema 300x8 mm column (Polymer Standards Service, RI) and a right angle light scattering detector was used for separation and detection respectively.

### **In vitro biocompatibility**

NIH 3T3 fibroblasts were cultured in DMEM (Mediatech, Manassas, VA) containing 10 % fetal bovine serum (FBS) (Lonza, Walkersville, MD) and 1% penicillin/streptomycin (Lonza, Walkersville, MD) and expanded under standard culture conditions at 37 °C with 5%  $\text{CO}_2$  until sufficient quantities were obtained. Human aortic endothelial cells (HAEC) (Lonza, Walkersville,

MD) (passage 6-8) were cultured in MCDB 131 medium (Mediatech, Manassas, VA) containing 10% FBS and 1% penicillin/streptomycin, and supplemented with 1 ng/ml epithelial growth factor (EGF), 2 ng/ml basic fibroblast growth factor (FGF2), 2 ng/ml insulin-like growth factor-1 (IGF1), 1 ng/ml vascular endothelial growth factor (VEGF) and 1 µg/ml hydrocortisone (all growth factors were from the same vendor, Sigma-Aldrich, St. Louis, MO). The medium including all the supplements is referred to as the complete medium.

For lactate dehydrogenase (LDH) assay (n=4), 3-(4,5 -dimethylthiazol-2-yl)-2,5-diphenyl tetrazolium bromide (MTT) assay (n=4) and live/dead assay (n=4),  $5 \times 10^3$  cells per well were seeded in 96-well plates one day before the experiment. PED, PEAD or PEI dissolved in the complete medium at the desired concentrations (10, 5, 2, 1 mg/ml for PED and PEAD; 10, 1, 0.1, 0.01 mg/ml for PEI) was added into each well. The complete medium alone was used as the control. After 24 h incubation, LDH activity in the culture medium was measured by a CytoTox 96® Non-Radioactive Cytotoxicity Assay kit (Promega, Madison, WI). Cell metabolic activity was determined by a Vybrant® MTT Cell Proliferation Assay Kit (Invitrogen, Carlsbad, CA) according to a modified protocol [100]. The level of caspase-3 was measured using an EnzChek® Caspase-3 Assay Kit (Invitrogen, Carlsbad, CA). Cell viability was analyzed by using a LIVE/DEAD® Viability/Cytotoxicity Kit (Invitrogen, Carlsbad, CA). The absorbance and fluorescence were recorded by a SynergyMX plate reader (Biotek, Winooski, VT).

### **In vivo biocompatibility**

Male Sprague Dawley rats with an average body weight of 300 g were used and cared for in compliance with a protocol approved by the Institutional Animal Care and Use Committee of the University of Pittsburgh. Under isoflurane anesthesia, 1 mg of PEAD or PEI in 100 µl saline (0.9%) was injected subcutaneously into the back of each animal. The animals were sacrificed at post-injection day 3, 14 and 28. The tissue surrounding the injection site and major

organs including lung, liver and kidney were harvested and fixed in 10 % formalin. Cross-sections (4  $\mu\text{m}$  thick, longitudinal axial cut) were stained with hematoxylin and eosin (H & E) to examine inflammation or any adverse effects using an inverted microscope Eclipse Ti (Nikon, Melville, NY) equipped with a RETIGA-SRV digital camera (QImaging, BC, Canada).

### **Zeta potential and dynamic light scattering (DLS) measurement**

All polymer solutions were prepared at the concentration of 1 mg/ml in deionized water and saline respectively. All zeta potential measurement was carried out in water and DLS was performed in both water and saline. For [PEAD:DNA] complex formation, 10  $\mu\text{l}$  of plasmid (pEYFP-N1) solution (1  $\mu\text{g}/\mu\text{l}$ ) was titrated with different amounts of PEAD solution. 750  $\mu\text{l}$  of deionized water or saline was added to dilute the complex before the measurement. For [PEAD:HA] complex formation, 100  $\mu\text{l}$  of HA solution (1 mg/ml) was titrated with increasing amounts of PEAD solution. 1 ml of deionized water or saline was added for dilution, and 750  $\mu\text{l}$  of solution was used for zeta potential and particle size measurement on a Zetasizer Nano ZS (Malvern, Westborough, MA).

### **Scanning electron microscopy (SEM)**

The SEM samples were prepared by mixing PEAD with DNA (mass ratio of PEAD to DNA: 1.5) or hyaluronic acid (mass ratio: 4) to form the complex. The complexes were dropped on aluminum stubs, lyophilized, sputtered with gold and viewed with a Leo 1530 SEM (10 kV, 3 nm spot size) (Carl Zeiss SMT, Peabody, MA).

## **Statistical analysis**

The results of in vitro biocompatibility assays were analyzed by ANOVA with post-hoc Bonferroni correction. The value of the control group was compared with that of each PEAD concentration individually. A  $p$  value < 0.05 was considered significant.

### **3.1.3 Results and discussion**

#### **Synthesis and characterization of PEAD**

The synthesis of PEAD starts from a polycondensation reaction between t-BOC aspartic acid and EGDE under the catalysis of TBAB. Deprotection of t-BOC formed the intermediate, PED, with ~94 % yield. The conjugation of t-BOC arginine to PED and then deprotection of t-BOC produced PEAD which comprises three parts derived from arginine, aspartate and ethylene glycol (Fig. 2). Because removal of DMF by repeated precipitation caused a significant loss of PEAD, the yield of the arginine conjugation step is 33 %. Clearly, a more efficient purification method needs to be developed to increase the yield in the future.

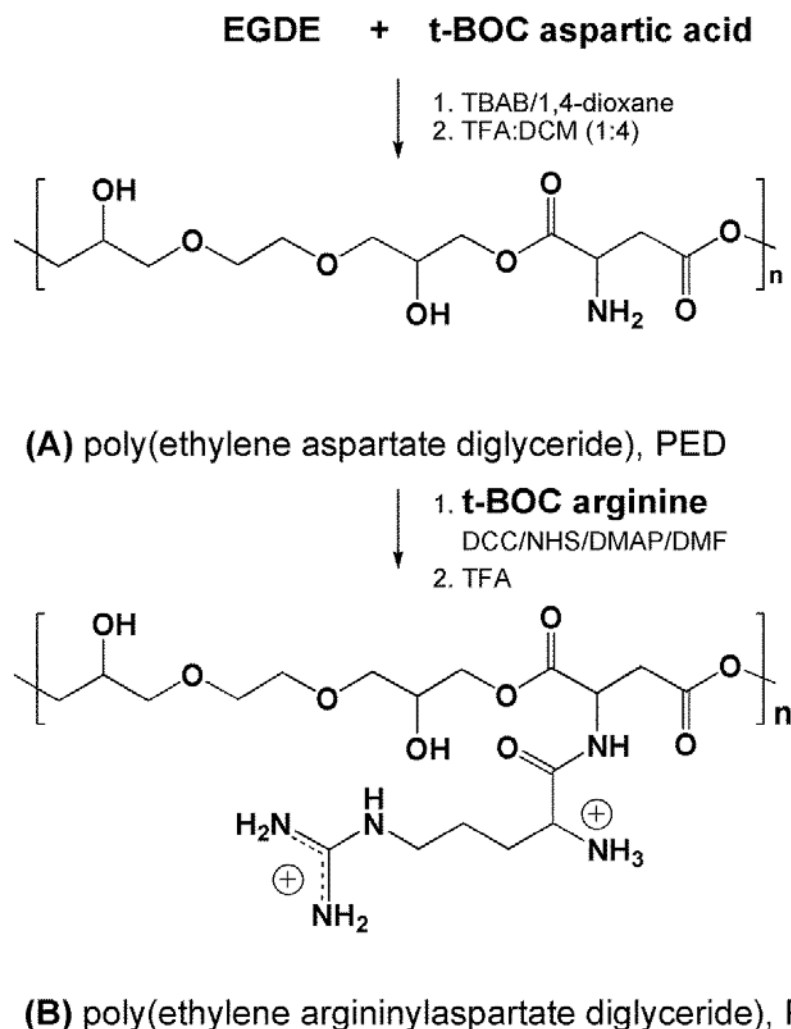


**Figure 2.** Synthetic routes and chemical structures of PEAD and its intermediate. Poly(ethylene aspartate diglyceride), PED, was synthesized by polycondensation of t-BOC aspartic acid and EGDE catalyzed by TBAB in DMF or 1,4-dioxane followed by removal of t-BOC in 20 % TFA in dichloromethane. PEAD was synthesized by conjugation of t-BOC arginine to the aspartic amino group under the activation of DCC, NHS and DMAP followed by deprotection using TFA. The chemical shifts in  $^1\text{H}$  NMR for the key functional groups are marked on the structure.

The structure of the polymer was analyzed using NMR, IR, and GPC. The  $^1\text{H}$  NMR spectrum showed two chemical shifts at 1.7 and 1.9 ppm corresponding to the  $\beta$  and  $\gamma$  methylene protons on the arginine moiety (Fig. 3). The chemical shift at 4.1 ppm was from the  $\alpha$

hydrogen of the aspartate moiety. The ethylene glycol portion produced a multiplet between 3.4 to 3.9 ppm. The conversion of deprotected primary amine to arginine was nearly quantitative according to NMR integration of arginine proton "c" and the rest of the protons of PEAD. The intermediate, PED, had a weight average molecular weight ( $M_w$ ) of 73,750 Da with a polydispersity index (PDI) of 1.18. The polymerization was performed either in DMF or 1,4-dioxane. 1,4-dioxane yielded polymers with a higher molecular weight and a lower polydispersity (Fig. 3). The molecular weight of the intermediate was higher than those of the final products because the deprotection of t-BOC by TFA can also cleave the ester bonds of the backbone. IR spectrum revealed a clear difference between PED and PEAD. PED had two distinct peaks at 1668 and 1733  $\text{cm}^{-1}$  corresponding to the ester bonds in the polymer backbone. The guanidine group on arginine increased the intensity of the absorption between 1635-1670  $\text{cm}^{-1}$  and broadened the absorption between 3000-3500  $\text{cm}^{-1}$  (Fig. 4).

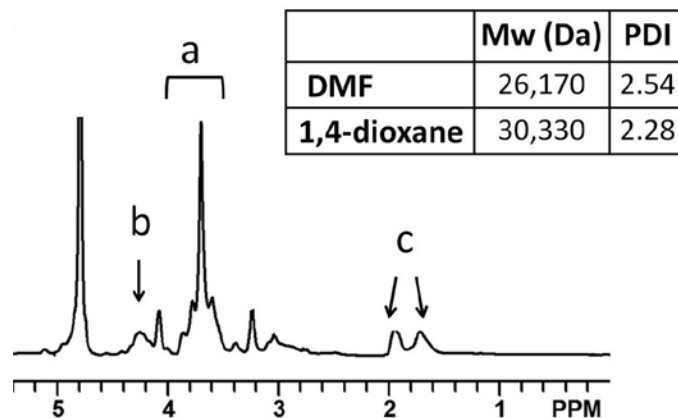


**Figure 3.**  $^1\text{H}$  NMR spectrum of PEAD shows proton signals consistent with functional groups derived from arginine, aspartate and ethylene glycol. The solvent used in NMR,  $\text{D}_2\text{O}$ , has a sharp signal at 4.79 ppm. The inset summarizes the GPC result. Polycondensations performed in 1,4-dioxane have higher  $M_w$  and smaller PDI.

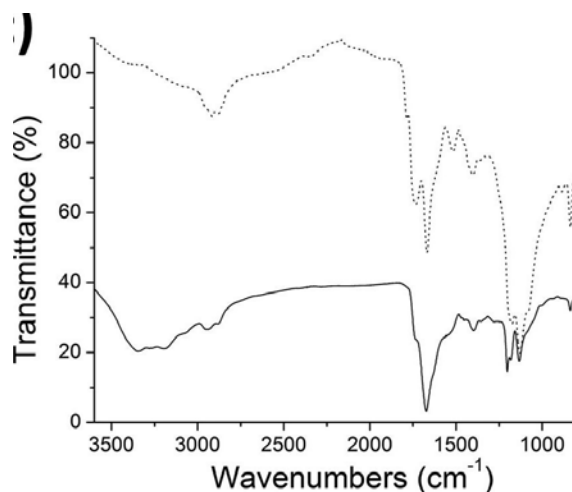


**Figure 4.** FTIR spectrum reveals that PED has strong absorption at 1668 and 1733  $\text{cm}^{-1}$  due to the ester bonds connecting EGDE and aspartate (dotted line). PEAD has strong absorption in the region (1635-1750  $\text{cm}^{-1}$ ) and (3000-3500  $\text{cm}^{-1}$ ) supposedly contributed by the amide bonds connecting arginine and aspartate and guanidinium groups of arginine moiety (solid line).

In our previous study, different catalysts and solvents were examined for the same polycondensation reaction; it was found that TBAB was a good catalyst, and 1,4-dioxane was an appropriate solvent in terms of yield and molecular weight [99]. The monomers used in this study were more polar, but the results showed a similar trend with respect to solvent.

As a polyester, PEAD was expected to be hydrolysable. To test the degradability, PEAD was dissolved in PBS containing 0.5% FBS, and the intensity of the scattered light was measured at different time points (Fig. 5). The polymer signal was clearly visible after 30 days. The steady drop of the intensity of the scattered light suggested that PEAD degraded gradually via simple hydrolysis under test conditions.

<b>Time point (days)</b>	<b>RALS Intensity (mV)</b>	<b>Percentage (%)</b>
<b>0</b>	141.6	100
<b>7</b>	109.9	77.6
<b>14</b>	89.6	63.3
<b>30</b>	85.2	60.2

**Figure 5.** The degradation of PEAD as determined by the change of light scattering with time. The intensity of the peak at retention time 5.3 min gradually decreased. This demonstrated that PEAD is degradable but the process is slow under the testing conditions.

### **Examination fibroblasts and endothelial cytotoxicity**

To study the cytocompatibility of PEAD, in vitro assays were performed using NIH 3T3 fibroblasts and HAECs. NIH 3T3 fibroblasts were chosen because they have been used extensively to test polycation cytocompatibility [101]. Furthermore, HAECs could represent non-immortalized human cells. In addition to PEAD, the cytocompatibility of the intermediate, PED, was also tested. Therefore it was able to estimate the influence of arginine conjugation on biocompatibility. The results were all compared with the widely used polycation, PEI. After incubation with various concentrations of polycations for 24 h, a series of assays including LDH, MTT, caspase-3 activity, and live/dead assays were performed to determine the cytocompatibility of PEAD.

When testing PEAD with NIH 3T3 fibroblasts, LDH assay revealed that 1 mg/ml of PEAD did not compromise cell membrane integrity (Fig. 6a). MTT assay showed that 5 mg/ml did not reduce cellular metabolism. There was no activation of caspase-3 at any of the concentrations tested. Live/dead assay showed that 5 mg/ml of PEAD had no impact on the ratio of live to dead cells. When testing the intermediate PED with NIH 3T3 fibroblasts, no cell membrane damage was observed at any concentrations tested (Fig. 6b). MTT assay showed that 5 mg/ml of PED

caused a significant reduction in cell metabolism. Live/dead assay showed that 5 mg/ml of PED reduced the ratio of live to dead cells to 68 %. Overall, it was concluded that 1 mg/ml of PEAD or 2 mg/ml of PED did not cause cytotoxicity to NIH 3T3 cells. On the contrary, PEI showed high cytotoxicity; 0.01 mg/ml PEI was cytotoxic as indicated by all three assays (Fig. 6c). This is consistent with our prior results using primary baboon smooth muscle cells [95].

When testing PEAD with HAECs, LDH in the culture medium elevated and the metabolic activity dropped when the concentration of PEAD reached 10 mg/ml (Fig 6d). No increase in caspase-3 activity was observed at any concentration as NIH 3T3. Live/dead assay suggested that cell viability dropped when the concentration of PEAD reached 5 mg/ml. For PED, only MTT assay showed that cell metabolism was compromised when the concentration reached 5 mg/ml (Fig. 6e). Other assays revealed no difference with the control group. Overall, no cytotoxicity to HAECs was observed up to 5 mg/ml PEAD or 2 mg/ml PED. Compared to PEAD or PED, 0.01 mg/ml of PEI showed significant cytotoxicity to HAECs as it did to NIH 3T3 cells (Fig. 6f).

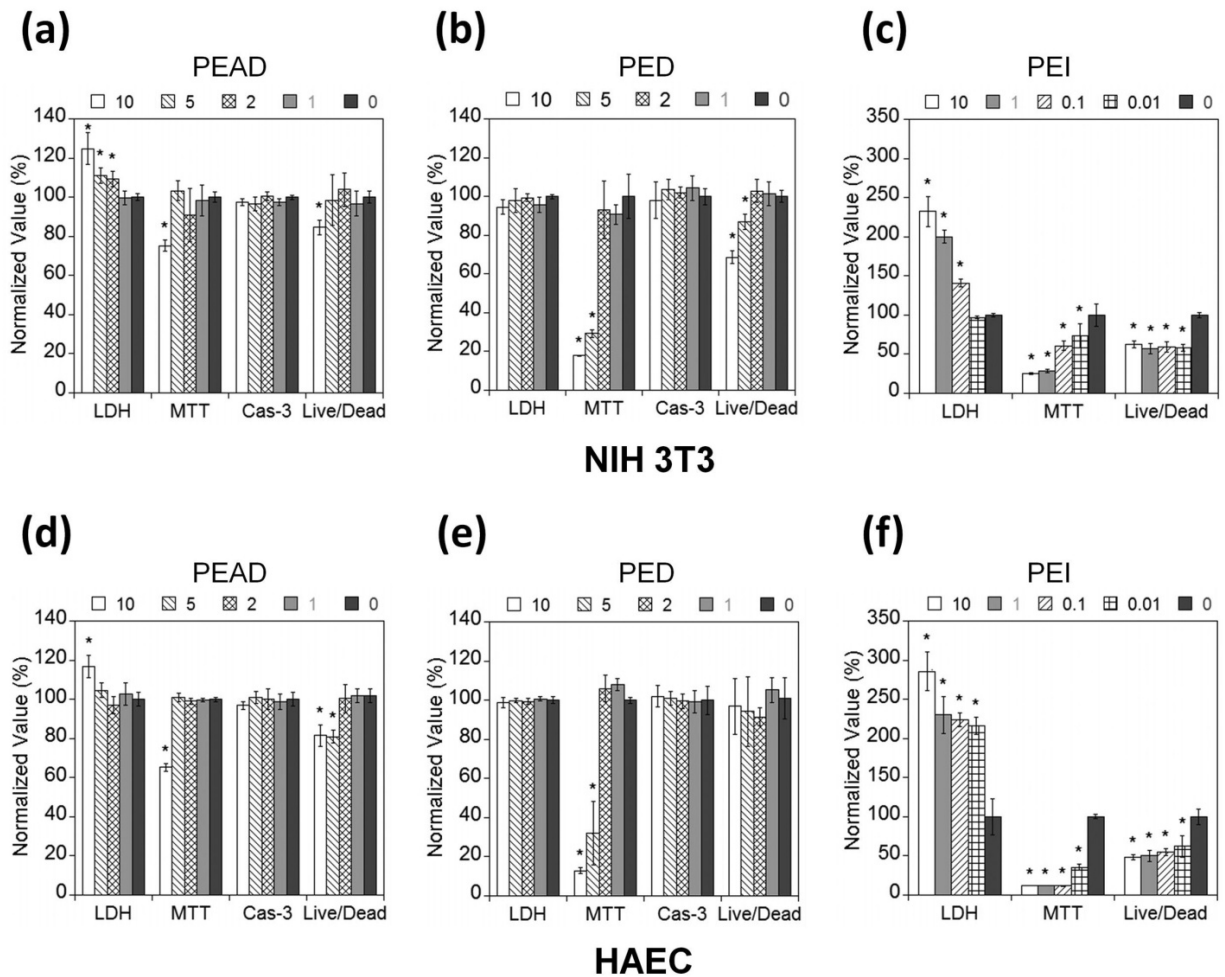


**Figure 6.** Comparison of in vitro biocompatibility of PEAD, PED and PEI by NIH 3T3 (a-c) and HAECs (d-f). For NIH 3T3 cells, PEAD did not compromise cell membrane at 1 mg/ml, reduce cellular metabolism at 5 mg/ml, or activate caspase-3 for all concentrations tested, and also had no impact on the ratio of live to dead cells at 5 mg/ml (a). PED reduced cellular metabolism and reduced the ratio of live to dead cells to 68 % when the concentration reached 10 mg/ml (b). PEI, however, showed high cytotoxicity; 0.01 mg/ml PEI was cytotoxic as indicated by all three assays (c). For HAECs, PEAD elevated LDH in the culture medium and dropped metabolism at 10 mg/ml, and also lowered cell viability at 5 mg/ml (d). PED compromised cellular metabolism when the concentration reached 5 mg/ml (e). 0.01 mg/ml of PEI showed significant cytotoxicity

to HAECs as it did to NIH 3T3 cells (f). Overall, the in vitro study demonstrated that PEAD and PED have much higher biocompatibility than PEI. \* $p$  value < 0.05.

According to the results of MTT assays reported previously using L929 mouse fibroblasts, many existing polycations had  $IC_{50}$  values lower than 0.5 mg/ml. These include poly-L lysine (PLL), poly(diallyl-dimethyl-ammonium chloride), poly(vinyl pyridinium bromide) and diethylaminoethyl dextran, or 0.1 mg/ml polyethylenimine (PEI) [94]. MTT assays showed that even at 10 mg/ml, PEAD only reduced the metabolic activity to 75 % and 65 % for NIH 3T3 and HAECs respectively. In addition, PEI and PLL have been demonstrated to induce apoptosis in multiple cell lines according to caspase-3 assays [87]. In contrast, caspase-3 activity showed no significant increase at any concentration tested for PEAD and PED. Previous accounts of different polycation toxicities were obtained using a variety of cell lines, but common observation was that synthetic polycations have low biocompatibility in genera [87,90]. PEAD was tested with both cell line and immortalized human cells. Combined, the in vitro assays indicated that PEAD showed no cytotoxicity to either NIH 3T3 cell line or primary HAECs, at 1 mg/ml. Structurally, the difference between PED and PEAD is that the latter carries arginine. The biocompatibility of PEAD and PED showed no difference at 2 mg/ml. At 5 to 10 mg/ml, the biocompatibility of PEAD appeared to be higher than PED. This is opposite of the inverse relationship between charge density and biocompatibility observed in other series of polycations and the mechanism awaits further investigation [90].

### **Examination of in vivo biocompatibility by subcutaneous injection**

To complement the in vitro studies, the in vivo biocompatibility of PEAD was further investigated. 100  $\mu$ l of PEAD solution (10 mg/ml) was injected subcutaneously in rats. 3, 7 and 28 days post-injection were chosen to observe the progression of acute to long term effects of

PEAD injection. No discernable difference was observed between the tissue responses at the different time points. The micrographs show that hematoxylin and eosin (H & E) staining of the tissues harvested at day 3 displayed normal tissue architecture for the connective tissue and the muscle surrounding the injection site (Fig. 7) and major organs including lung, liver and kidney (Fig. 8). No appreciable inflammation or necrosis was observed. In addition, there were no associated atypical or transformed malignant cells. However, under identical conditions, PEI caused severe damage to the connective tissues and muscles surrounding the injection site. The connective tissues were widely infiltrated by neutrophils and plasmocytes, and showed extensive inflammation. The muscle fibers in the injection zone showed severe degeneration and necrosis accompanied by significant inflammatory infiltrates.

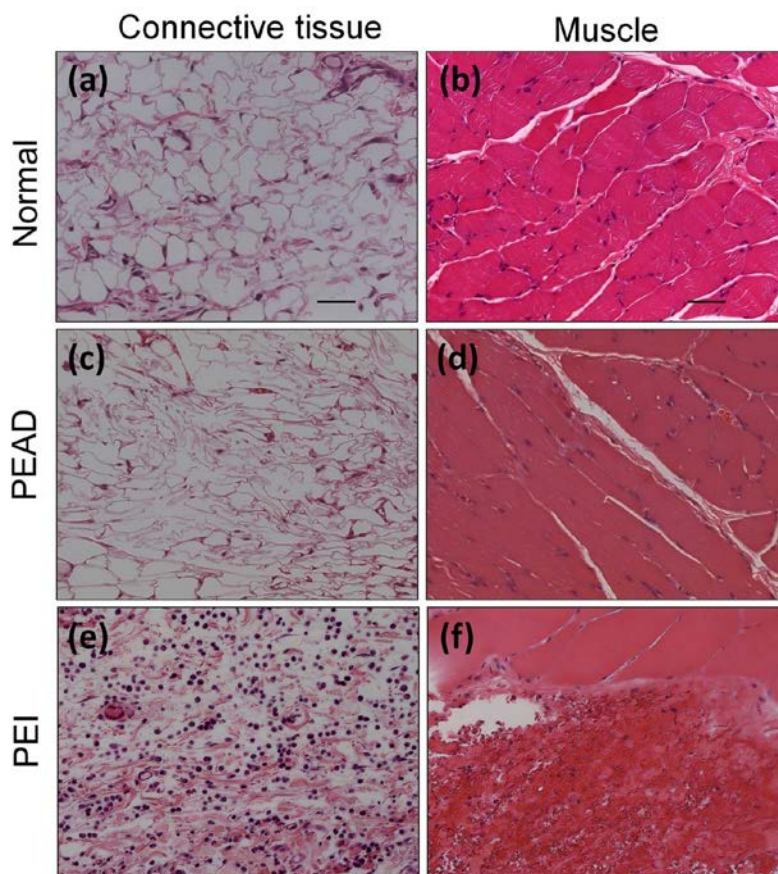


**Figure 7.** Comparison of in vivo biocompatibility of PEAD and PEI by H&E staining. The tissues from the healthy animals were used as the controls, (a) connective tissues and (b) muscles. The

animals injected with PEAD exhibited no difference from healthy controls 3 day post-injection. No appreciable inflammation or necrosis was observed at the injection site, (c) and (d). PEI, however, showed serious cytotoxicity to the tissues. (e) The connective tissues were widely infiltrated by neutrophils and plasmocytes and exhibited extensive inflammation. (f) The muscle fibers were degenerated and suffered significant necrosis. Scale bar = 50  $\mu$ m. The same was observed for tissues harvested at days 7 and 28.

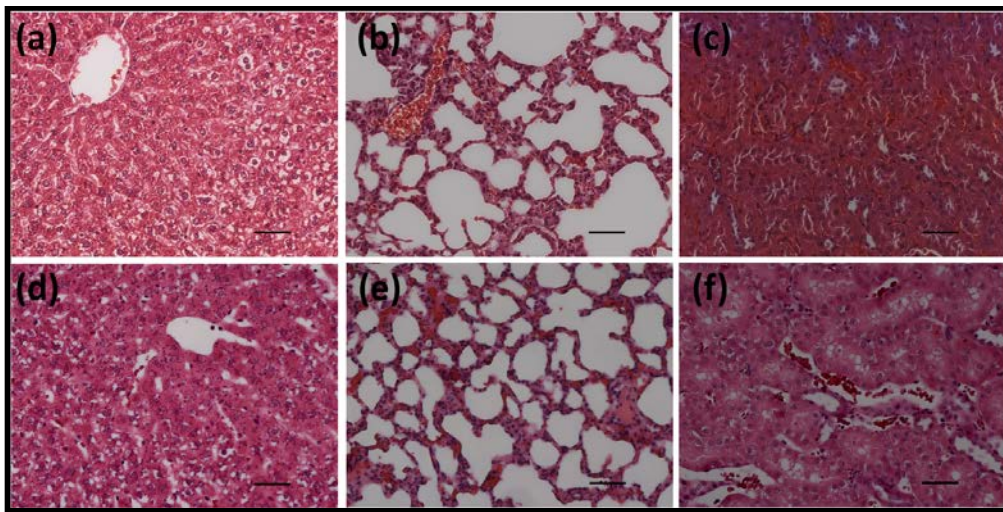


**Figure 8.** H & E staining of tissues harvested at day 3 post-injection. Both PEAD (a-c) and PEI (d-f) showed normal morphology. Liver: (a) and (d). Lung: (b) and (e). Kidney: (c) and (f). Scale bar = 50  $\mu$ m.

PEI is currently the most widely used polycation in gene delivery. Although the *in vivo* efficacy has been demonstrated, its high cytotoxicity is still an issue which compromises the clinical value. Tail-vein injection of 0.02 mg of PEI (25 kDa) in mice can cause necrosis and apoptosis in the lung, liver, spleen and kidney [94]. Similarly, according to our previous experiment, injecting 0.2 mg of PEI (10 kDa) intraperitoneally caused severe necrosis and apoptosis in the liver of mice at day 1 post injection [95]. Here, at least 1 mg of PEAD was shown to have no *in vivo* cytotoxicity when injected subcutaneously whereas the same amount

of PEI caused serious damage to the tissue at the injection site. It is possible that a larger amount of PEAD could be injected without causing adverse reactions in vivo. 1 mg of PEAD was tested because this was expected to be the upper limit of our in vivo applications [102].

### **Zeta potential measurement of [PEAD:polyanion] complexes**

Under physiological conditions, PEAD bears  $> 1$  positive charge per repeating unit and should interact strongly with negatively charged macromolecules through Coulombic attraction. DNA (plasmid pEYFP-N1) and hyaluronic acid (HA) were chosen to represent two important classes of biological polyanions, nucleic acids and glycosaminoglycans. Upon addition of PEAD to DNA solution, the zeta potential changed from negative to neutral and then positive (Fig. 9). At a PEAD to DNA mass ratio of approximately 1.5, the complex became neutral, indicating that all negative charges on the DNA were neutralized by PEAD. Adding more PEAD after this isoelectric point was reached caused [PEAD:DNA] complexes to become positively charged, reaching a plateau at +23.9 mV which is similar to the potential of PEAD (+23.1mV). The same trend was observed during the addition of PEAD into hyaluronic acid. The isoelectric point for [PEAD:HA] complex was obtained at a polycation/polyanion mass ratio of approximately 4. The only difference was that the plateau potential of [PEAD:HA] complex was +11.1 mV, lower than that of [PEAD:DNA] complex. It was hypothesized that different plateau potentials are caused mainly by intrinsic properties such as viscosity and solubility of individual biological polyanions. Because zeta potential measurement does not account for these factors, [PEAD:DNA] and [PEAD:HA] complexes exhibited similar patterns but have different zeta potentials. The polyvalent nature of the interactions between PEAD and a polyanion suggests that the molecular weight of the polymeric components will affect their affinity. Therefore molecular weight of PEAD is expected to offer a convenient control of its interaction with polyanions in a similar fashion as poly(L-argininate glyceryl succinate) [96].

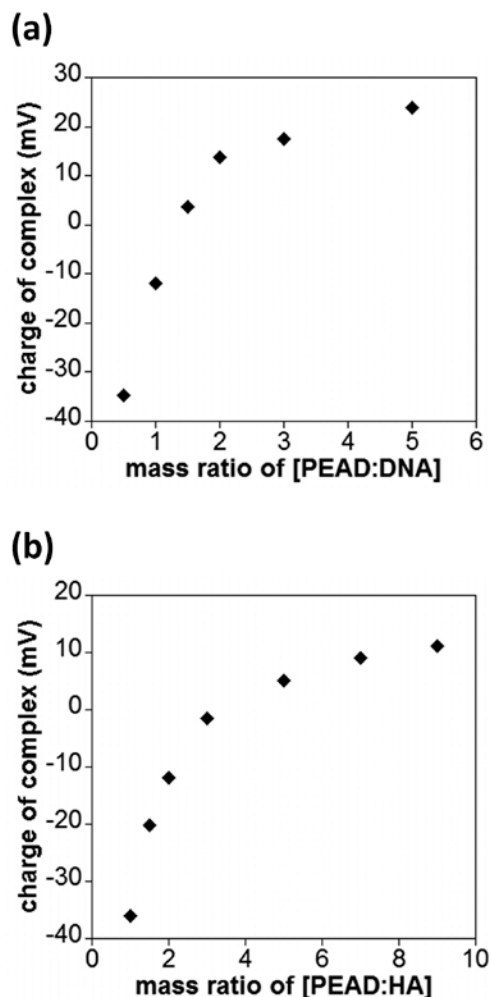


**Figure 9.** Monitoring Zeta potential during the titration of biological polyanions with PEAD suggested that PEAD had high affinity toward negatively charged macromolecules. (a) As more PEAD is added, the zeta potential of the [PEAD:DNA] complexes shifted from negative to neutral and then reached a plateau at approximately +23 mV. At the mass ratio close to 1.5, the complex is neutral. (b) The titration of [PEAD:HA] complex followed a similar pattern with a neutral complex formed at the mass ratio of 4.

### Size measurement of [PEAD:polyanion] complexes

Dynamic light scattering (DLS) was used to measure the hydrodynamic volume of macromolecules. DLS offers useful information on size of the [PEAD:polyanion] coacervate

even though DLS assumes the coacervate is spherical. In deionized water the average diameter of the [PEAD:DNA] complex at the isoelectric point was 245 nm with a standard deviation of 53 nm. In saline, the diameter decreased to 150 nm with a standard deviation of 30 nm. Compared to [PEAD:DNA] complex, [PEAD:HA] complex had a much larger diameter in deionized water reaching 1,236 nm with a standard deviation of 124 nm, but in saline the diameter dropped significantly to 240 nm with a standard deviation of 20 nm. These results suggest that increasing ionic strength reduces the interaction between PEAD and polyanions. Differences between [PEAD:DNA] and [PEAD:HA] are likely caused by differences in size and electrostatic properties of individual polyanions. Furthermore, DLS and GPC data are consistent with a mostly linear structure of the polymer. Based on DLS measurement, the hydrodynamic diameter of PEAD is 5.9 nm. The corresponding MW would be 214.2 kD, 257.0 kD, and 50.8 kD for globular, starburst, and linear polymers respectively. GPC analysis indicates that Mw of PEAD is approximately 30 kD. This matches the linear polymer (50.8 kD) best, therefore, PEAD is most likely linear.

### **SEM micrographs of [PEAD:polyanion] complexes**

PEAD immediately forms a turbid solution with DNA or HA upon mixing. To reveal the morphology of the resultant ionic complexes, SEM was used to investigate the complexes at the isoelectric points. The micrograph shows that [PEAD:DNA] complex is mainly composed of fibers, beads, and sheets (Fig. 10a). The diameters of the fibers cover a wide range from sub-micron to nanometers. [PEAD:HA] complex shares similar structures with [PEAD:DNA] complex, however, the fiber diameters are larger and there are more sheets and fewer beads (Fig. 10b). The factors that lead to the morphological differences between [PEAD:HA] and [PEAD:DNA] complexes are currently under investigation.

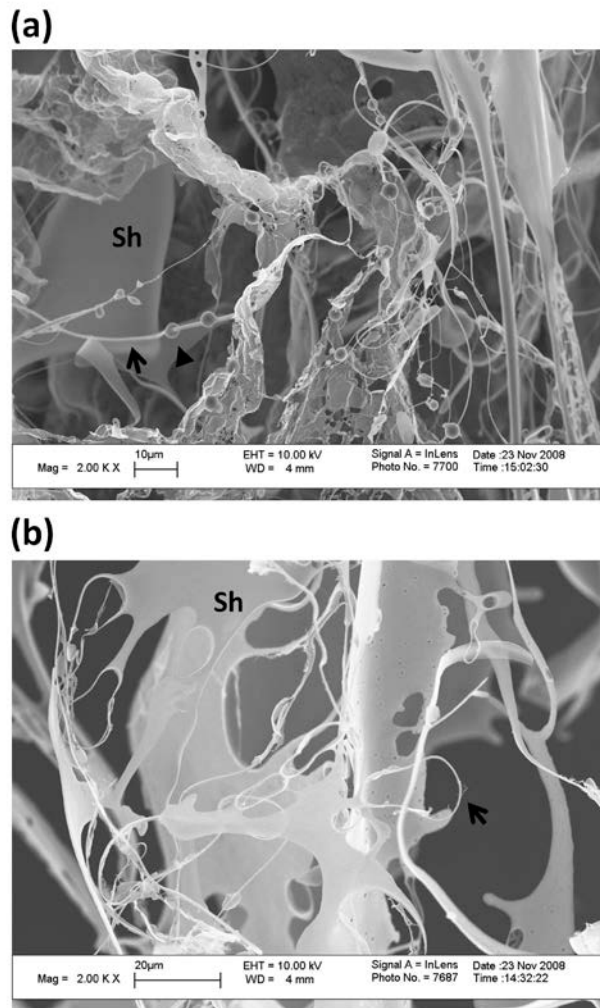


**Figure 10.** Scanning electron micrographs of the ionic complexes. (a) [PEAD:DNA] complex consists mainly of fibrous structures (arrow). The diameters of the fibers are typically less than 1 µm. In addition, it also contains beads (arrowhead) and sheets (sh). 2,000X, scale bar = 10 µm. (b) [PEAD:HA] complex is mainly fibrous in nature and the fibers (arrow) have larger diameters. There are also sheet-like structures (sh) in the complex. 2,000X, scale bar = 20 µm.

### 3.1.4 Summary

In the prior study, our laboratory proposed a design principle for biocompatible polycations: a biocompatible polycation should be biodegradable and made from endogenous cations [95]. Here, this study followed the same principle and applied a simple chemistry to synthesize a new arginine-based biodegradable polycation to further test this design. The reaction parameters can be adjusted easily to generate a series of polycations with different physical and chemical properties. PEAD assembles with biological polyanions and spontaneously forms three-dimensional structures in aqueous solution. PEAD offers higher biocompatibility than conventional polycations and may lead to advancements in many areas of biotechnology and medicine.

### **3.2 APPLICATION OF [PEAD:HEPARIN] IN GROWTH FACTOR DELIVERY**

Growth factors are potent molecules that regulate cell functions including survival, self renewal, differentiation and proliferation. High-efficacy delivery of growth factors will be a powerful tool for regenerative medicine. Decades of intense research have significantly advanced the field of controlled delivery. There is, however, still a great unmet need for new methods that can improve overall efficacy of growth-factor delivery. Here, we report a new growth factor delivery vehicle formed by self assembly of heparin and a biocompatible polycation, poly(ethylene argininy laspartate diglyceride) (PEAD). Of the many heparin-binding growth factors, we chose FGF2 and NGF to demonstrate the potential of the [PEAD:heparin] delivery vehicle. The delivery vehicle incorporates both growth factors with high efficiency, controls their release, maintains the bioactivity of FGF2 and increases the bioactivity of NGF relative to bolus delivery. [PEAD:heparin] appears to be a promising delivery matrix for many heparin-binding growth factors and may lead to efficient growth factor delivery for a variety of diseases and disabilities.

### 3.2.1 Introduction

Extracellular growth factors are usually associated with extracellular matrix (ECM) and rarely exist in free forms [103,104,105]. This allows for growth factors to be stored in the ECM which enables a rapid response to extracellular stimuli. This is highly beneficial because the activation of a growth factor expressing gene can take hours [106]. Growth factor binding also changes the conformation of the growth factors and modulates their interactions with receptors and their bioactivities [107,108,109]. Furthermore, the association can protect the growth factors from proteolytic degradation [110]. Heparan sulfate, a major component of the ECM, is a highly-sulfated glycosaminoglycan with high affinity to a large variety of growth factors [111,112]. Heparin has a similar structure to heparan, binds many growth factors, and is more readily available and more widely used in the research and application of growth factors [113]. We therefore decided to exploit the affinity between heparin and growth factors to achieve high-efficiency delivery of heparin-binding growth factors.

In order to maintain the native properties and function of heparin, we chose to use intact heparin without covalently linking heparin to the delivery matrix. A biocompatible polycation was chosen to ionically bind heparin to form the delivery vehicle. PEAD was a biodegradable polycation with high biocompatibility. Because of the high charge density, PEAD bound strongly to heparin and consequently incorporates growth factors with high efficiency. [PEAD:heparin] can control the release of the growth factors for over 30 days in a nearly linear fashion. More importantly, [PEAD:heparin] complex maintained the bioactivity of fibroblast growth factor-2 (FGF2) and increased the bioactivity of nerve growth factor (NGF) when compared with bolus delivery. This new delivery vehicle was expected to be applicable to any heparin-binding growth factor and represent an innovative method of delivering single or multiple growth factors.

### 3.2.2 Experimental section

#### Synthesis of PEAD

The detailed synthetic procedures of PEAD are described in the supporting material. Briefly, PEAD was synthesized in two steps. (i) Ethylene glycol diglycidyl ether (EGDE) and t-BOC protected aspartic acid were polymerized through a polycondensation reaction in 1,4-dioxane under the catalysis of tetra-*n*-butylammonium bromide (TBAB). The t-BOC protective group was removed by 1:4 trifluoroacetic acid (TFA):dichloromethane (DCM) to generate the intermediate, poly(ethylene aspartate glyceride) (PED). (ii) Conjugation of t-BOC arginine to PED was performed by a dicyclohexylcarbodiimide (DCC)/N-hydroxysuccinimide (NHS)/4-dimethylaminopyridine (DMAP) coupling reaction in dimethylformamide (DMF) followed by the second deprotection of t-BOC with TFA to yield PEAD. The chemical structure was characterized using a Mercury 400 NMR (Varian, Palo Alto, CA) and a Nicolet IR-100 spectrometer (Thermo Fisher Scientific, Waltham, IL).

#### Gel permeation chromatography (GPC) analysis

The molecular weights of PEAD and heparin (Alfa Aesar, Ward Hill, MA) were measured with a PL-GPC 50 Plus- RI equipped with a PD 2020 light scattering detector (Varian, MA). For PEAD, two MesoPore 300x7.5 mm columns and 0.1% of LiBr in DMF were used as the stationary phase and mobile phase respectively. For heparin, the PL aquagel OH-40 and PL aquagel OH-30 columns were used as the stationary phase and the buffer solution containing 0.2 M NaNO<sub>3</sub> and 0.01 M NaH<sub>2</sub>PO<sub>4</sub>, pH 7 was used as the mobile phase.

### **Zeta potential measurement**

PEAD and heparin solutions were prepared in deionized water at a concentration of 1 mg/ml. 100  $\mu$ l of heparin solution was titrated with PEAD solution. 750  $\mu$ l of water was added to dilute the complex before the measurements were taken. Zeta potentials were measured by a Zetasizer Nano Z (Malvern, Westborough, MA). The results were reported as mean with  $\pm$  deviation for 30 measurements. The same instrument was used to measure and compare the hydrodynamic diameter of [heparin:FGF2] and [PEAD:heparin:FGF2] by dynamic light scattering.

### **Dimethylmethylene blue assay**

Dimethylmethylene blue (DMB) was used for quantification of sulfated glycosaminoglycans according to published protocols [114,115]. Briefly, 20  $\mu$ l of heparin solution (1 mg/ml) was mixed with different volumes of PEAD solution (1 mg/ml). Deionized water was added to the complex solution to reach a final volume of 220  $\mu$ l. After a 5 min centrifugation at 12,100 g, 50  $\mu$ l of supernatant was added to DMB working solution containing 10.7  $\mu$ g of 1,9-dimethylmethylene blue chloride (Polysciences, Warrington, PA) in 55 mM formic acid. The absorbance at 520 nm was determined by a SynergyMX plate reader (Biotek, Winooski, VT). A series of heparin solutions of known concentrations were used as standards to calculate the concentration of heparin in the supernatant.

The amount of PEAD in the supernatant was quantified by an anionic dye, orange II (Acros Organics, Geel, Belgium) [116]. Briefly, 50  $\mu$ l supernatant was added to 20  $\mu$ l orange II solution (1mM) and gently agitated for 10 min. After centrifugation at 12,100 g for 5 min, 50  $\mu$ l was used for absorption measurement at 484 nm. A series of PEAD solutions of known concentrations were used as standards to calculate the concentration of PEAD in the supernatant.

## **Scanning electron microscopy (SEM)**

The SEM samples were prepared by mixing PEAD with heparin (mass ratio of PEAD to heparin: 5) to form the complex. The complex was dropped on an aluminum stub, lyophilized, sputtered with gold and viewed with a Leo 1530 SEM (10 kV, 3 nm spot size) (Carl Zeiss SMT, Peabody, MA).

## **Growth factor loading efficiency**

The loading efficiency of FGF2 was determined by an indirect enzyme-linked immunosorbent assay (ELISA). Briefly, 100 ng of bolus FGF2 or [PEAD:heparin:FGF2] was added to a 96-well plate and left overnight to allow protein adsorption. After blocking by bovine serum albumin (BSA), a rabbit anti-FGF2 polyclonal antibody (PeproTech, Rocky Hill, NJ) was used for recognition followed by a secondary antibody, goat anti-rabbit IgG HRP (Sigma-Aldrich, St. Louis, MO) and then a chromagen substrate, 3,3',5,5'-tetramethylbenzidine (TMB) (Promega, Madison, WI). The absorbance at 450 nm was recorded by a SynergyMX plate reader (Biotek, Winooski, VT). The loading efficiency of NGF was determined by a sandwich ELISA using a commercial kit, NGF E<sub>max</sub><sup>®</sup> ImmunoAssay Systems (Promega, Madison, WI). Briefly, an anti-NGF polyclonal antibody was coated on a 96-well plate. After blocking by BSA, [PEAD:heparin:FGF2] was added for incubation, followed by the recognition of an anti-NGF monoclonal antibody and an anti-rat IgG HRP.

## **Growth factor release profile**

FGF2 and NGF were labeled with <sup>125</sup>I. Briefly, 100 µl of FGF2 (0.1 mg/ml) or NGF (0.2 mg/ml) was transferred to a Pierce Iodination Tube (Thermo Fisher Scientific, Waltham, IL). 15-20 µl of carrier-free Na<sup>125</sup>I (PerkinElmer, Waltham, MA) was added to the tube, and the reaction

proceeded for 2 min. The crude reaction mixture was purified by size exclusion chromatography and the product was stored at -20 °C.

The controlled delivery matrix was formed by combining 100 ng of growth factor with 0.1 ng of <sup>125</sup>I labeled growth factor to 10 µl of heparin (10 mg/ml) followed by the addition of 50 µl of PEAD solution (10 mg/ml). The solution was gently mixed and centrifuged at 12,100 g for 5 min. After removal of the supernatant, 500 µl of 0.9% saline was added to cover the pellet. At predetermined time points (day 1, 4, 7, 14, 19, 28, 33 and 42), the supernatant was collected and replaced with fresh saline. The radioactivity of the collected supernatant was measured by a Packard Cobra II Gamma Counter (PerkinElmer, Waltham, MA) to determine the amount of the released growth factor.

### **FGF2 bioactivity**

FGF2 bioactivity was determined by its stimulatory effects on the proliferation of human aortic endothelial cells (HAECs). Briefly, HAECs were cultured on a 24-well plate with MCDB 131 medium (Mediatech, Manassas, VA) supplemented with 10% fetal bovine serum (FBS), 1% L-glutamine and 50 µg/ml ascorbic acid. A cell culture insert (BD Biosciences, San Jose, CA) with 1.0 µm pores was placed in each well. 100 ng of FGF2 (PeproTech, Rocky Hill, NJ) alone or [PEAD:heparin:FGF2] was added on the insert. Two control groups were applied in the study: (1) basal medium: medium without supplemental growth factors, and (2) Endothelial cell (EC) culture supplement: medium containing 1 ng/ml epithelial growth factor (EGF), 2 ng/ml FGF2, 2 ng/ml insulin-like growth factor-1 (IGF1), 1 ng/ml vascular endothelial growth factor (VEGF) and 1 µg/ml hydrocortisone as provided by the supplier of HAECs (Sigma-Aldrich, St. Louis, MO). After culturing for 4 days, the proliferation of HAEC was determined by a CyQuant Cell Proliferation Assay (Invitrogen, Carlsbad, CA). All results were normalized to the basal medium group.

## **NGF bioactivity**

NGF bioactivity was determined by its ability to stimulate neuronal differentiation of PC-12 cells. [117] PC-12 cells were maintained in Dulbecco's Modified Eagle Medium (DMEM) (Mediatech, Manassas, VA) supplemented with 1.0% horse serum (HS) and 0.5% FBS. Delivery vehicle [PEAD:heparin], bolus NGF (Promega, Madison, WI), NGF stabilized by heparin [heparin:NGF] or delivery matrix [PEAD:heparin:NGF] was added to the cell culture insert. The controls were basal medium without NGF and bolus NGF. All NGF groups contained 10 ng of NGF. On day 4 and day 7, five fields were randomly selected and the phase contrast images were acquired using an inverted microscope Eclipse Ti (Nikon, Melville, NY) equipped with a RETIGA-SRV digital camera (QImaging, BC, Canada). The neurite lengths were measured using NIH ImageJ software version 1.42. The average length of the ten longest neurites was reported with standard deviation.

## **Statistical analysis**

ANOVA followed by post-hoc Bonferroni test was used to analyze the data for the bioactivity of FGF2 and NGF. Data is presented as mean  $\pm$  standard deviations. \*  $p$  value < 0.05; \*\*  $p$  value < 0.01.

### **3.2.3 Results**

#### **Zeta potential measurement of [PEAD:heparin] complex**

PEAD was synthesized by polycondensation of aspartic acid and ethylene glycol diglycidyl ether (EGDE), followed by the conjugation of arginine which provided positive charges

to the polymer. PEAD has two cationic groups (amine and guanidine) per repeating unit, thus it interacts strongly with heparin, the most negatively charged natural polymer, through Coulombic forces. We observed that heparin solution became turbid upon addition of PEAD as the negative charge of heparin was neutralized (Fig. 11). The highest turbidity was reached with a PEAD to heparin mass ratio of 5, indicating that the [PEAD:heparin] complex is likely neutral at this ratio. We used zeta potential titration to analyze the charge of the complex. The zeta potential of the complexes shifted from -45 mV at a mass ratio of 1, to neutral at the mass ratio close to 5 and to +23.2 mV at a ratio of 10 (Fig. 12). The zeta potential at the plateau (+23.2 mV) was similar to that of pure PEAD (+23.1 mV), suggesting that the complex was completely saturated with PEAD. The titration revealed that at a PEAD to heparin mass ratio close to 5 (molar ratio of 3.4), PEAD completely neutralized the negative charges of heparin. Because the binding between PEAD and heparin is based on ionic interaction, we also observed that ionic strength of the delivery matrix solution affected the binding between PEAD and heparin. When PEAD and heparin were mixed in 10-fold saline (9 % NaCl<sub>(aq)</sub>), no coacervate was observed by the naked eye. We can therefore conclude that ionic interaction is the major force between PEAD and heparin.

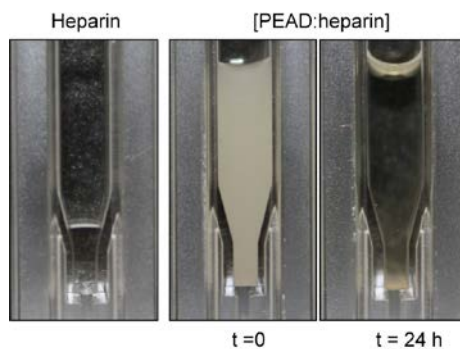


**Figure 11.** Macroscopic observation of [PEAD:heparin] complex. Both heparin and PEAD have excellent solubility in aqueous solution. Addition of PEAD into heparin solution neutralized the negative charge of heparin and formed insoluble [PEAD:heparin] coacervate. The complex settled down to the bottom after 24 h.

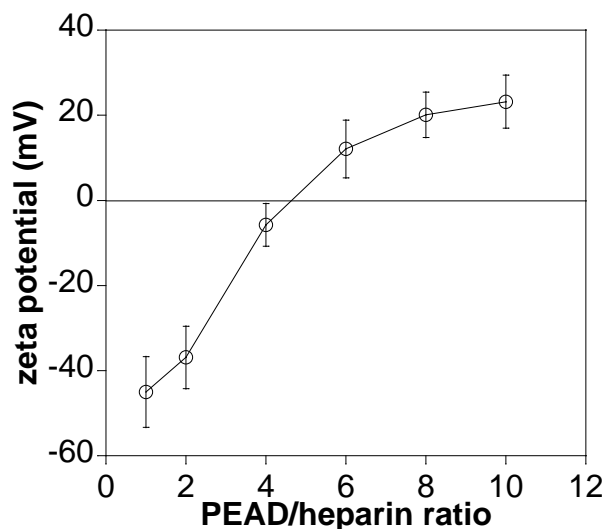


**Figure 12.** Binding of PEAD to heparin monitored by zeta potential titration. The [PEAD:heparin] complex reached isoelectric point at a PEAD:heparin mass ratio close to 5 (molar ratio 3.4). Over-titration with PEAD gave the complex excessive positive charge that leveled off at +23.2 mV at a mass ratio of 10. Data represent the average and the standard deviation of 30 measurements.

### DMB binding assay of [PEAD:heparin] complex

The ionic interaction of PEAD and heparin decreased their solubility in water and the polymers formed a coacervate. We calculated the binding affinity between PEAD and heparin by measuring the amount of each left in the supernatant. Heparin quantification was performed using a heparin binding dye, dimethylmethylene blue (DMB). The results suggest that the amount of heparin in the supernatant decreased gradually with the addition of PEAD (Fig. 13). Maximum binding of heparin, 98.7%, was reached with a PEAD to heparin mass ratio of 5. Similarly, using an anionic dye, orange II, we quantified the amount of PEAD in the supernatant at a mass ratio of 5 to be 5.0%.

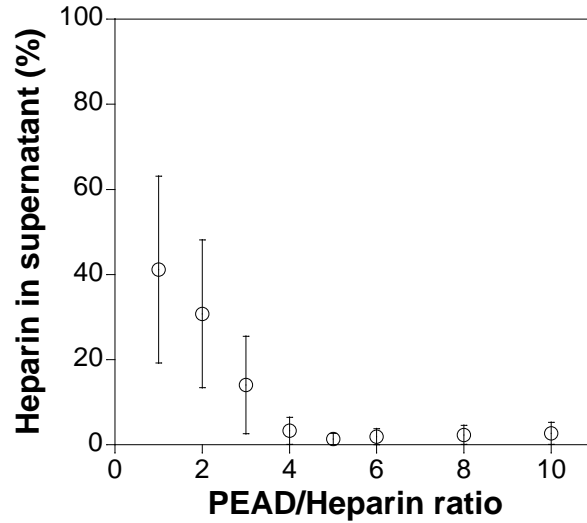
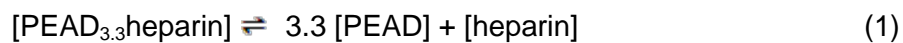


**Figure 13.** Binding of PEAD to heparin as monitored by DMB assay. The amount of heparin in the solution phase decreased as PEAD was added until maximal binding at a PEAD:heparin mass ratio of 5 where only 1.33% of heparin was left in the supernatant. At ratios greater than 5, excessive positive charge on the complex likely caused a slight reduction in coacervation. Data represent an average of four independent assays.

According to the GPC analysis, the weight-average molecular weight ( $M_w$ ) of PEAD is 30,330 Da (PDI = 2.28) and that of heparin is 20,700 Da (PDI = 1.20). These values and the amount of PEAD, heparin, and [PEAD:heparin] complex was used to calculate the stoichiometry of [PEAD:heparin]. The result revealed that approximately 3.3 PEAD molecules bind to 1 heparin molecule. The dissociation constant ( $K_d$ ) of PEAD and heparin was  $1.55 \times 10^{-10}$  as calculated according to the following equations:



$$K_d = \frac{[\text{PEAD}]^{3.3}[\text{heparin}]}{[\text{PEAD}_{3.3}\text{heparin}]} \quad (2)$$

## SEM of [PEAD:heparin] complex

We examined the morphology of [PEAD:heparin] complex using scanning electron microscopy (SEM). The micrographs revealed that a neutral [PEAD:heparin] complex was largely composed of ribbon-like structures with globular domains of various sizes dispersed throughout the matrix (Fig. 14a). The diameters of the ribbons ranged from nanometers to micrometers. The globules might originate from heparin as the micrograph of heparin showed mainly beads with diameters below 1 $\mu$ m (Fig. 14c). On the other hand, the ribbon-like morphology was likely generated by PEAD (Fig. 14d). Dynamic light scattering measurement revealed that [heparin:FGF2] has a hydrodynamic diameter of 181.9 nm with a polydispersity index of 0.478. Addition of PEAD significantly increased the diameter to 540.8 nm with a polydispersity index of 0.489.

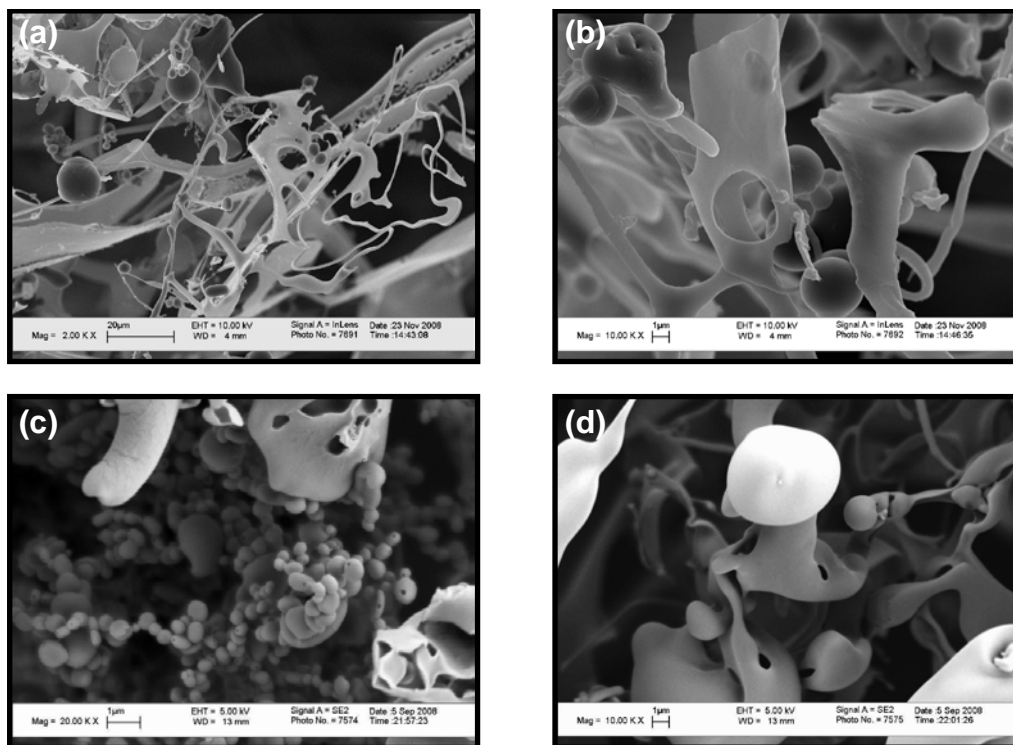


**Figure 14.** Scanning electron micrographs of the [PEAD:heparin] complex at (a) Low magnification (2,000 X) and (b) High magnification (10,000 X). The complex consists of ribbon-

like structure and beads with diameters ranging from nanometers to a few microns. (c) Heparin contains beads with diameters in the sub-micron range (20,000 X). (d) PEAD contains mostly ribbon-like structures (10,000 X).

### **Growth factor loading efficiency of [PEAD:heparin] complex**

Loading efficiency is another critical parameter of effective growth factor delivery. We examined growth factor loading efficiency of [PEAD:heparin] by ELISA. Less than 0.01% of FGF2 was detected in the supernatant by an anti-FGF2 polyclonal antibody. Similarly, less than 0.02% of NGF was detected in the supernatant. This data indicates that [PEAD:heparin] can incorporate more than 99% of FGF2 and NGF.

### **Release of growth factors bound to [PEAD:heparin]**

To investigate the release rate of the incorporated growth factors from the delivery vehicle we determined the release profiles of [PEAD:heparin]-bound growth factors by measuring the radioactivity of the supernatant. FGF2 release showed an initial burst of approximately 10% after one day (Fig. 15a). Thereafter, the release was nearly linear and sustained through the end of the 42-day experiment. At day 42, [PEAD:heparin:FGF2] complex still contained about 60% of FGF2. As expected, NGF showed a faster release profile due to its lower affinity for heparin. The initial burst released almost 20%, followed by a sustained release for 20 days (Fig. 15b). At day 20, [PEAD:heparin:NGF] complex still contained approximately 30% of NGF and the coacervate was radioactive. The residual NGF could be bound too tightly to [PEAD:heparin] and unable to be released by simple diffusion, however the remaining growth factor may be released if exposed to enzymes such as heparinase or esterase. Overall, the release profile of each growth factor reflected its respective heparin-binding affinity. The initial burst is likely caused by loosely adsorbed growth factors and growth factors physically trapped

in the delivery vehicle. This could be avoided, in part, by washing the delivery matrix immediately after its formation.

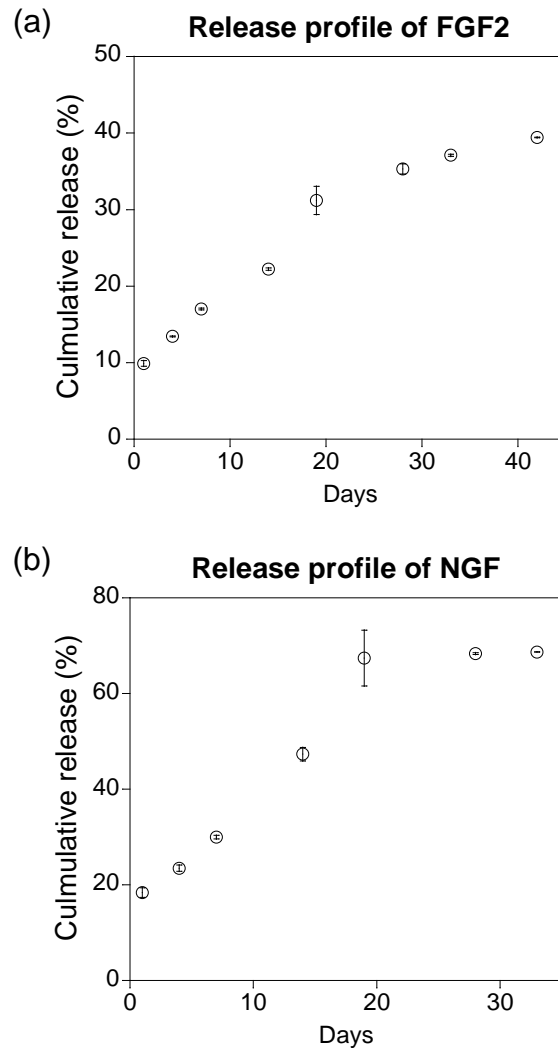


**Figure 15.** Release profiles of growth factors bound to [PEAD:heparin] indicating that [PEAD:heparin] complex can control the release of the incorporated growth factors. (a) FGF-2: The initial burst (~10%) was limited to day 1 only. Thereafter the release was nearly linear and lasted for at least 42 days. (b) NGF: The initial burst was approximately 20% and the steady release was sustained for 20 days, at which point it reached a plateau. The remaining NGF may be too tightly bound to [PEAD:heparin], making it difficult to be released by simple diffusion under the test conditions. The quicker release of NGF compared to FGF-2 matches its weaker affinity for heparin.

## Bioactivity of FGF2 delivered by [PEAD:heparin]

The most important feature of a growth factor delivery vehicle is its ability to maintain the bioactivity of its bound growth factors. We tested the ability of [PEAD:heparin] to maintain the bioactivity of FGF2 and NGF, chosen because of their high and low heparin affinities; the  $K_d$  values for FGF2 and NGF are 2.0 and 600 nM, respectively [118]. To evaluate FGF2 bioactivity, we compared the proliferation of human aortic endothelial cells (HAECs) cultured in basal medium, medium supplemented with manufacturer-supplied EC culture supplement, medium with bolus FGF2, and medium with [PEAD:heparin:FGF2]. After 4 days of culture, bolus FGF2 and [PEAD:heparin:FGF2] promoted higher proliferation than the basal medium and EC culture supplement groups (Fig. 16). Cell proliferation in the presence of [PEAD:heparin:FGF2] was 2.69 times higher than that of the basal medium and 1.26 times higher than that of EC culture supplement. There was no statistical difference between cell proliferation for bolus FGF2 and [PEAD:heparin:FGF2], suggesting that FGF2 bioactivity was well preserved in the delivery matrix.

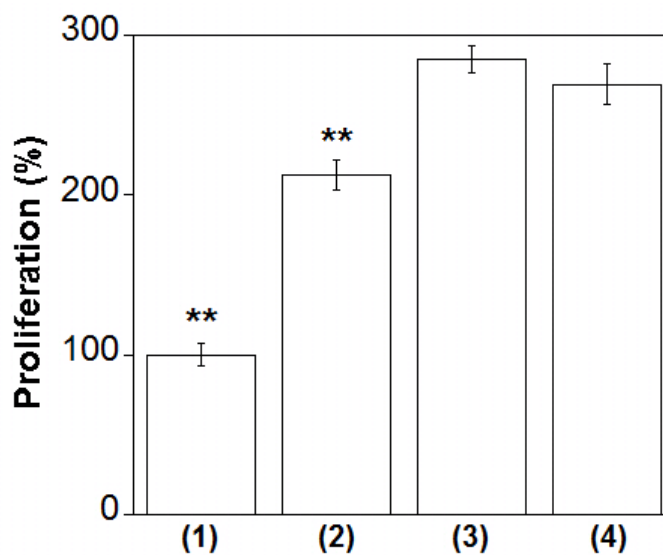


**Figure 16.** HAEC proliferation under different culture conditions: 1. basal medium, 2. EC culture supplement, 3. bolus FGF-2, and 4. [PEAD:heparin:FGF-2]. Data represent the average of 3

independent experiments and standard deviation. \*\* indicates  $p$  value  $< 0.01$  when comparing bolus FGF-2 or [PEAD:heparin:FGF-2] to the controls (groups 1 and 2). For both bolus FGF-2 and [PEAD:heparin:FGF-2], HAECs exhibited significantly higher proliferation after 4 days of culture. There was no statistical difference observed between bolus and [PEAD:heparin:FGF-2] suggesting that the delivery vehicle maintains FGF-2 bioactivity well.

### **Bioactivity of NGF delivered by [PEAD:heparin]**

NGF is known to have a lower heparin affinity than FGF2 [17]. To examine the bioactivity of NGF we chose to use the common and well-established cell line, PC-12. Upon stimulation by NGF, PC-12 cells would start to differentiate into neuron-like cells and begin to extend neurites. Neurite length is widely used as an index to determine NGF bioactivity [18]. This study included five groups: control (neural basal medium without NGF), delivery vehicle [PEAD:heparin], bolus NGF, [heparin:NGF], and [PEAD:heparin: NGF]. After 4 days of culture, all three NGF-containing groups had significantly longer neurites than the control and the delivery vehicle groups which displayed reduced or no neurite extension (Fig. 17a). There was no statistical difference between the control group and the delivery vehicle group. This suggests that the delivery vehicle had no bioactivity. The [heparin:NGF] group showed significantly longer neurite extension than the bolus group. On day 4 there was no statistical difference between [PEAD:heparin:NGF] and the bolus or [heparin:NGF] group. However, after 7 days, there was a statistically significant difference between each group (Fig. 17a, b). For bolus NGF and [heparin:NGF], the neurite lengths decreased between day 4 and day 7, suggesting reduced NGF activity. [PEAD:heparin:NGF], on the contrary, continued to promote differentiation and stimulate neurite extension, increasing average neurite length 2.3 fold from day 4 to day 7 (48  $\mu\text{m}$  to 108  $\mu\text{m}$ ). On day 7, the average neurite length of the [PEAD:heparin:NGF] group was 2.8 times and 3.6 times longer than that of the [heparin:NGF] and bolus group, respectively,

indicating that the [PEAD:heparin] delivery vehicle most effectively maintains and potentiates NGF bioactivity.

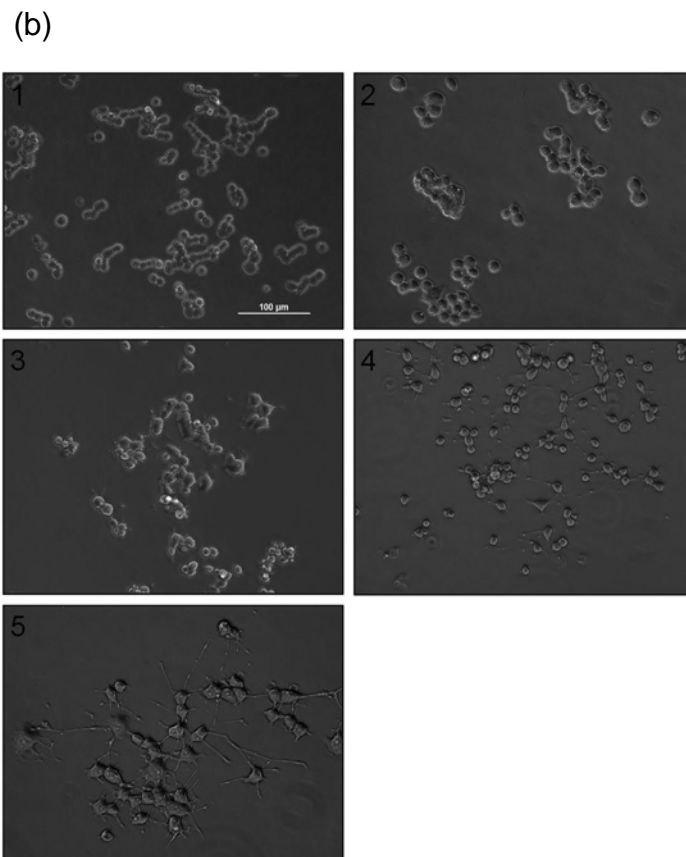
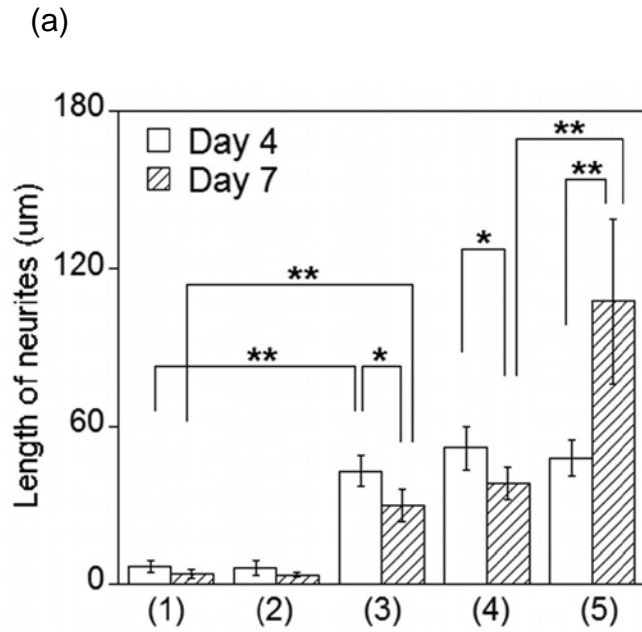


**Figure 17.** PC-12 cell differentiation stimulated by NGF: 1. control, 2. [PEAD:heparin], 3. bolus NGF, 4. [heparin:NGF] and 5. [PEAD:heparin:NGF]. (a) Three independent experiments were

performed. Data represent the average length of the ten longest neurites with standard deviation. \*  $p$  value < 0.05; \*\*  $p$  value < 0.01. At 4 days, [heparin:NGF] and [PEAD:heparin:NGF] showed similar bioactivity and were more effective than bolus NGF, control, and [PEAD:heparin]. However, [PEAD:heparin:NGF] was the only group to exhibit continued extension of neurites beyond day 4. The average neurite length reached 108  $\mu\text{m}$  which was significantly longer than that of either the bolus or [heparin:NGF] group. (b) Phase contrast images of the PC-12 cells at day 7. Only PC-12 cells cultured in the presence of [PEAD:heparin:NGF] fully spread out and generated an extensive network of neurites. Bolus NGF and [heparin:NGF] groups not only exhibited atrophy in neurites, but also cell soma.

### **3.2.4 Discussion**

Growth factor delivery using natural or synthetic materials has great therapeutic potential in biomedicine and biotechnology. In regenerative medicine, controlled release of growth factors has been applied in many applications including angiogenesis [119,120], nerve repair [121,122] and bone and cartilage regeneration [123,124]. Important parameters in growth factor delivery include bioactivity, loading efficiency and controlled release rate. Native growth factors are usually bound to, protected and controlled by the ECM, often through heparan sulfate. Heparin shares a similar structure with heparan sulfate and is widely used in growth factor delivery. However, heparin stabilized growth factors are water soluble and not amenable to controlled release by heparin alone. To solve this problem and improve the efficacy of growth factor

therapy, much research effort has been devoted to mimicking the structure of heparin or immobilizing heparin in order to regulate the distribution of heparin-binding growth factors. For example, Wenk, E. *et al.* decorated silk fibroin with sulfonic acid moieties by a diazonium reaction to mimic natural heparin [125]. Tae, G. *et al.* functionalized heparin with hydroxybenzotriazole and crosslinked with polyethylene glycol (PEG) to form a hydrogel [126]. Nilasaroya, A. *et al.* modified heparin with glycidyl methacrylate then photopolymerized with PEG dimethacrylate [127]. Seal, B. L. *et al.* attached heparin-binding sequences (12 to 17-mer) to PEG arms to conjugate heparin [128]. Similarly, Rajangam, K. *et al.* integrated heparin-binding sequences (15-mer) to immobilize heparin on the surface of self-assembled nanofibers [129]. Johnson, P.J. *et al.* applied a bi-domain chimera containing the heparin-binding sequence (12-mer) to immobilize heparin in the fibrin gel [130]. The advantage of the latter three methods is that heparin was not covalently modified and was able to interact with growth factors directly, thus fully preserving the natural bioactivity of heparin. In the research reported here, a polycation interacts directly with native heparin without modification. The advantages of this approach are that PEAD is easily synthesized and provides a cost-effective platform for intact-heparin-based growth factor delivery. Furthermore, the affinity between PEAD and heparin is extremely high, and thus it is expected to incorporate high amount of heparin-binding growth factors and control their release well. This is complemented with the ability to retain and promote growth factor bioactivity as demonstrated in the *in vitro* assays.

PEAD interacts strongly with heparin and neutralizes its inherent negative charges. This charge neutralization decreases the solubility of individual molecules and induces the formation of a coacervate immediately upon mixing. The coacervate confines the growth factor; furthermore heparin binds the growth factors. These two factors together control the release of the growth factors. We believe that the release kinetics of growth factors bound to [PEAD:heparin] can be tailored by: (i) The amount of heparin used in complex formation. More heparin is expected to slow the release of the growth factor. (ii) The properties of PEAD such as

molecular weight and charge density can alter its interaction with heparin which in turn, modifies the release kinetic of the growth factors. These properties can be easily adjusted during polymer synthesis.

Regarding the bioactivity of growth factors bound to [PEAD:heparin] complex, the results demonstrated that the bioactivity of the growth factors studied was well maintained or even enhanced compared to bolus and heparin-protected growth factors. [PEAD:heparin:FGF2] promoted HAEC proliferation to the same level as bolus FGF2 up to day 4 (Fig. 16). Since the release profile indicates that only 13% of the loaded FGF2 was released during the first 4 days (Fig. 17a), it can be deduced that [PEAD:heparin:FGF2] is able to prolong the activity of FGF2 compared to the bolus form. The neurite outgrowth study using PC-12 cells further supports this conclusion, showing a substantial increase in average neurite length after 7 days for cells cultured in [PEAD:heparin:NGF] compared to all other groups. The average neurite length for the bolus and [heparin:NGF] groups at day 7 were shorter than those of day 4, indicating that the bioactivity of bolus NGF and [heparin:NGF] could not be sustained over a long period of time.

There are a few possible non-exclusive mechanisms to explain the enhanced bioactivity of NGF by [PEAD:heparin]: (i) [PEAD:heparin] complex incorporates the growth factors in a coacervate and shields them from proteolytic degradation, thereby extending the half life of the growth factor. (ii) The binding of the growth factors to [PEAD:heparin] complex concentrates the growth factors and consequently more growth factors are simultaneously presented to the target cells. (iii) Compared to bolus growth factor or heparin-bound growth factor alone, [PEAD:heparin]-bound growth factor allows for release in a temporally and spatially controlled manner.

[PEAD:heparin] complex also exhibited the ability to release growth factors in a steady fashion (Fig. 15). Furthermore, PEAD has several specific features that enhance its usefulness in growth factor delivery: (i) Because of its high biocompatibility and the high affinity between

heparin and many growth factors, it is possible to deliver greater amounts of heparin-binding growth factors if clinically necessary. (ii) The charge density of PEAD can be adjusted easily by changing the molar ratio of arginine used in conjugation. It is highly possible that the charge density would affect the interaction between PEAD and heparin and therefore alter the release kinetics of growth factors. This will be investigated more thoroughly in future experiments. (iii) The assembly of PEAD, heparin and growth factors is performed in an aqueous solution, thus the bioactivity of the growth factor is better maintained than approaches that require organic solvents. (iv) [PEAD:heparin:growth factors] are injectable suspensions allowing for minimally invasive administration.

### **3.2.5 Summary**

This study investigates a new growth factor delivery vehicle formed by self assembly of a polycation and heparin. The association of growth factors, native heparin, and PEAD in an aqueous buffer is expected to maximize the interactions between heparin and the growth factors. We have demonstrated that [PEAD:heparin] complex can load heparin-binding growth factors with high efficiency, control their release in a steady manner and maintain or enhance their bioactivity. Furthermore, the polycation is easily synthesized and cost effective compared to existing delivery strategies which utilize the entire heparin-binding domain. The results suggest that this delivery vehicle warrants extensive further investigations.

#### **4.0 THERAPEUTIC ANGIOGENESIS VIA FGF2 COACERVATE**

Therapeutic angiogenesis via growth factor delivery has potential in treatment of many human diseases, especially cardiovascular-related. However, due to the insufficient bioactivity of the delivered factors, the nascent blood vessels usually do not have enough stability and regress over time. Here, the ability of [PEAD:heparin] coacervates to deliver an angiogenic factor was examined in two in vivo models.

## **4.1 IN VIVO ANGIOGENIC ACTIVITY OF FGF2 COACERVATE**

FGF2, a potent angiogenic factor, has the ability to induce the proliferation of endothelial cells, similar to vascular endothelial growth factor. In addition, FGF2 has ability to stimulate mural cells to associate and stabilize the endothelial tubes. We anticipate that if the bioactivity of FGF2 is well preserved, mature blood vessels will be generated even at low dosage of applied FGF2. In a rodent model, FGF2 containing coacervate was subcutaneously injected and long term angiogenesis was monitored. For comparison, the hemoglobin concentration at the injection site was measured. The expression of associated markers was evaluated to determine the maturity of neovasculature. It was expected that the [PEAD:heparin] coacervate can effectively enhance the bioactivity of FGF2.

### **4.1.1 Introduction**

Angiogenesis is a physiological process involving the formation of nascent vasculature from existing blood vessels. The complex interactions between endothelial cells and mural cells including vascular smooth muscle cells and pericytes are highly coordinated by various signals

[131,132]. Therapeutic angiogenesis is promising in treating many human diseases especially coronary and peripheral ischemia [133,134]. Among various approaches to therapeutic angiogenesis, delivery of growth factors is the most simple and direct because it doesn't need viral vectors in gene therapy or cells in cell therapy. Direct injection of free growth factors failed to demonstrate efficacy in clinical trials [135]. Therefore, appropriate controlled delivery strategy for growth factor is highly desirable and extensively studied. However, loading capacity and long term efficacy still present significant challenges to growth factor delivery.

In the human body, most secretory growth factors are associated with extracellular matrix usually through interactions with glycosaminoglycans. Glycosaminoglycans are negatively charged linear polysaccharides that can have different composition, function and distribution in the body [136]. Together with other extracellular matrix molecules, glycosaminoglycans provide a substratum for cell attachment [137]. Furthermore, their interaction with growth factors is critical in many biological processes such as development [138,139] and cancer progression [140,141]. Heparin and heparan sulfate are well studied glycosaminoglycans for their high affinity to a variety of growth factors including heparin-binding epidermal growth factor (HB-EGF), fibroblast growth factor (FGF) and vascular endothelial growth factor (VEGF) families [142]. Heparin can modulate the conformation of the growth factors [143,144], protect them from proteolytic cleavage [145] and potentiate their bioactivity [146]. Incorporation of heparin in a delivery vehicle is therefore a promising approach to preserve the bioactivity of the delivered growth factors [147,148].

The FGF family is well known for its high affinity to heparin which modulates the interaction between FGFs and their receptors. As revealed by the crystal structure, the heavily anionic heparin brings the cationic sequences on FGF and its receptor closely together and stabilizes the ternary complex largely through polyvalent ionic interactions [149]. In order to mimic the interactions between these three components, a synthetic polycation substituted the heparin-binding sequence of the FGF receptor and form a ternary complex containing the

polycation, heparin and FGF. We designed a polycation, poly(ethylene argininylaspartate diglyceride) (PEAD) with excellent biocompatibility to conjugate heparin and a potent angiogenic factor, FGF2 [150,151]. The complex of heparin and FGF2 is soluble in water and not amenable to controlled local delivery. The addition of PEAD neutralized the excess negative charge of heparin and immediately induced the formation of [PEAD:heparin:FGF2] coacervates. This anchors FGF2 and enabled its controlled release. Charge interaction between PEAD and heparin was utilized instead of covalent modification of heparin in an effort to minimize the perturbation of the functions of heparin. As a result, FGF2 released from the coacervate induced much more potent angiogenic responses than free FGF2 in mice: mural cell participation significantly increases and the neo-vasculature is mature and persists to at least 4 weeks.

#### **4.1.2 Experimental section**

##### **Synthesis of PEAD**

PEAD was synthesized in two steps: (1) Ethylene glycol diglycidyl ether and t-BOC protected aspartic acid were polymerized through a polycondensation reaction in 1,4-dioxane under the catalysis of tetra-*n*-butylammonium bromide. The t-BOC protective group was removed by stirring in 1:4 trifluoroacetic acid (TFA):dichloromethane to yield the intermediate, poly(ethylene aspartate glyceride). (2) Conjugation of t-BOC arginine to poly(ethylene aspartate glyceride) was performed by a standard dicyclohexylcarbodiimide/*N*-hydroxysuccinimide coupling reaction in dimethylformamide followed by the removal of t-BOC with TFA to obtain

PEAD. The chemical structure was characterized using an UltraShield Plus 600 NMR (Bruker BioSpin) and a Nicolet iS10 spectrometer (Thermo Fisher Scientific).

### **Delivery vehicle preparation and scanning electron microscopy**

For preparation of the delivery vehicle, PEAD dissolved in deionized water was mixed with heparin solution under constant stirring and the solution immediately became cloudy as the delivery vehicle (empty coacervate) formed. The complex was dropped on an aluminum stub, lyophilized, sputtered with gold, and the morphology was examined by a Jeol 6335 field emission gun SEM (Jeol).

### **Analysis of FGF2 loading efficiency by Western blotting**

PEAD and heparin were each dissolved in normal saline (0.9 % NaCl<sub>(aq)</sub>) to obtain 10 mg/ml solutions. For preparation of the coacervate, 100, 500 ng or 1,000 ng of FGF2 (PeproTech) was first mixed with 10  $\mu$ l of the heparin solution and then 50  $\mu$ l of the PEAD solution. The coacervate was equilibrated at room temperature for 15 min followed by centrifugation at 12,100g for 10 min. The supernatant and the pellet were mixed with the common sample buffer and denatured at 95°C for 5 min. 15 % of sodium dodecyl sulfate polyacrylamide gel electrophoresis (SDS-PAGE) was utilized for separation followed by protein blotting on a polyvinylidene fluoride (PVDF) membrane. A rabbit anti-human FGF2 polyclonal antibody (PeproTech) was applied for recognition followed by a secondary horse peroxidase conjugated anti-rabbit IgG antibody (Sigma). The intensity of the individual band was determined by NIH ImageJ software and compared with that of the FGF2 loading solution.

### **Protection from proteolysis by the coacervate**

Trypsin digestion of FGF2 was evaluated as previously described [152]. Briefly, FGF2 (100 ng) alone, heparin-bound FGF2 (100 µg of heparin and 100 ng of FGF2) or the coacervate (500 µg of PEAD, 100 µg of heparin and 100 ng of FGF2) was incubated with 2 µg of trypsin at 37°C for 30 min or 2 h. The digested solution was mixed with the sample buffer and denatured at 95°C for 5 min. Following the identical method, western blotting was utilized to examine the amount of intact FGF2.

### **Bioactivity of FGF2 in fibrin gel**

The fibrin gel (400 µl) was formed by mixing fibrinogen (4 mg/ml) solution with either 500 ng free FGF2 or the coacervate containing 50 µg PEAD, 10 µg heparin and 500 ng of FGF2, and thrombin in the basal medium. The gel was incubated at 37°C for 30 min and overlaid with 600 µl basal medium. After 24 h incubation, FGF2 in the medium was precipitated by addition of trichloroacetic acid (TCA) and centrifuged at 12,100g for 10 min. Ice-cold acetone was utilized to wash out residual TCA. The pellets were dissolved in sample buffer for SDS-PAGE and western blotting.

Endothelial tube formation was investigated at three FGF2 dosing levels (50, 250, and 500 ng/ml) using fibrin gel assay as described above. HUVECs (Lonza) were maintained in EGM-2 basal medium supplemented with growth factors according to the supplier's instruction. The experimental procedures of tube formation followed a published protocol (19). Briefly,  $8 \times 10^4$  cells (passage 7) were mixed with fibrinogen solution containing FGF2 (50, 250 or 500 ng) or the same amount of FGF2 in the coacervate. After addition of thrombin, the whole solution was gelled at 37°C for 30 min. The gel was last overlaid with 600 µl of the basal medium to provide the basic nutrient. After incubation for 3 days, the phase contrast images were taken by a microscope.

### **Chemotaxis of pericytes induced by coacervate**

Human pericytes were isolated following the established method [153]. For the chemotaxis experiment,  $1.0 \times 10^4$  pericytes (passage 7) were added in Transwell® inserts (pore size of 8  $\mu\text{m}$ ) and placed in a 24-well plate containing blank solution, delivery vehicle, 100 ng of FGF2 or the coacervate having 100 ng of FGF2. After incubation for 12 h, nonmigrating cells were removed with cotton swabs and migrating cells were stained by Quant-iT™ PicoGreen® (Invitrogen). The fluorescent images were taken by an inverted microscope Eclipse Ti (Nikon).

### **Animal care and subcutaneous injection**

Male Balb/cJ mice (Jackson Laboratory) with an average age of 6-7 weeks were used and cared for in compliance with a protocol approved by the Institutional Animal Care and Use Committee of the University of Pittsburgh. Under isoflurane anesthesia, 65  $\mu\text{l}$  of saline, delivery vehicle (500  $\mu\text{g}$  of PEAD and 100  $\mu\text{g}$  of heparin), free FGF2 (500 ng of FGF2) or the coacervate (500  $\mu\text{g}$  of PEAD, 100  $\mu\text{g}$  of heparin and 500 ng of FGF2) was subcutaneously injected in the left back of the mice through a 31G insulin needle. The right back which did not receive injection served as the contralateral control. All groups contained 4 to 8 mice.

### **Hemoglobin quantification**

The animals were sacrificed at post-injection week 1, 2 and 4. The subcutaneous tissue having a dimension of 1.5 cm x 1.5 cm was harvested at the injection site and the contralateral site. The hemoglobin in the harvested tissue was extracted by addition of in 500  $\mu\text{l}$  of the hemolysis buffer containing 17 mM of Tris-HCl (pH 7.4) and 0.75 wt% ammonium chloride and incubation for 24 h. The absorbance at 410 nm corresponding to the hemoglobin Soret band was recorded by a SynergyMX plate reader (Biotek) [154]. All values were normalized to that of the saline injection.

## **Immunofluorescent staining**

The harvested subcutaneous tissue was embedded and frozen in Tissue-Tek OCT compound (Sakura Finetek USA). Sections of 5  $\mu\text{m}$  thickness were cut with a cryo-microtome and stored at  $-80^{\circ}\text{C}$ . For CD31 staining, a rat anti-mouse CD31 monoclonal antibody (BD Biosciences) was applied first followed by a Cy3-conjugated anti-rat IgG antibody (Invitrogen). For  $\alpha$ -SMA staining, a FITC-conjugated anti- $\alpha$ -SMA monoclonal antibody (Sigma) was utilized according to the provided instruction. For PDGFR- $\beta$  staining, a goat anti-mouse PDGFR- $\beta$  polyclonal antibody (R&D Systems) was applied first followed by an Alexa Fluor 488-conjugated anti-goat IgG antibody (Invitrogen). For VWF staining, a FITC-conjugated anti-VWF antibody (US Biological) was used. For desmin staining, a rabbit anti-desmin polyclonal antibody (sigma) was applied first followed by an Alexa Fluor 594-conjugated anti-rabbit IgG antibody (Invitrogen). For calponin staining, a rabbit anti-mouse calponin-1 monoclonal antibody (Millipore) was applied first followed by an Alexa Fluor 594-conjugated anti-rabbit IgG antibody. All slides were last counterstained with DAPI (Invitrogen). The fluorescent images were taken using a Fluoview 500 Confocal microscope (Olympus).

## **Quantitative analysis of immunofluorescent staining**

For quantification of CD31- or  $\alpha$ -SMA-positive cells, six low magnification (200X) fields containing the highest number of CD31- or  $\alpha$ -SMA-positive cells were selected for each group following a previously published criteria [155]. The number of CD31- or  $\alpha$ -SMA-positive cells in the field were counted and confirmed by DAPI-positive nuclei. The value was divided by the area of the tissue and normalized to that of the saline group. For comparison of the number and the size of blood vessels, CD31-positive blood vessels in three low magnification (200X) fields of the free FGF2 or the coacervate group were determined and measured by NIS-Elements software (Nikon).

## Statistical analysis

Student's *t*-test was used for pair comparison between the coacervate and free FGF2 for the chemotaxis experiment or free FGF2 for the in vivo experiment. ANOVA followed by post-hoc Bonferroni test was utilized to compare the number of CD31- and  $\alpha$ -SMA-positive cells between all conditions. Data is presented as mean  $\pm$  standard deviations. \**p* value < 0.05; \*\**p* value < 0.01.

### 4.1.3 Results

#### Interactions between PEAD, heparin and FGF2

This research used poly(ethylene argininylaspartate diglyceride) (PEAD) that consists of aspartic acid, arginine and diglyceride moieties. The amino and guanidine groups were positively charged under physiological conditions and enable PEAD to interact strongly with heparin, the most negatively-charged glycosaminoglycan. This charge interaction was employed to load heparin-binding growth factors into the delivery vehicle. PEAD lowered the solubility of [heparin:FGF2] complex in water by forming a coacervate through charge interactions (Fig. 18). [PEAD:heparin:FGF2] coacervates aggregated over time and settled at the bottom of the vessel as an oil droplet after 24 h of standing. The droplet was easily resuspended by agitation, which returns the solution to the turbid state. Scanning electron microscopy revealed that the

morphology of the [PEAD:heparin:FGF2] mainly consists of globular domains that can fuse with each other to form strands (Fig. 19).



**Figure 18.** The three components dissolve well in water individually as represented here by heparin. Adding FGF2 induces no apparent changes in solubility. Upon addition of PEAD, the solution turns cloudy. Charge neutralization between the polycation and heparin forms the [PEAD:heparin:FGF2] coacervate which is insoluble in the aqueous solution, enabling local delivery of FGF2. Upon standing for 24 h, the coacervate aggregates to the bottom of the tube.

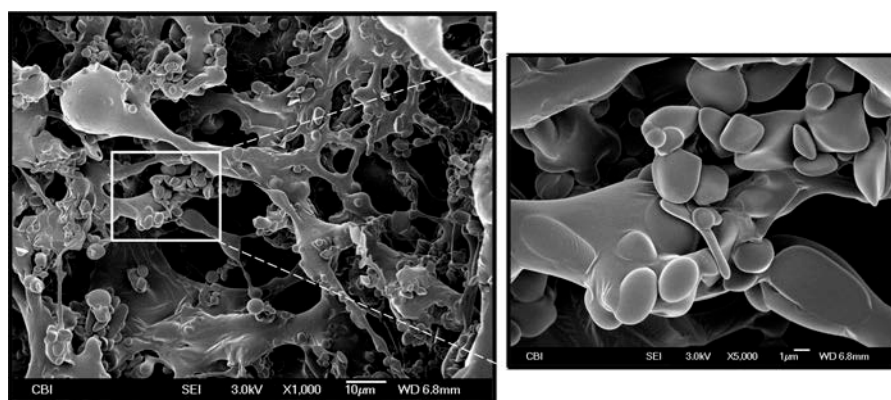


**Figure 19.** SEM micrograph revealed that [PEAD:heparin:FGF2] mainly consisted of globular domains that fuse together. The globular nature of the coacervate is more distinguishable at higher magnification. Scale bars: 10 µm (low magnification) and 1 µm (high magnification).

An effective delivery vehicle should have high loading efficiency in addition to controlled release of the cargo. We tested the loading efficiency of the delivery vehicle by western blot. Following the centrifugation of the coacervate, the amount of FGF2 in the supernatant and the coacervate were compared to the amount in the original loading solution. Comparison of the band intensity of western blot using NIH ImageJ found no FGF2 in the supernatant. Furthermore, the amount of FGF2 in the coacervate when 100, 500, and 1,000 ng of FGF2 was used (Fig. 20) is statistically the same as the loading solution suggesting nearly 100% loading efficiency. We expect the loading efficiency will also be near 100% for higher amount of growth factors because of the large excess of heparin relative to growth factor. We ended the test at 1,000 ng because the subsequent in vivo examination used only 500 ng FGF2.

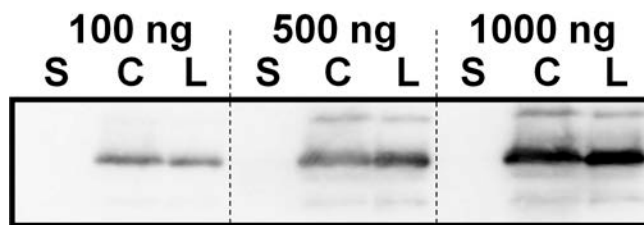


**Figure 20.** The loading efficiency is >95% for FGF2 (500  $\mu$ g PEAD, 100  $\mu$ g heparin, FGF2 range tested: 100 - 1000 ng). Western blot demonstrated that the intensity of the coacervate and the loading solution is the same. S: FGF2 in the supernatant after centrifugation. C: FGF2 in the settled coacervates. L: total amount of FGF2 in the loading solution.

Most free growth factors degrade quickly in vivo; therefore bolus injection has very low efficacy. Because heparin can protect growth factors from proteolytic cleavage, we examined if heparin in the coacervate retains its protective capability. When treated with a broad spectrum protease, trypsin, all free FGF2 was degraded within 0.5 h (Fig. 21, column I). On the other hand, heparin protected FGF2 from trypsin digestion (Fig. 21, column II) and so did the

coacervate (Fig. 20, column III). An average of 86.1% of FGF2 was present in the coacervate 2 h after trypsin treatment demonstrating that heparin retained its protective effect.

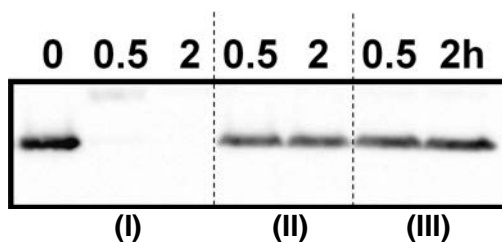


**Figure 21.** Protection from proteolysis by the coacervate. FGF2 and trypsin (mass ratio 1:200) was incubated for 30 min or 2 h at 37°C. The results indicated that free FGF2 (I) was completely degraded within 0.5 h. On the other hand, heparin (II) and the coacervate (III) protected FGF2 from degradation for at least 2h.

In order to examine the ability of the coacervate to localize FGF2 in the tissue, we used fibrin gel to mimic the *in vivo* environment. The gel was overlaid with medium and the amount of FGF2 in the medium was determined after 24 h by western blotting. A significantly lower amount of FGF2 was detected in the medium of the coacervate group indicating that the coacervate can effectively localize FGF2 (Fig. 22). To investigate potential endothelial response to FGF2 released from the coacervate, human umbilical vein endothelial cells (HUVECs) were embedded in the fibrin gel as previously described [156]. Different concentrations of FGF2 were tested for their ability to induce tube formation. After three days, free FGF2 did not induce tube formation at any concentration (Fig 23). Most cells were round with a few spread-out cells scattered throughout the gel. On the other hand, HUVECs in the coacervate groups formed a clearly visible network of nascent endothelial tubes at 250 and 500 FGF2 ng/ml FGF2. This indicated that the FGF2 coacervate may induce more potent localized angiogenesis *in vivo* than free FGF2.

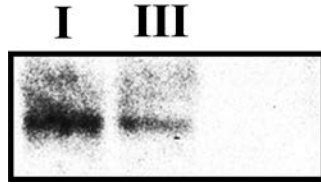


**Figure 22.** The coacervate localized FGF2 release in fibrin gel. Fibrin gels were prepared with free FGF2 or FGF2-containing coacervate. The amount of FGF2 in the medium was determined by western blot. Less FGF2 was present in the medium of the coacervate group suggesting that FGF2 was localized better in the fibrin gel than the free FGF2 group.

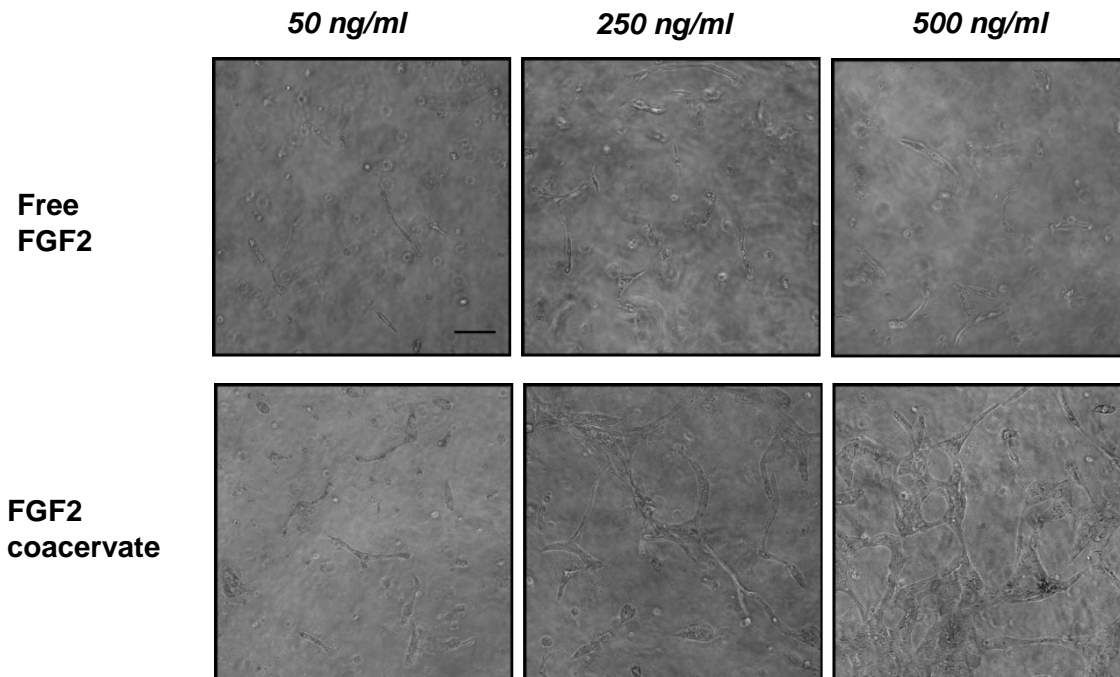


**Figure 23.** Endothelial tube formation in fibrin gels. HUVECs mixed with free FGF2 (50, 250 or 500 ng/ml) or the same amount of FGF2 in the coacervate were encapsulated in the fibrin gel. After incubation of 3 days, the coacervate induced extensive tube network formation at 250 and 500 ng/ml of FGF2. On the contrary, FGF2 alone induced sparse tube formation at all growth factor concentrations. Scale bar: 100  $\mu$ m.

The bioactivity of FGF2 was further examined by using mural cells that are important in the stabilization of blood vessels. Pericytes are actively involved in early angiogenesis, and their recruitment is critical to stabilize the newly formed vessels. Chemotaxis assays using pericytes revealed that both free FGF2 and the coacervate had higher chemotactic activities than the control groups which were basal medium and the delivery vehicle. More importantly, pair-wise comparison between the coacervate and free FGF2 yielded a  $p$ -value lower than 0.05 revealing a higher chemotactic activity of FGF2 released from the coacervate (Fig. 24).

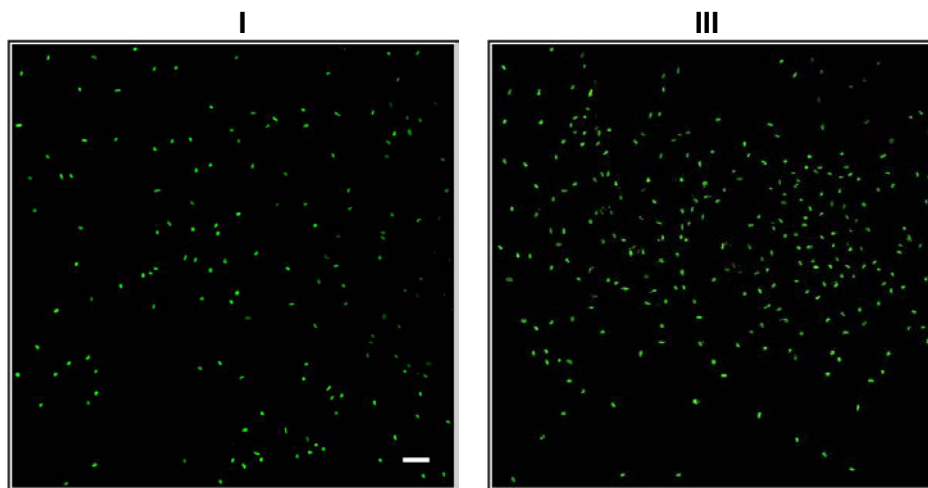


**Figure 24.** Chemotaxis of pericytes by the coacervate. After incubation for 12 h, migrated pericytes were stained by PicoGreen. Quantitative comparison suggested that the coacervate induced significantly higher extent of chemotaxis than free FGF2 ( $254 \pm 44$  vs.  $108 \pm 14$  per  $\text{mm}^2$ ,  $p < 0.05$ , Student's  $t$ -test). Scale bar: 100  $\mu\text{m}$ .

### **[PEAD:Heparin:FGF2] promotes more potent angiogenesis than free FGF2**

In order to examine the *in vivo* efficacy of the coacervate, the coacervate containing 500 ng of FGF2 was injected subcutaneously in the back of male BALB/cJ mice and compared its angiogenic capability to that of saline, delivery vehicle and 500 ng of free FGF2 respectively (Fig. 25). Macroscopic observation of the coacervate group revealed extensive formation of

blood vessels at the injection site whereas the contralateral site showed no difference from normal tissue (Fig. 26). Hematoxylin and eosin staining revealed that the gross appearance of the saline and delivery vehicle groups are indistinguishable suggesting the delivery vehicle itself had no angiogenic effect (Fig. 27). Free FGF2 induced aggregation of nucleated cells, but few blood vessels were identified. On the contrary, the coacervate showed significant blood vessel formation with closed circles of nucleated cells surrounded by muscle bundles (arrow). The lumen of vessel was filled with red cells further supporting the function of the nascent blood vessels.

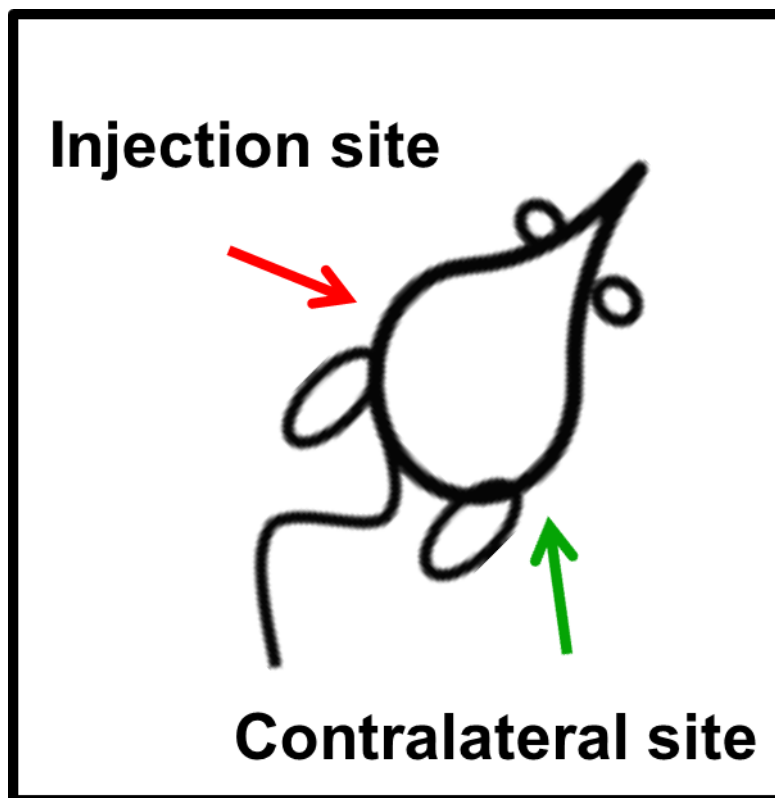


**Figure 25.** Subcutaneous injection of FGF2 coacervate

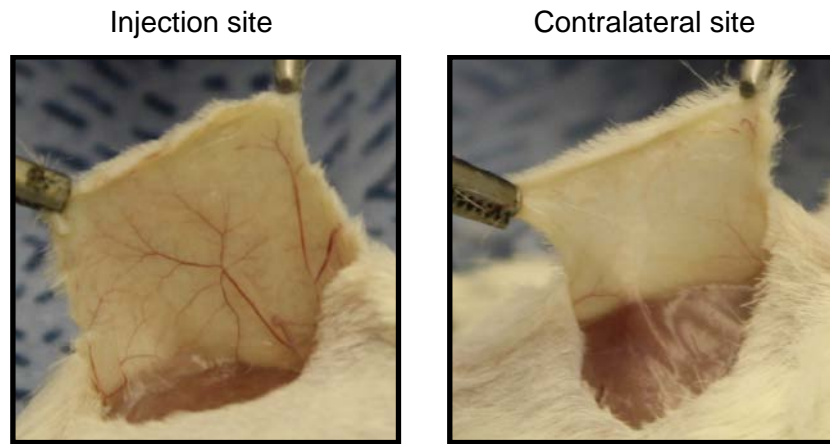


**Figure 26.** Macroscopic observation of subcutaneous tissue showed that the coacervate clearly induced new blood vessel formation at the injection site (2-week pictures from the same mouse).

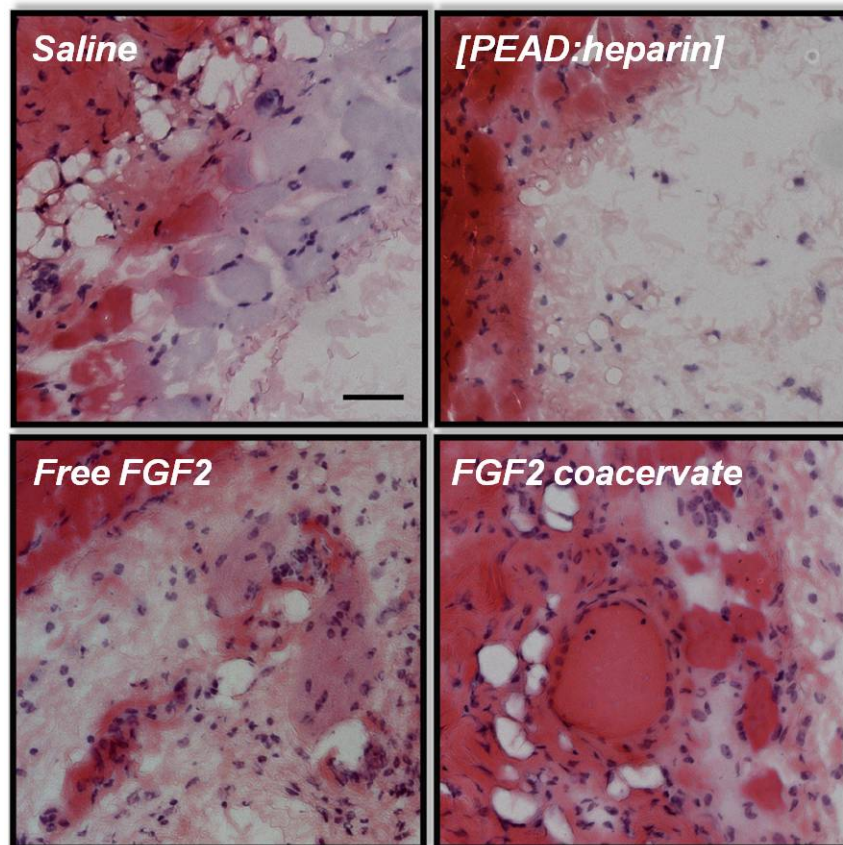


**Fig 27.** Hematoxylin and eosin staining of subcutaneous tissues after 4 weeks. For the saline, delivery vehicle and free FGF2 groups, there were no clear growth of vasculature in the

subcutaneous region. The coacervate group, on the contrary, revealed the feature of blood vessel which had a closed inner layer of nucleated cells surrounded by smooth muscle bundles (arrow). Scale bar: 50  $\mu\text{m}$ .

As an indirect measure of blood vessel density, the amount of hemoglobin in the tissue at the injection site at 1, 2, and 4 week post-injection was quantified using a previously published method [157]. All the groups had no significant difference at week 1. The coacervate group had higher amounts of hemoglobin than any other groups at week 2 and 4 (Fig. 28). On the other hand, bolus injection of free FGF2 showed no statistical difference in hemoglobin content from saline and delivery vehicle groups at any time point. After 4 weeks, the coacervate group still exhibited a significantly higher amount of hemoglobin than all control groups suggesting the long term stability of the newly formed blood vessels and the bioactivity of FGF2 released from the coacervate. The ratio of hemoglobin at the injection and contralateral site revealed that angiogenic responses were spatially controlled for the coacervate whereas the free FGF2 group showed no difference (Fig. 29). This correlated well with the macroscopic observation that the angiogenic activity of the coacervate was localized at the injection site. For the free FGF2 group, the ratio was close to 1 at every time point and was significantly lower than that of the coacervate after 2 weeks. This combined with the insignificant change of hemoglobin from saline control suggested that bolus injection of 500 ng FGF2 had little angiogenic potency. Overall, the histological examination demonstrated the high efficacy of the coacervate in promoting angiogenesis and the spatial control of FGF2 release from the coacervate.

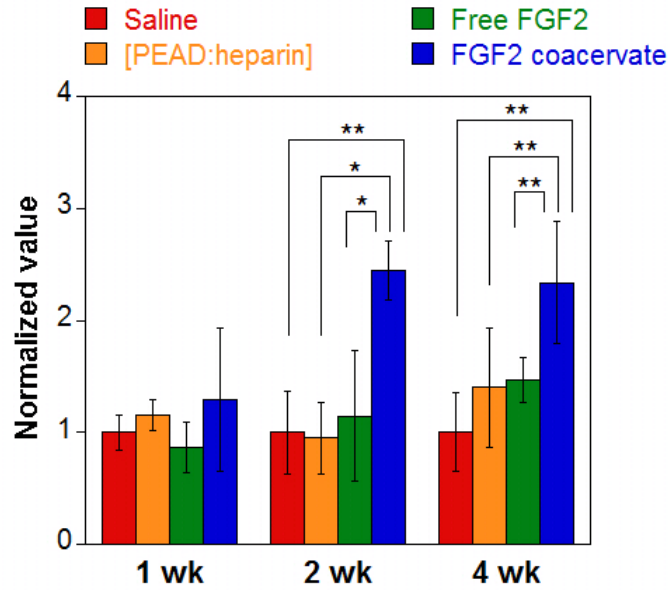


**Fig 28.** Hemoglobin quantification compared the extent of angiogenesis between different groups. The result suggested that the coacervate group had a higher amount of hemoglobin 2 weeks post-injection whereas free FGF2 did not have statistical difference between the saline and delivery vehicle groups. This difference lasted at least for 4 weeks. (mean± s.d.,  $n=4-8$  for each condition) Normalized to the saline group. One-way ANOVA followed by Bonferroni correction was applied for multiple comparisons. \* $p<0.05$ , \*\*  $p<0.01$ .

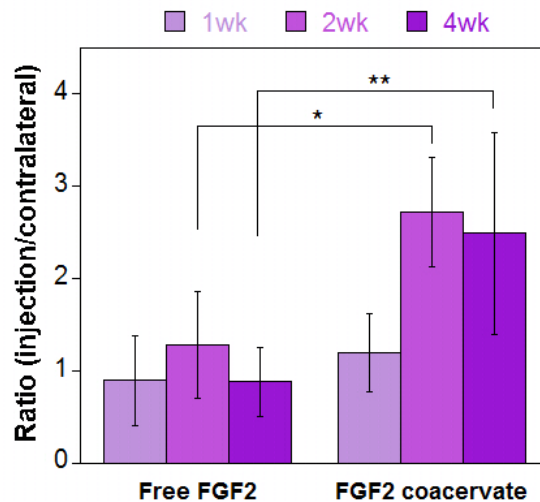


**Figure 29.** The ratio of hemoglobin at the injection sites and the contralateral sites. For the coacervate, the ratio was significantly higher than that of the free FGF2 group. The result

explained that FGF2 was well localized at the injection site by the delivery vehicle. Student's *t*-test was used as a statistical tool. \* $p < 0.05$ , \*\*  $p < 0.01$ .

### **[PEAD:Heparin:FGF2] stimulates proliferation of endothelial and mural cells**

The more potent angiogenesis induced by the coacervate warranted further study on the effects of the released FGF2 on cell functions. Two specific markers closely associated with angiogenesis was utilized: CD31 for endothelial cells and  $\alpha$ -smooth muscle actin ( $\alpha$ -SMA) for mural cells (pericytes or smooth muscle cells). Both the coacervate and free FGF2 promoted more endothelial cells (CD31-positive) than saline and the delivery vehicle qualitatively 1 week post-injection, (Fig. 30). This was attributed to the proliferation of endothelial cells stimulated by FGF2. On the other hand, only a small number of mural cells ( $\alpha$ -SMA-positive) were present in all groups. After 2 weeks, higher number of endothelial cells can still be found at the presence of the coacervate and free FGF2. However, the coacervate also induced a significant amount of mural cells. More importantly, the blood vessels in the coacervate group were well organized into circles of endothelial cells surrounded by mural cells. This difference was even more pronounced after 4 weeks. Compared to the coacervate, the other three groups were similar in that most endothelial cells lacked support by mural cells. Higher magnifications of the vessels in the coacervate group showed distinctive structure of blood vessels with aligned endothelial cells closely associated and surrounded by mural cells (Fig. 31).

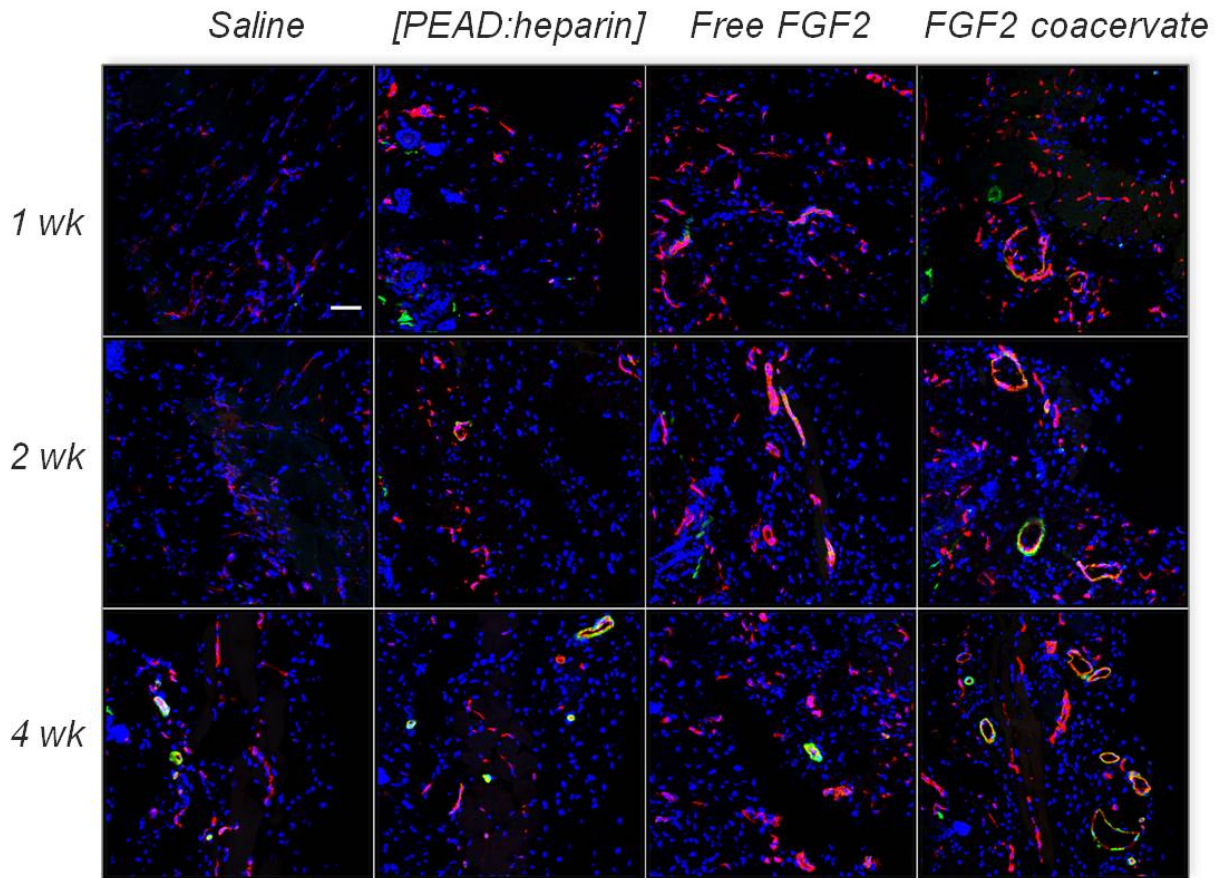


**Figure 30.** Representative confocal micrographs showed the distribution of blood-vessel associated markers CD31 (endothelial cell, red) and  $\alpha$ -SMA (mural cell, green) of each group at three time points. Both the free and coacervate FGF2 groups revealed a higher quantity of endothelial cells than saline control after 1 week, but only the coacervate induced an increase of  $\alpha$ -SMA expression after 2 weeks. The circular vessel-like structures were observed in the field. After 4 weeks, more endothelial and mural cells were present in the coacervate group demonstrating the long term efficacy of the FGF2 coacervate. Scale bar: 50  $\mu$ m.

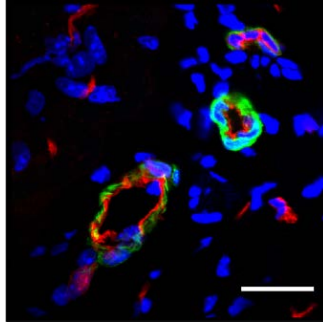


**Figure 31.** High magnification revealed the maturation of the blood vessels induced by the coacervate. The endothelial tubes were clearly surrounded by mural cells. Scale bar: 50  $\mu\text{m}$ .

Quantification of the endothelial and mural cells was consistent with higher angiogenic potency of the coacervate. Six low magnification (200x) fields for each group were chosen to quantify the number of endothelial and mural cells. The result suggested that the coacervate increased the number of endothelial cells by 120%, 95% and 47% relative to that of the saline, delivery vehicle and free FGF2 (Fig. 32). All the comparisons were statistically significant with  $p$  values lower than 0.01 supporting the coacervate induced more proliferation of endothelial cells. The free FGF2 group had more CD31-positive cells than the saline group ( $p < 0.01$ ); whereas the delivery vehicle group showed no difference from the saline group ( $p = 0.81$ ) revealing that the delivery vehicle itself had little effect to the proliferation of endothelial cells. More striking difference was the number of mural cells. Significant amount of mural cells were observed in the coacervate group. The quantification of mural cells demonstrated that the coacervate group was 6.71, 3.39 and 2.02 folds higher than that of the saline, delivery vehicle and free FGF2 groups respectively ( $p < 0.01$  for all comparison). Again, the free FGF2 group induced more mural cells than saline ( $p < 0.05$ ), but the delivery vehicle had no difference from saline ( $p = 0.89$ ).

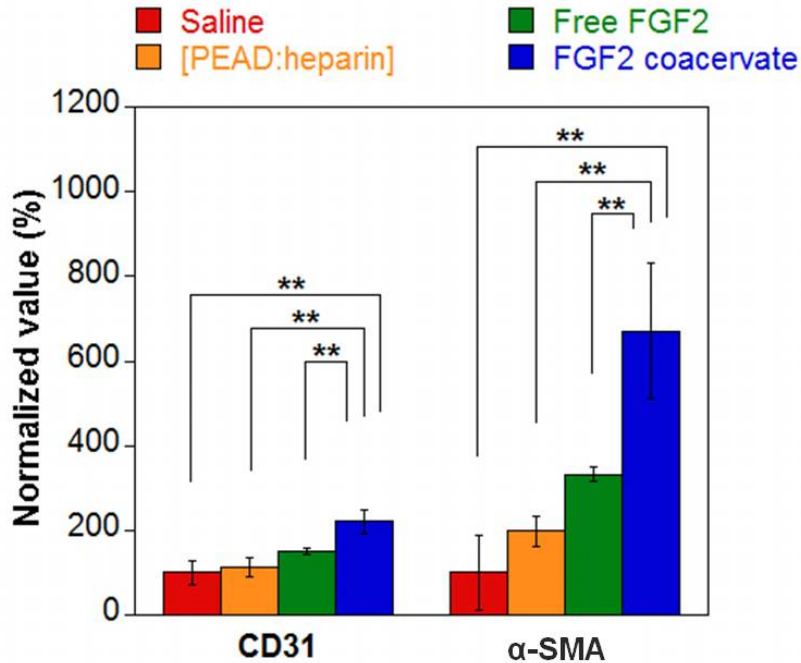


**Figure 32.** Comparison of CD31 and  $\alpha$ -SMA expression in the 4 injected groups. The number of endothelial cells in the coacervate group was higher than those of the control groups by 47% to 120%. More significantly, the number of mural cells in the coacervate group was 2.02 folds of that in the free FGF2 group. One-way ANOVA followed by Bonferroni correction, \* $p < 0.05$ ; \*\* $p < 0.01$ .

Furthermore, the number and the size of the blood vessels in free FGF2 and coacervate groups was compared by counting CD31-positive blood vessels and measuring their area according to a previously published procedure [158]. The average number of blood vessels in the coacervate group was higher than that of the free FGF2 group ( $63.5 \pm 3.6$  vs.  $46.0 \pm 7.7$  per  $\text{mm}^2$ ,  $p < 0.05$ ) (Fig. 33). This is consistent with the above data that showed the coacervate group induced more vascular cell proliferation and the injection site contains more hemoglobin (Figs. 28, 29). Comparison of the size of the blood vessels revealed that the coacervate group had more blood vessels per  $\text{mm}^2$  for all three size groups including  $< 400 \mu\text{m}^2$  ( $34.1$  vs.  $28.6$ ),  $400$ - $1,000 \mu\text{m}^2$  ( $20.6$  vs.  $15.9$ ) and  $> 1,000 \mu\text{m}^2$  ( $8.7$  vs.  $1.6$ ). It is worth noting that blood vessels with

areas larger than  $1,000 \mu\text{m}^2$  all had abundant  $\alpha$ -SMA expression and are likely arterioles and venules. Collectively, the immunohistochemical analysis strongly supported higher angiogenic potency of the FGF2 coacervate.

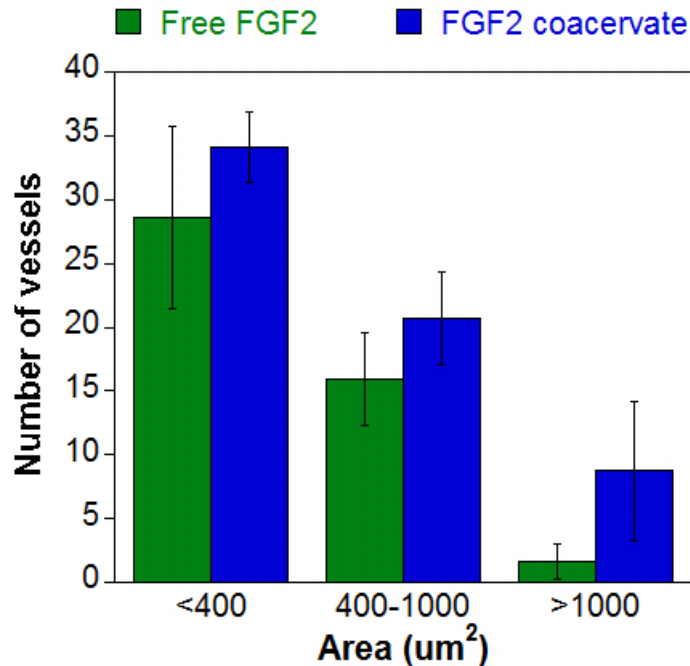


**Figure 33.** Comparison of the number of blood vessels in a given size range between free and coacervate FGF2 groups as previously described; the value represents the cumulative number of all the slides examined (24). The coacervate induced more blood vessel formation than free FGF2. Furthermore, the coacervate group contained more large vessels ( $>1,000\mu\text{m}^2$ , likely associated with arterioles and venules).

### **[PEAD:Heparin:FGF2] coacervate promotes neovasculature maturation by recruiting mural cells**

The maturity of newly formed blood vessels is critical for their stability and function. Thus, we studied the maturation of neovasculature induced by the coacervate from early to late stages of angiogenesis. For the early angiogenic process, CD31 was co-stained with a pericyte

specific marker, platelet derived growth factor receptor- $\beta$  (PDGFR- $\beta$ ) [159]. The result observed many CD31-positive endothelial cells clustered with PDGFR- $\beta$ -positive cells in the coacervate group 1 week post-injection (Fig. 34). On the contrary, no association of pericytes and endothelial cells was observed in the free FGF2 group. This difference again demonstrated the efficacy of the coacervate in maintaining the bioactivity of FGF2.

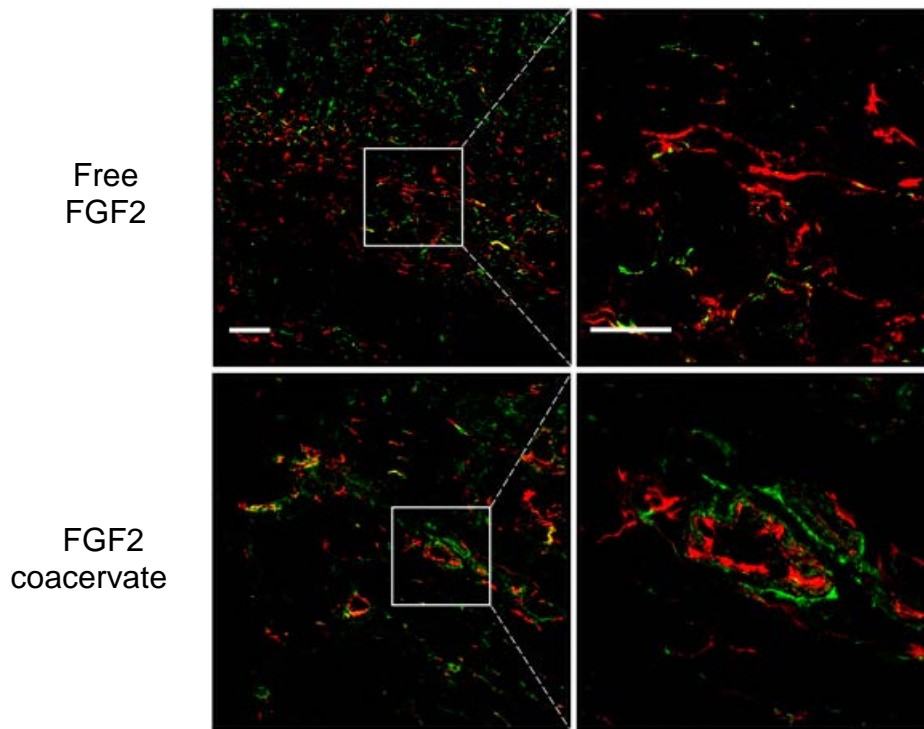


**Figure 34.** The co-localization of CD31-positive and PDGFR- $\beta$ -positive cells suggested the coacervate quickly recruited pericytes to interact with endothelial cells in the nascent vessels. This phenomenon was absent in the free FGF2 group. Scale bar: 50  $\mu$ m.

For long term vessel maturity, the markers associated with vascular functions were examined. Von Willebrand factor (VWF), an important protein involved in hemostasis was stained to show the potential of the nascent blood vessels to participate in hemostasis. It was found that the coacervate induced strong expression of VWF (Fig. 35). The overlap of CD31

and VWF signals indicated that the nascent endothelial cells were functional. Desmin, a component of intermediate filament expressed in mural cells is a widely used marker to study perivascular structure. Desmin was observed to co-express in  $\alpha$ -SMA-positive blood vessels (Fig. 36). Additionally,  $\alpha$ -SMA-negative but desmin-positive blood vessels were also found in the field. This likely reflected the distribution of vessel sizes and the heterogeneity of pericytes which had low  $\alpha$ -SMA expression at capillary levels [160]. Calponin mediate contractile responses of vascular smooth muscle cells; and we co-stained this important marker with  $\alpha$ -SMA to evaluate the functionality of nascent blood vessels. The result showed again that more and larger blood vessels were induced by the coacervate than by free FGF2 (Fig. 37). Overall, the results of immunohistochemical analysis demonstrated that more mature vasculature was induced by the coacervate, which correlated well with the higher local hemoglobin concentration at the injection site.

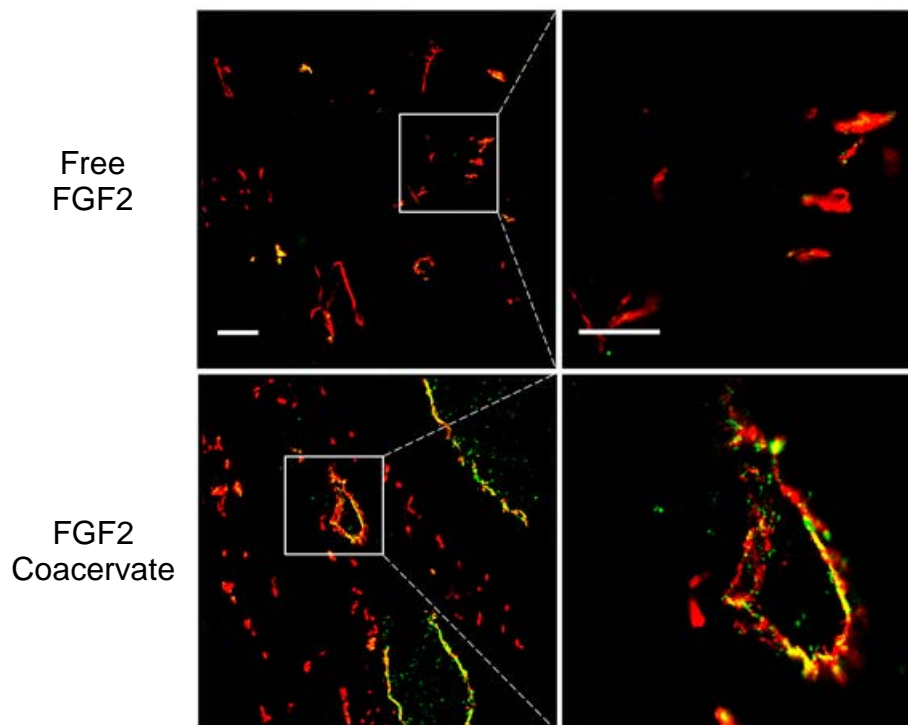


**Figure 35.** Significant co-localization (green + red = yellow) of VWF- and CD31-positive cells suggested that the endothelial cells in the nascent vessels can potentially participate in hemostasis. Scale bar: 50  $\mu$ m.

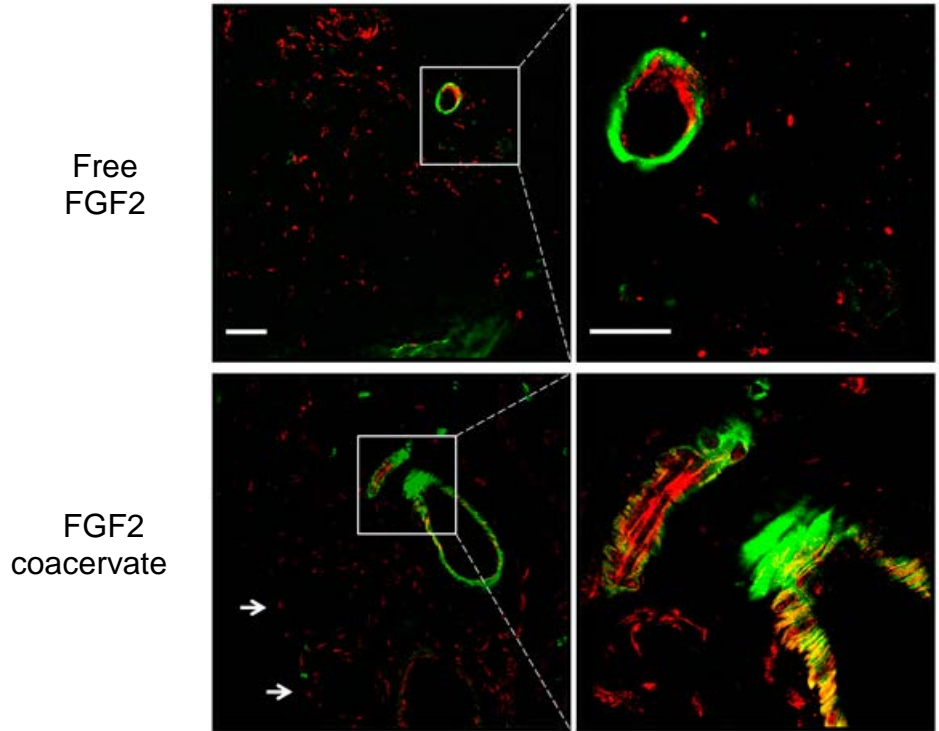


**Figure 36.** Both  $\alpha$ -SMA and desmin are markers for mural cells. Their expression pattern revealed that larger vessels co-expressed these markers whereas smaller vessels were dominated by the expression of desmin (arrows). Scale bar: 50  $\mu$ m.

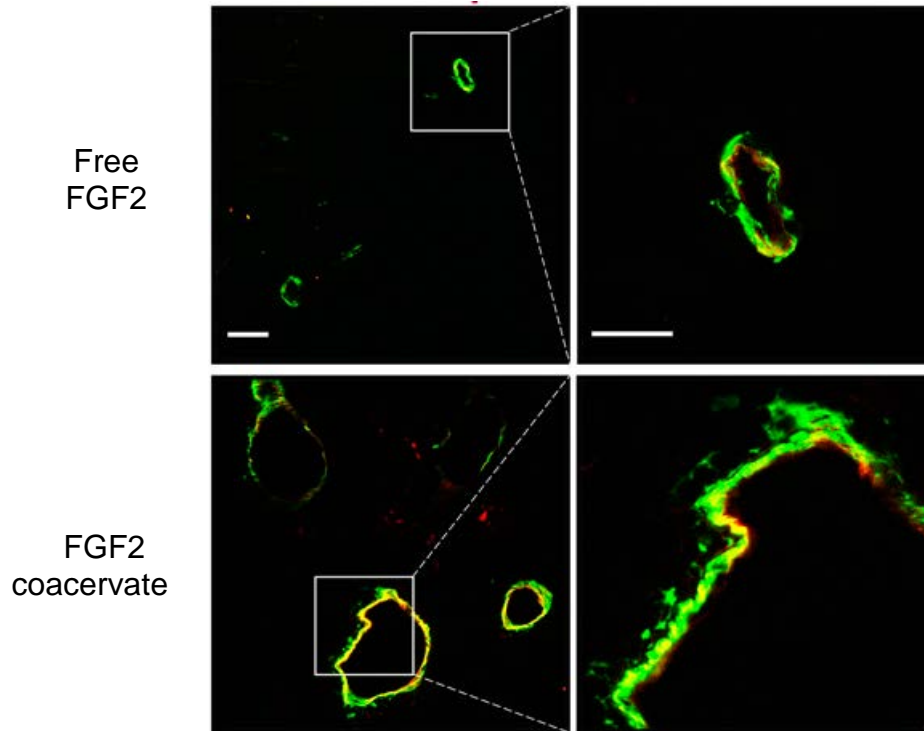


**Figure 37.** Calponin, a calmodulin associated with vascular smooth muscle cells contraction, was co-stained with  $\alpha$ -SMA to examine the potential functionality of the new blood vessels. The result indicated that the blood vessels in the coacervate group had abundant expression of calponin. In addition, the blood vessels were much larger in the coacervate group than those in the free FGF2 group. Scale bars: 50  $\mu$ m.

#### 4.1.4 Discussion

The goal is to develop an injectable platform that is easily administered even in a basic clinic. Thus, a coacervate was formed by simple mixing of three water soluble components: a

biocompatible polycation, heparin and a heparin-binding growth factor. The resultant coacervate has very low viscosity and is injectable via a 31 G needle (outer diameter: 0.26 mm) or a catheter. The loading efficiency of FGF2 is nearly 100% according to the results of both ELISA and western blot [151]. The coacervate delivery platform is highly effective with a low dosage of 500 ng FGF2. In many test results reported here, there are insignificant differences between free FGF2, saline, and the delivery vehicle. The 500 ng dosage is much lower than what is commonly used in the literature. The injectability combined with high loading efficiency and efficacy of the coacervate may enable new opportunities of growth factor treatment for certain diseases such as cardiac infarct where only a small volume can be injected and wound must be minimal.

Therapeutic angiogenesis via exogenous growth factors including FGF2, VEGF and PDGF has been examined extensively to treat human ischemic diseases [161,162] that resulted in huge progress in understanding of growth factor signaling and its interaction with the host. However, there has yet to be a clear demonstration of clinical benefits [135]. Typically, the treatment group showed improvement at the early stage but had no significant difference from the placebos in long term observation [163]. This has been attributed to the lack of stability of the nascent blood vessels. Current approach to solve this challenge is co-delivery of multiple growth factors to boost the long term stability of the neovasculature [164,165]. Often, a growth factor can stimulate a range of cells to accomplish physiological events such as embryonic development, angiogenesis, vasculogenesis, and wound healing [166,167,168]. FGF2 binding to FGF receptors dimerizes the receptors, activates their tyrosine kinases and triggers the downstream signaling pathways [169]. For endothelial cells, FGF2 is a potent mediator that can promote their proliferation, migration, differentiation and stimulate the expression of VEGF to initiate angiogenesis [170]. In addition, FGF2 can recruit pericytes to newly formed blood vessels [171] and promote the survival and proliferation of vascular smooth muscle cells [172]. Both pericytes and smooth muscle cells substantially enhance the stability of the

neovasculature. Consequently, mature vasculature is achievable if the bioactivity of FGF2 is well maintained. The challenge is that the delivery system must maintain the bioactivity of the growth factors and release them with appropriate spatiotemporal control. By designing the delivery system de novo, we developed a coacervate that maintained the bioactivity of FGF2 well and enabled formation of mature vasculature with the controlled release of a single growth factor.

#### **4.1.5 Summary**

The current study evaluates the angiogenic activity of a heparin-based coacervate using a rodent model. Only one injection of the coacervate is required for sustained angiogenesis. Furthermore, the blood vessels formed are mature and stable to at least 4 weeks. The FGF2 coacervate has a much higher angiogenic efficacy than free FGF2. Further investigations include the effectiveness of this platform in ischemic animal models and in vivo imaging of the blood vessels to monitor flow and potential vasoresponsiveness. Because the polyvalent charge interaction is critical to the formation and stability of the coacervate, we expect efficient control of growth factor release by tailoring charges and size of PEAD as we demonstrated in a related polycation [96]. It is expected this new delivery platform will be useful in the controlled release of many heparin-binding growth factors that control important biological functions.

## **4.2 POST-MYOCARDIAL INFARCTION ANGIOGENESIS BY FGF2 COACERVATE**

As demonstrated in the previous section, [PEAD:heparin] coacervate enhances angiogenic activity of FGF2 and induces neovasculature with substantial maturity. The results are promising; however, healthy animals have normal physiological activities and do not reflect the pathological environment. Consequently, I decided to investigate the utility of coacervate in ischemic animals. I chose a mouse myocardial infarction model because it is well established and widely adopted. It closely mimics human heart attack and can better verdict the usefulness of this novel platform clinically.

### **4.2.1 Introduction**

Myocardial infarction (MI) characterized by permanent blockage of coronary artery is the leading cause of death in developed countries. MI results in several physiological consequences, including ischemia, inflammation, fibrosis and loss of cardiomyocytes, which collectively compromise the contractile capability of heart. Ischemia is the most serious outcome because without sufficient blood supply the remaining cardiomyocytes would dye and the

overload would cause heart failure eventually. Consequently, promoting angiogenesis is expected to be an effective treatment in protecting remaining cardiomyocytes. FGF2-containing coacervate was applied in a disease model that mimics the human MI (Fig. 38). Single injection of saline, delivery vehicle (500  $\mu$ g of PEAD and 100  $\mu$ g of heparin), free FGF2 (500 ng of FGF2) or FGF2 coacervate (500  $\mu$ g of PEAD, 100  $\mu$ g of heparin and 500 ng of FGF2) was compared to evaluate the efficacy of the coacervate-delivered FGF2. Histological analysis included hematoxylin and eosin staining for gross observation and Masson's trichrome staining for fibrosis. Both staining provided valuable information about the area of infarction. Additionally, CD31,  $\alpha$ -SMA and VWF staining were utilized to stain endothelial cells and mural cells to determine the extent of angiogenesis. Functional recovery measured by echocardiography gave a comprehensive evaluation to conclude the effectiveness of FGF2 coacervate in the ischemic heart disease.

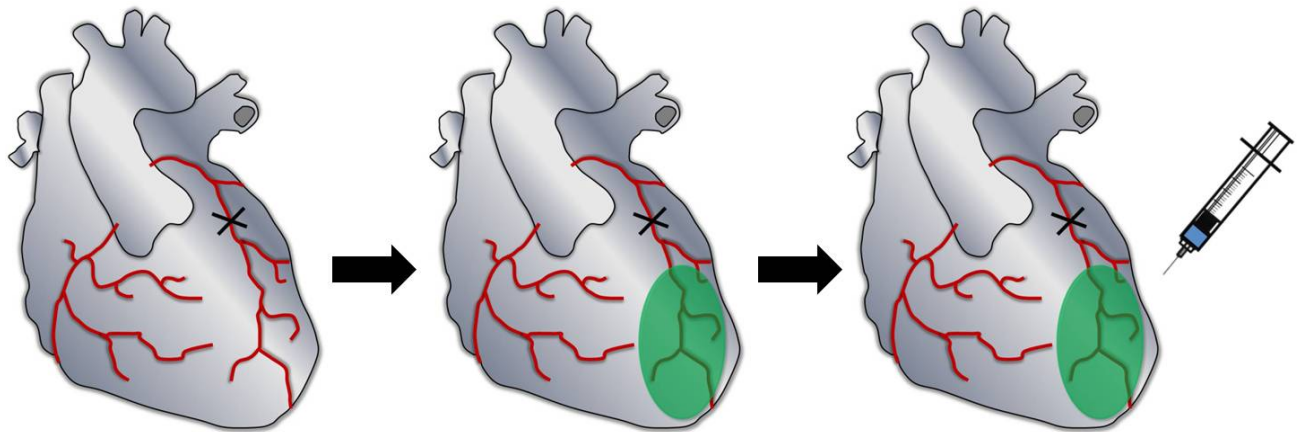


**Figure. 38** Mouse acute MI model. Left anterior descending artery is ligated to induce myocardial infarction in BALB/cJ mice. FGF2-containing coacervates or control solutions are injected within 5 minutes.

## 4.2.2 Experimental section

### Acute myocardial infarction model

The surgical procedures utilized to induce MI are briefly described below. 10-week-old BALB/cJ mice were intubated with a catheter for mechanical ventilation with an anesthetic gas mixture using a small animal ventilator. The left thoracic cavity was opened with an incision through the fourth intercostal space. The ribs and overlying muscle were separated and retracted with 5-0 silk sutures on each side of the incision. For creation of MI injury in the anterior wall of the left ventricle, the pericardium was cut to expose the heart, and the left anterior descending coronary artery was permanently ligated with an 8-0 Prolene suture. Within 5 min, solution was injected with an insulin syringe equipped with a 30G needle into the center of the infarct and in the peri-infarct region (Fig. 38). A successful injection into the myocardium can be determined visually under a surgical microscope by the marked change in color (pink to grey) and the formation of a gentle bump underneath the epicardium of the injection site. Once the injection was complete, the chest was closed in three layers (rib-intercostal space, overlying muscle, and skin) with 4-0 Vicryl absorbable sutures. Each mouse was observed post-operation until it had recovered from the anesthesia before returning to the animal holding room.

After 6 weeks, each mouse was euthanized with a deep anesthesia of isoflurane followed by tail vein injection of 1M KCl for diastolic arrest of the heart. It was important to arrest the heart in diastole because the geometry of the left ventricle needs to be preserved to accurately determine the area of the engraftment and dimensions of the LV for histological assessment. The heart was harvested and frozen in liquid nitrogen for histological and immunofluorescent examination.

## **Echocardiography**

Echocardiograms were utilized to assess LV dimensions and systolic function at 2 time points (2 weeks and 6 weeks), as previously described [173]. Two-dimensional images were obtained at the midpapillary muscle level. Left ventricular end-diastolic area (EDA) and end-systolic area (ESA) were measured from short-axis images of the LV, and both LV end-diastolic dimension (EDD) and end-systolic dimension (ESD) were measured from at least 6 consecutive beats via M-mode tracing. To measure LV contractility, fractional area change (FAC) was calculated as  $FAC(\%) = [(EDA - ESA) / EDA] \times 100$ .

## **Immunofluorescent staining**

The harvested subcutaneous tissue was embedded and frozen in Tissue-Tek OCT compound (Sakura Finetek USA). Sections of 8  $\mu\text{m}$  thickness were cut with a cryo-microtome and stored at  $-80^{\circ}\text{C}$ . For CD31 staining, a rat anti-mouse CD31 monoclonal antibody (BD Biosciences) was applied first followed by a Cy3-conjugated anti-rat IgG antibody (Invitrogen). For  $\alpha$ -SMA staining, a FITC-conjugated anti- $\alpha$ -SMA monoclonal antibody (Sigma) was utilized according to the provided instruction. For VWF staining, a FITC-conjugated anti-VWF antibody (US Biological) was used. All slides were last counterstained with DAPI (Invitrogen). The fluorescent images were taken using a Fluoview 500 confocal microscope (Olympus).

### 4.2.3 Results and discussion

#### FGF2 coacervate preserved ventricular function revealed by echocardiography

Our prior study (section 3.1) indicated that 500 ng of FGF2 delivered by [PEAD:heparin] induced significant angiogenesis and generated mature vessels. To examine its effect in ischemic heart diseases, identical amount of FGF2 coacervate was applied in an acute myocardial infarction model. In this model, the left anterior artery was ligated to create infarction followed by intramyocardial injection of FGF2 coacervate (n=6). The controls were saline (n=7), delivery vehicle (n=5) and free FGF2 (n=7). After 2 weeks, echocardiographic assessment observed the highest mean EDA ( $17.8 \pm 2.0 \text{mm}^2$ ) and ESA ( $12.5 \pm 1.6 \text{mm}^2$ ) in the saline group (Fig. 39). ANOVA-Tukey's HSD test showed that both values were significantly higher than those of the healthy controls (baseline). It suggested successful induction of MI leading to heart dilation. Statistically lower FAC ( $29.5 \pm 4.2\%$ ) of the saline group also pointed out that the contractile function was compromised. For the remaining groups, the FGF2 coacervate group had a mean ESA ( $9.1 \pm 1.6 \text{mm}^2$ ) and EDA ( $15.6 \pm 2.5 \text{mm}^2$ ) values lower than those of the delivery vehicle group (ESA  $12.3 \pm 1.3 \text{mm}^2$ ; EDA  $17.2 \pm 1.2 \text{mm}^2$ ) and the free FGF2 group (ESA  $12.8 \pm 1.9 \text{mm}^2$ ; EDA  $19.2 \pm 1.7 \text{mm}^2$ ). Furthermore, the FAC of the FGF2 coacervate group being  $41.8 \pm 3.7\%$  was higher than those of the delivery vehicle group ( $28.6 \pm 3.2\%$ ) and the free FGF2 group ( $33.2 \pm 7.0\%$ ). Pairwise comparison of ESA, EDA and FAC between the free FGF2 and the FGF2 coacervate groups all have *p* values lower than 0.01. Consequently, echocardiographic assessment concluded that FGF2 coacervate preserved better left ventricular function than free FGF2 2 weeks post-infarction.

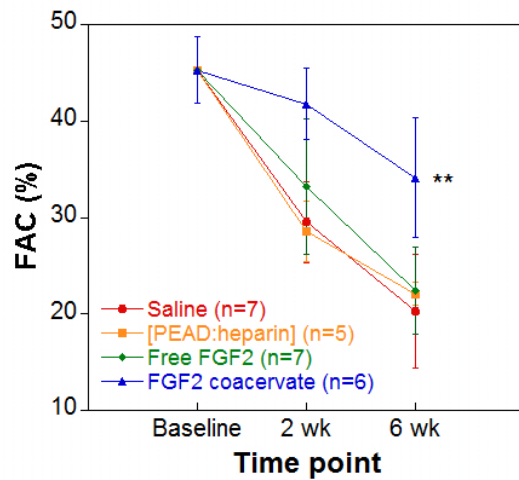
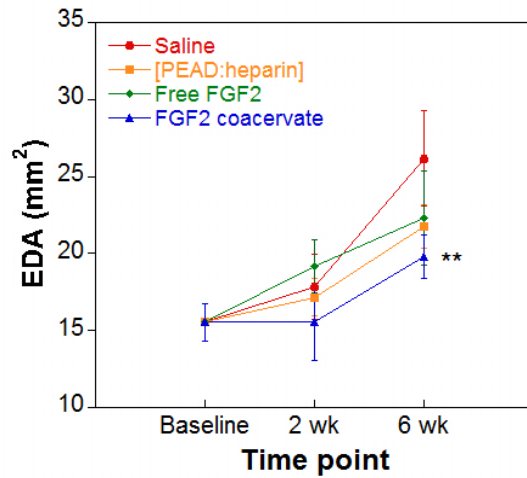
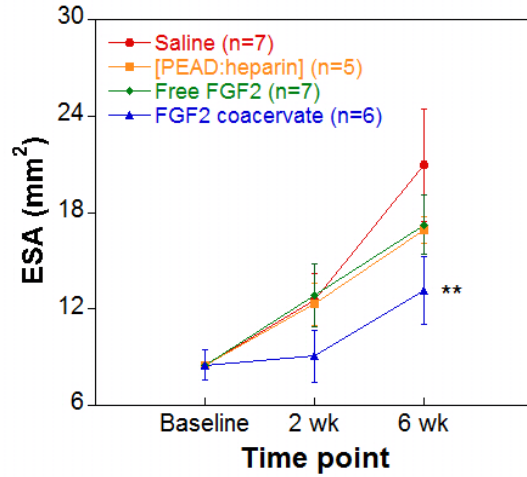


**Figure 39.** ESA and EDA data indicated that the left ventricle was not dilated in the coacervate group at 2 weeks, whereas all 3 control groups showed dilation indicating the coacervate delayed the onset of pathological remodeling. FAC data at 6 weeks indicated that heart

contractility of the coacervate group was 50% and 88% higher than free FGF2 and saline injection respectively. One-way within-subjects ANOVA followed by Tukey's HSD test was applied to compare individual treatment. \*\* indicated  $p$  value lower than 0.01 when FGF2 coacervate group was compared with all 3 control groups.

At 6 weeks, all experimental groups had significantly higher ESA and EDA and lower FAC than the healthy controls showing infarct reduced left ventricular function as time progresses. Among all experimental groups, the FGF2 coacervate group still had the lowest ESA ( $13.1 \pm 2.1 \text{ mm}^2$ ) and EDA ( $19.8 \pm 1.4 \text{ mm}^2$ ) and the highest FAC ( $34.1 \pm 6.2\%$ ), consistent with the result at 2 week; one-way within-subjects ANOVA followed by Tukey's HSD test suggested that these values were statistically different from those of the saline, delivery vehicle and free FGF2 groups. It pointed out that FGF2 coacervate delayed heart dilation and preserved contractile function. On the other hand, the free FGF2 group had no difference with the saline and delivery vehicle groups. Consequently, the result of echocardiography concluded that 500 ng of free FGF2 did not show significant effects in infarcted hearts whereas FGF2 delivered by the coacervate was effective enough to show benefit.

### **FGF2 coacervate preserved cardiac structure at early timepoint**

The histological analysis compared individual group at tissue level. For saline injection, hematoxylin and eosin staining showed that myocardial infarction seriously damaged the structure of cardiac fibers (Fig. 40). Compared to tissue at the remote zone, significant difference indicated that almost all cardiomyocyte fibers were lost in the infarct zone after 2 weeks. Actinin staining that recognized cardiomyocytes also indicated their loss caused by MI (Fig. 41). FGF2 coacervate, however, preserved certain cardiac structure in the infarct zone while it was not seen in delivery vehicle and free FGF2 injection (Fig. 42); these included actinin

staining further confirmed that infarction caused cardiomyocyte death at the infarct zone (Fig. 43). FGF2 coacervate was able to reduce cardiomyocyte death more effectively.

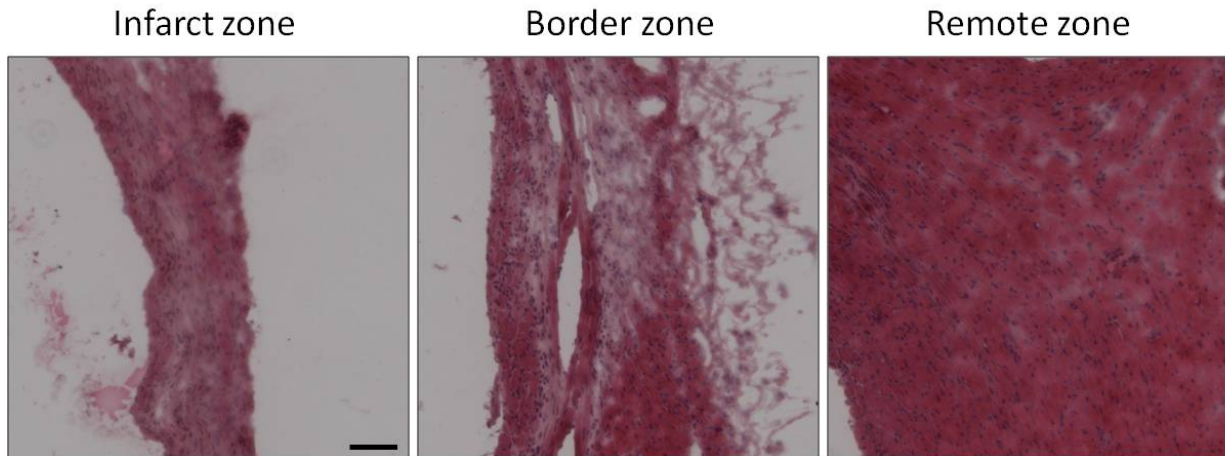


**Figure 40.** Hematoxylin and eosin staining revealed MI caused cardiomyocyte loss. Scale bar: 100  $\mu\text{m}$ .

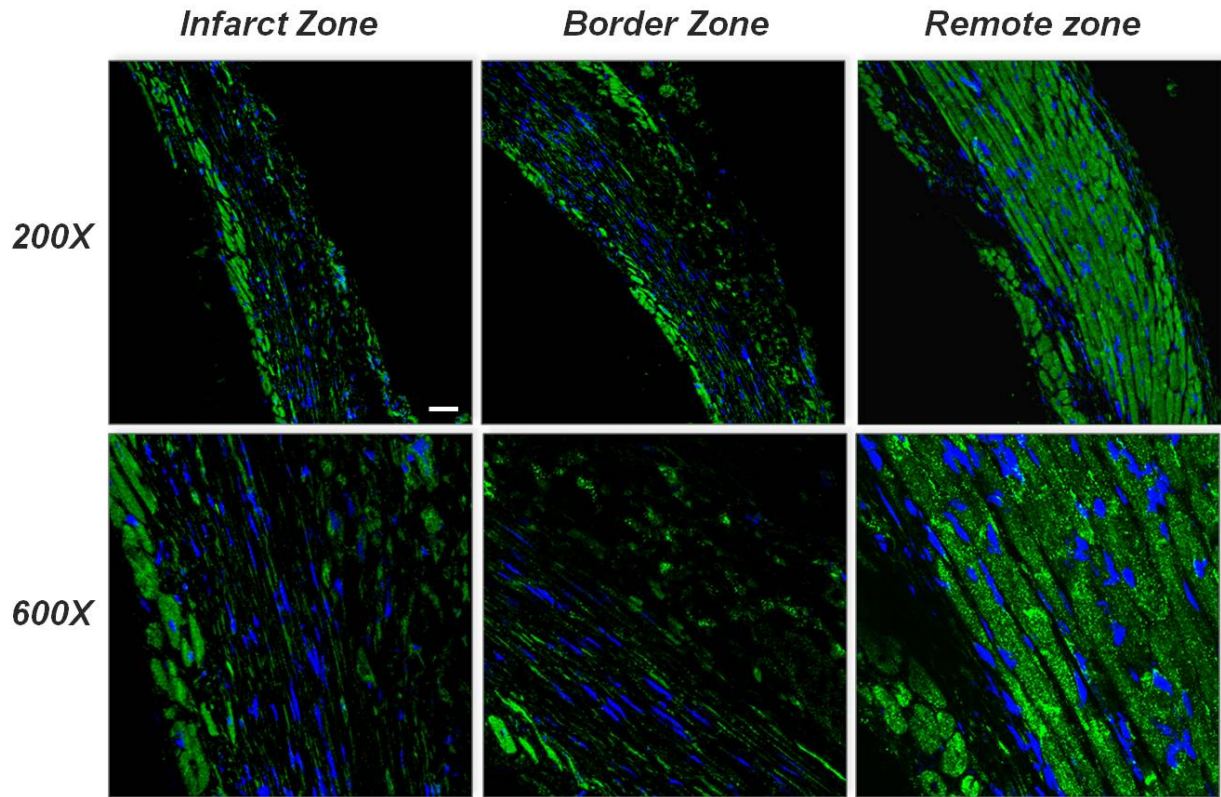


**Figure 41.** Actinin staining (green color) that labeled cardiomyocytes showed cardiomyocyte loss in the infarction and border zones. Scale bar: 50  $\mu$ m.

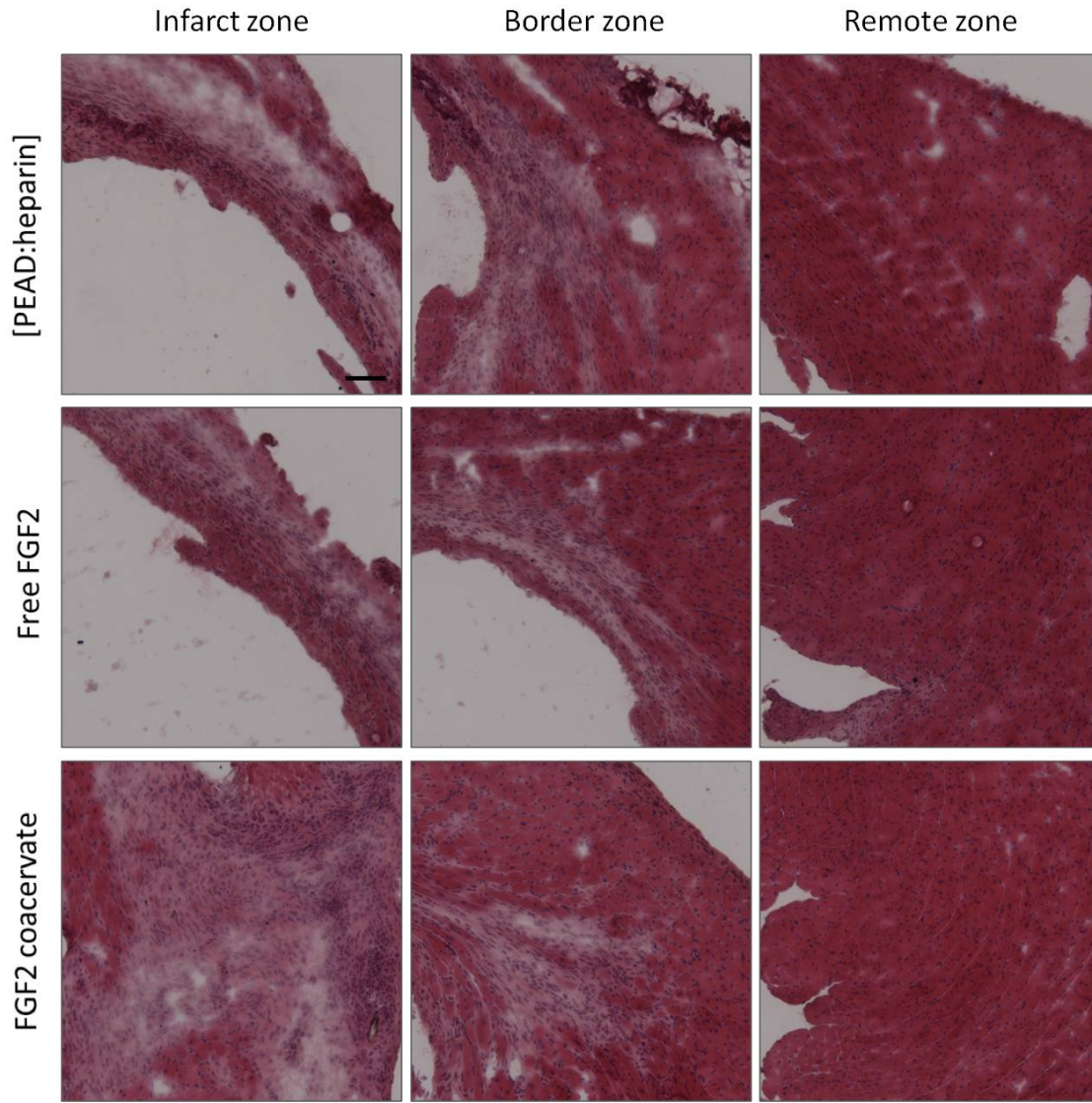


**Figure 42.** Hematoxylin and eosin staining indicated FGF2 coacervate group had thicker heart wall compared to [PEAD:heparin] and free FGF2 groups. Scale bar: 100  $\mu$ m.

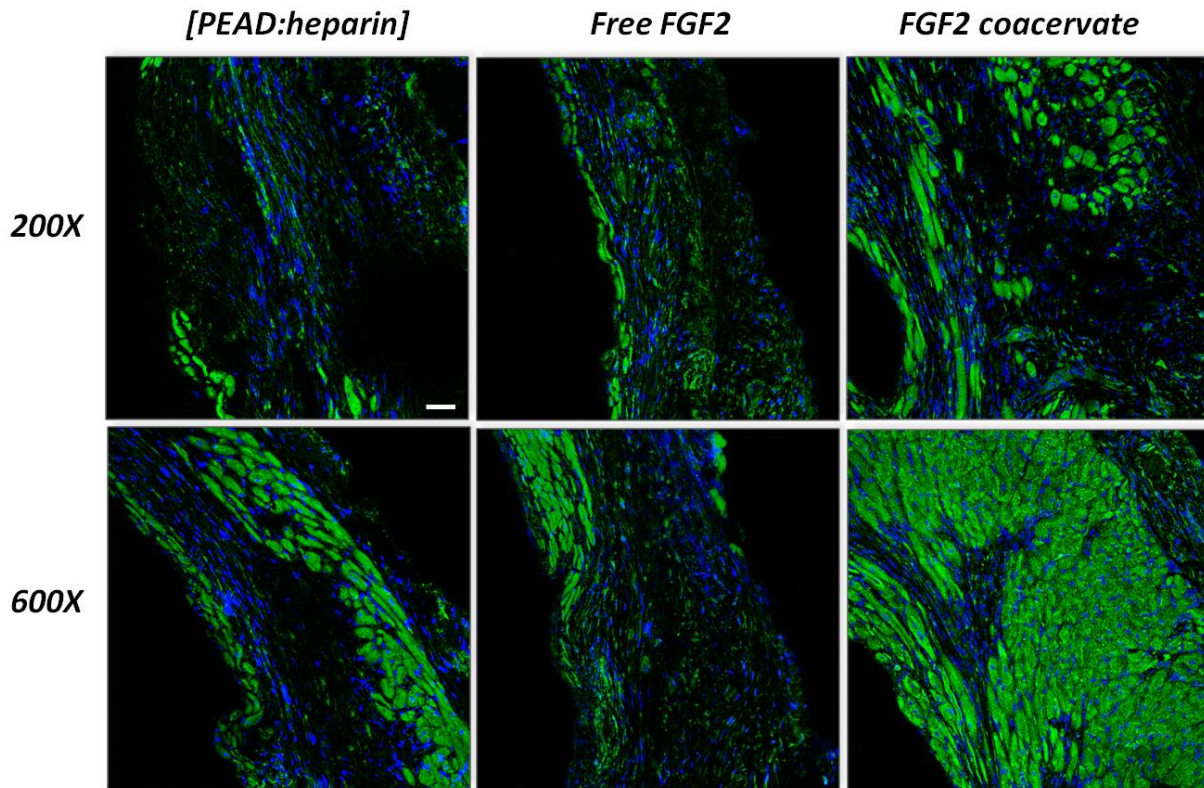


**Figure 43.** Actinin staining pointed out that more viable cardiomyocytes existed in the infarct zone for the FGF2 coacervate group. Scale bar: 50  $\mu$ m.

### **FGF2 coacervate had long term effect to reduce fibrosis**

Fibrosis is a result of pathological remodeling after myocardial infarction, in which fibrillar collagen plays a major structural role. Excess fibrosis stiffens the heart wall and lowers contractility. To evaluate the effect of FGF2 coacervate in fibrosis, Masson's trichrome staining was used to compare each group 6 weeks post-MI (Fig. 44). The staining showed that all experimental groups contained dense collagen fiber formation at the infarct zone along with heart wall thinning (data not shown). No difference was observed between all groups. At the border zone, nevertheless, the results revealed that the FGF2 coacervate group had less fibrotic tissue than the saline, delivery vehicle and free FGF2 groups. Hematoxylin and eosin staining

further confirmed that FGF2 coacervate preserved cardiac structure better at the border zone (Fig. 45).

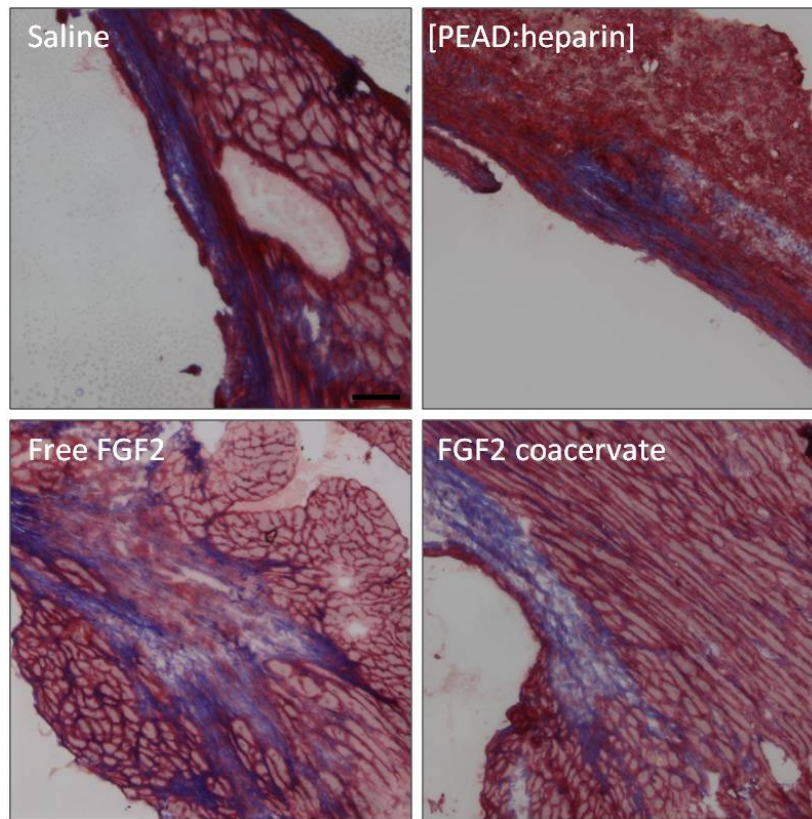


**Figure 44.** Masson's trichrome staining suggested FGF2 coacervate group had less fibrosis in the border zone compared to three control groups. Scale bar: 100  $\mu\text{m}$ .

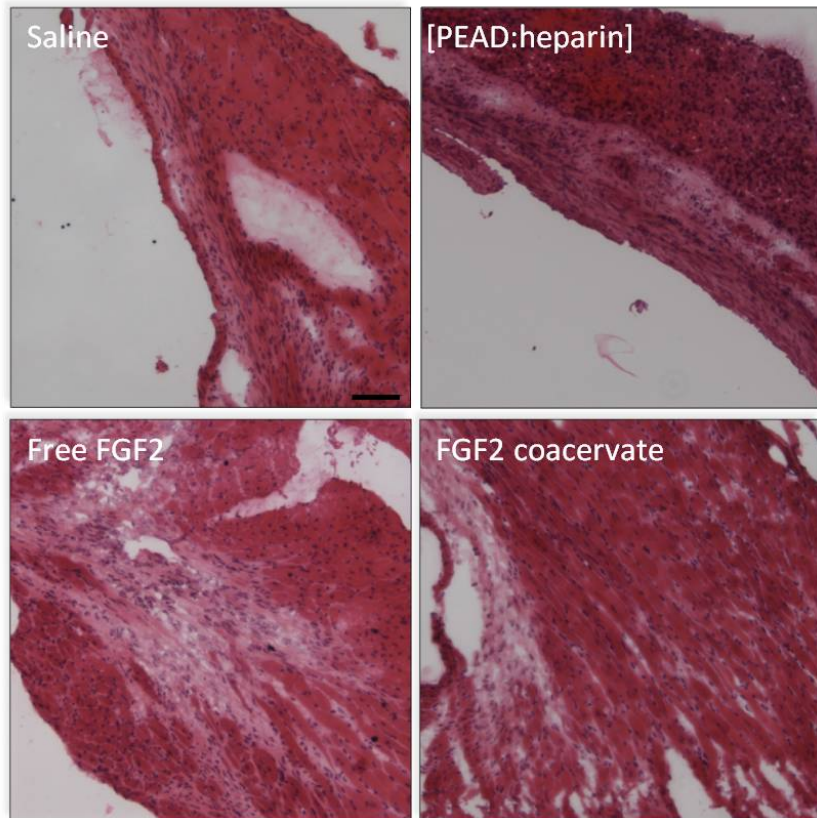


**Figure 45.** Hematoxylin and eosin staining showed that more cardiomyocytes were preserved in the border zone for the FGF2 coacervate group. Scale bar: 100  $\mu$ m.

### **FGF2 coacervate promoted more blood vessel formation**

When bioactivity is maintained, FGF2 promotes neovasculature formation and is expected to reduce damage caused by ischemic condition. The extent of angiogenesis was examined by staining of blood vessel-associated markers, VWF and CD31 for endothelial cells, and  $\alpha$ -SMA for mural cells (Fig. 46). For CD31 staining, the results showed that at the border zone, more blood vessels were observed for the FGF2 coacervate group. Its co-localization with VWF supported that these vessel were anatomically functional. Qualitatively, the number of vessels was higher and the size was larger. Co-staining of  $\alpha$ -SMA and CD31 revealed vasculature at the anterior wall of the left ventricle. The result demonstrated that  $\alpha$ -SMA and CD31 double positive vessels were clearly observed in the FGF2 coacervate group but not the

free FGF2 group (Fig. 47). It is possible that FGF2 coacervate preserved or protected larger vessels whereas free FGF2 was not effective enough to show this effect. However, it was also possible that these vessels grew from smaller vessels by stimulation of FGF2 coacervate. More study be necessary to address this result.

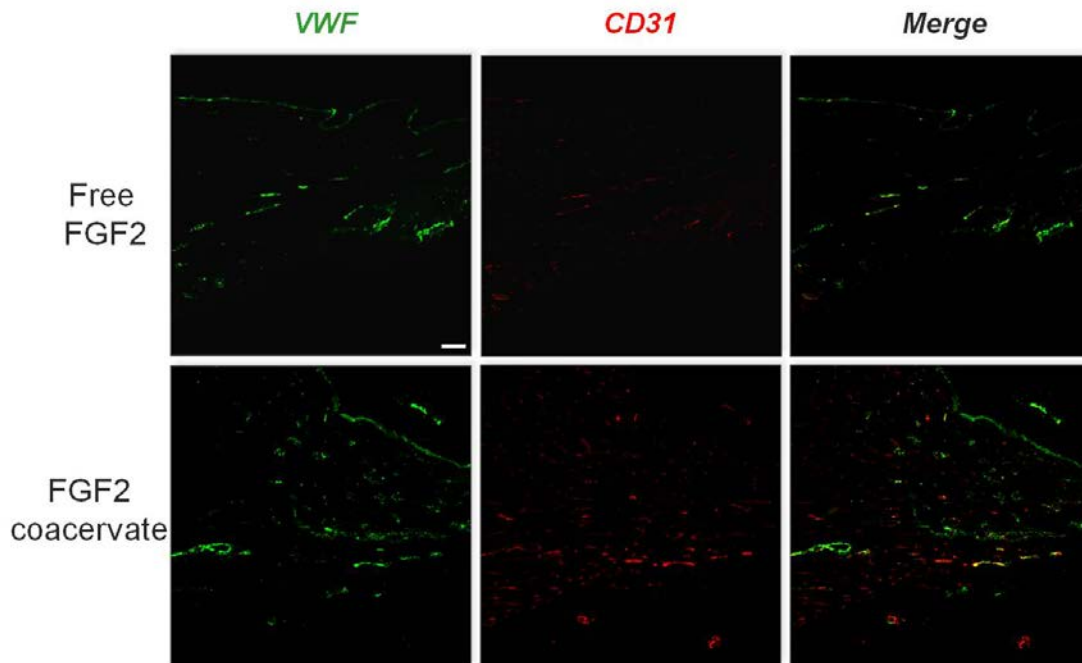


**Figure 46.** VWF (green color) and CD31 (red color) staining revealed FGF2 coacervate promoted more angiogenesis in the border zone than free FGF2. Scale bar: 50  $\mu\text{m}$ .

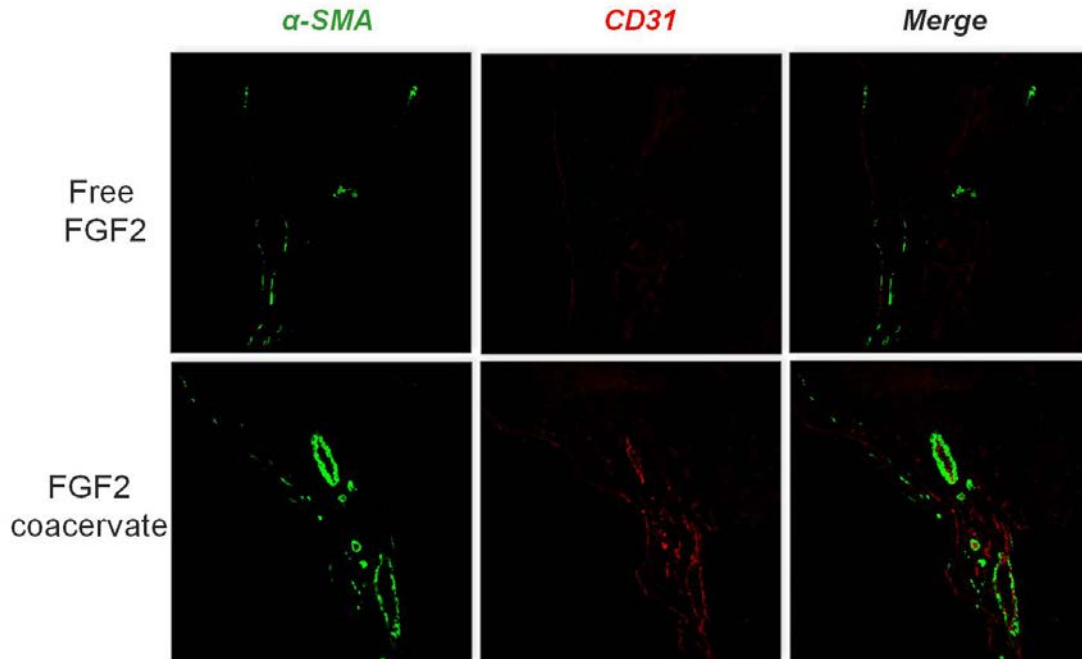


**Figure 47.**  $\alpha$ -SMA (green color) and CD31 (red color) staining demonstrated FGF2 coacervate preserved more angiogenesis at the anterior wall than free FGF2. Scale bar: 50  $\mu$ m.

#### 4.2.4 Summary

Successful angiogenesis can bring significance for infarcted heart in which blood supply is critical for survival of remaining cardiomyocytes. When FGF2 coacervate was injected in the infarct region, the effectiveness was demonstrated by delayed ventricular dilation and preserved cardiac function. The better contractile function is likely due to angiogenic activity of FGF2 and/or its ability of cardioprotection. Future study focusing on tailoring the dosage of FGF2 will be necessary to further evaluate the benefit of the coacervate in an ischemic heart.

## 5.0 CONCLUSION

Maximizing the bioactivity and prolonging the activity are critical for the success of growth factor therapy. A coacervate-based platform that mimics the binding between heparin, FGF and FGFR has been demonstrated to effectively enhance the bioactivity of growth factors and achieve promising outcomes in animal studies. Since heparin has high affinity to a variety of growth factors, this platform is expected to deliver different growth factors and has great utility in regenerative medicine. To our best knowledge, this is the first coacervate-based platform applied in controlled release of growth factors. Future study on its utility in translational medicine can include several directions:

Fundamentally, how [PEAD:heparin] coacervate enhances the bioactivity of heparin-binding factors is not fully understood. According to prior research, the condensation of growth factors by heparin enables more growth factors to interact with their receptors simultaneously. This so called polyvalency can amplify the downstream signaling and cause heparin-bound growth factors to be more potent than free factors. It is possible that the interaction between PEAD and heparin further condenses heparin-binding factors and consequently strengthens the polyvalent effect. To test this hypothesis, soluble [PEAD:heparin:growth factor] complex has to be isolated and its bioactivity has to be examined by in vitro or in vivo assays. In addition, it is also possible that growth factors that bind to [PEAD:heparin] coacervate has distinct conformation from the free or heparin-bound factors. Bioinformatics tools that model the macromolecular interaction are able to provide some information from the structural aspect.

For therapeutic angiogenesis, only one dose of FGF2 has been tested in both subcutaneous and MI models. We would like to compare different dosage of FGF2 in order to obtain the best outcome and also understand the therapeutic window of FGF2 coacervate. Furthermore, the half-lives of FGF2 delivered by [PEAD:heparin] coacervate which are also valuable information can be measured by biochemical or molecular biological methods. Lastly, tissue repair and regeneration always involve several pathways. FGF2 can be co-delivered with another heparin-binding factor that targets a different pathway, for example anti-inflammation or stem cell recruitment. We would expect that the synergistic effect can contribute to functional improvement significantly.

## REFERENCES

1. Roger VL, *et al.* (2011) Heart disease and stroke statistics—2011 update: a report from the American Heart Association *Circulation* 123(4):e18-e209.
2. <http://www.heart.org>
3. Risau W (1997) Mechanisms of angiogenesis. *Nature* 386(6626):671-674.
4. Carmeliet P, *et al.* (1996) Abnormal blood vessel development and lethality in embryos lacking a single VEGF allele. *Nature* 380(6573):435-439.
5. Gale NW & Yancopoulos GD (1999) Growth factors acting via endothelial cell-specific receptor tyrosine kinases: VEGFs, Angiopoietins, and ephrins in vascular development. *Genes & Development* 13(9):1055-1066.
6. Wijelath ES, *et al.* (2006) Heparin-II domain of fibronectin is a vascular endothelial growth factor-binding domain. *Circulation Research* 99(8):853-860.
7. Takeshita S, *et al.* (1994) Therapeutic angiogenesis. A single intraarterial bolus of vascular endothelial growth factor augments revascularization in a rabbit ischemic hind limb model. *The Journal of Clinical Investigation* 93(2):662-670.
8. Lee RJ, *et al.* (2000) VEGF gene delivery to myocardium: deleterious effects of unregulated expression. *Circulation* 102(8):898-901.
9. Hacein-Bey-Abina S, *et al.* (2003) LMO2-associated clonal T cell proliferation in two patients after gene therapy for SCID-X1. *Science* 302(5644):415-419.
10. Taniyama Y, *et al.* (2002) Local delivery of plasmid DNA into rat carotid artery using ultrasound. *Circulation* 105(10):1233-1239.
11. Nguyen DN, Green JJ, Chan JM, Langer R, & Anderson DG (2009) Polymeric materials for gene delivery and DNA vaccination. *Advanced Materials* 21(8):847-867.
12. Williams PD & Kingston PA (2011) Plasmid-mediated gene therapy for cardiovascular disease. *Cardiovascular Research* 91(4):565-576.
13. Lazarous DF, *et al.* (1997) Pharmacodynamics of basic fibroblast growth factor: route of administration determines myocardial and systemic distribution. *Cardiovascular Research* 36(1):78-85.

14. Bethel A, Kirsch JR, Koehler RC, Finklestein SP, & Traystman RJ (1997) Intravenous basic fibroblast growth factor decreases brain injury resulting from focal ischemia in cats. *Stroke* 28(3):609-616.
15. Laham RJ, *et al.* (1999) Intracoronary and intravenous administration of basic fibroblast growth factor: myocardial and tissue distribution. *Drug Metabolism and Disposition* 27(7):821-826.
16. Losordo DW & Dimmeler S (2004) Therapeutic angiogenesis and vasculogenesis for ischemic disease. *Circulation* 109(22):2692-2697.
17. Takahashi K & Yamanaka S (2006) Induction of pluripotent stem cells from mouse embryonic and adult fibroblast cultures by defined factors. *Cell* 126(4):663-676.
18. Maherali N, *et al.* (2007) Directly Reprogrammed Fibroblasts Show Global Epigenetic Remodeling and Widespread Tissue Contribution. *Cell Stem Cell* 1(1):55-70.
19. Leeper NJ, Hunter AL, & Cooke JP (2010) Stem cell therapy for vascular regeneration. *Circulation* 122(5):517-526.
20. Meller R (2009) The Role of the Ubiquitin proteasome system in ischemia and ischemic tolerance. *The Neuroscientist* 15(3):243-260.
21. Brevetti G, Giugliano G, Brevetti L, & Hiatt WR (2010) Inflammation in peripheral artery disease. *Circulation* 122(18):1862-1875.
22. Marzouk SAM, Buck RP, Dunlap LA, Johnson TA, & Cascio WE (2002) Measurement of extracellular pH, K<sup>+</sup>, and lactate in ischemic heart. *Analytical Biochemistry* 308(1):52-60.
23. Mehta JL & Li DY (1999) Inflammation in ischemic heart disease: Response to tissue injury or a pathogenetic villain? *Cardiovascular Research* 43(2):291-299.
24. Le KN, *et al.* (2009) Vascular regeneration by local growth factor release is self-limited by microvascular clearance. *Circulation* 119(22):2928-2935.
25. Yancopoulos GD, *et al.* (2000) Vascular-specific growth factors and blood vessel formation. *Nature* 407(6801):242-248.
26. Park JE, Keller GA, & Ferrara N (1993) The vascular endothelial growth factor (VEGF) isoforms: differential deposition into the subepithelial extracellular matrix and bioactivity of extracellular matrix-bound VEGF. *Molecular Biology of the Cell* 4(12):1317-1326.
27. Ruhrberg C, *et al.* (2002) Spatially restricted patterning cues provided by heparin-binding VEGF-A control blood vessel branching morphogenesis. *Genes & Development* 16(20):2684-2698.
28. Olsson A-K, Dimberg A, Kreuger J, & Claesson-Welsh L (2006) VEGF receptor signalling ? in control of vascular function. *Nat Rev Mol Cell Biol* 7(5):359-371.

29. Soker S, Takashima S, Miao HQ, Neufeld G, & Klagsbrun M (1998) Neuropilin-1 is expressed by endothelial and tumor cells as an isoform-specific receptor for vascular endothelial growth factor. *Cell* 92(6):735-745.
30. Kawamura H, *et al.* (2008) Neuropilin-1 in regulation of VEGF-induced activation of p38MAPK and endothelial cell organization. *Blood* 112(9):3638-3649.
31. Tongers J, Roncalli JG, & Losordo DW (2008) Therapeutic angiogenesis for critical limb ischemia. *Circulation* 118(1):9-16.
32. Hedman M, *et al.* (2003) Safety and feasibility of catheter-based local intracoronary vascular endothelial growth factor gene transfer in the prevention of postangioplasty and in-stent restenosis and in the treatment of chronic myocardial ischemia. *Circulation* 107(21):2677-2683.
33. Ripa RS, *et al.* (2006) Intramyocardial injection of vascular endothelial growth factor-A165 plasmid followed by granulocyte-colony stimulating factor to induce angiogenesis in patients with severe chronic ischaemic heart disease. *European Heart Journal* 27(15):1785-1792.
34. Alfranca A (2009) VEGF therapy: a timely retreat. *Cardiovascular Research* 83(4):611-612.
35. Yla-Herttuala S, Rissanen TT, Vajanto I, & Hartikainen J (2007) Vascular endothelial growth factors: biology and current status of clinical applications in cardiovascular medicine. *J Am Coll Cardiol* 49(10):1015-1026.
36. Tafuro S, *et al.* (2009) Inducible adeno-associated virus vectors promote functional angiogenesis in adult organisms via regulated vascular endothelial growth factor expression. *Cardiovascular Research* 83(4):663-671.
37. Ornitz DM, *et al.* (1996) Receptor specificity of the fibroblast growth factor family. *Journal of Biological Chemistry* 271(25):15292-15297.
38. Zhang X, *et al.* (2006) Receptor specificity of the fibroblast growth factor family. *Journal of Biological Chemistry* 281(23):15694-15700.
39. Venkataraman G, Raman R, Sasisekharan V, & Sasisekharan R (1999) Molecular characteristics of fibroblast growth factor–fibroblast growth factor receptor–heparin-like glycosaminoglycan complex. *Proceedings of the National Academy of Sciences* 96(7):3658-3663.
40. Sawada A, *et al.* (2001) Fgf/MAPK signalling is a crucial positional cue in somite boundary formation. *Development* 128(23):4873-4880.
41. Werner S, *et al.* (1992) Large induction of keratinocyte growth factor expression in the dermis during wound healing. *Proceedings of the National Academy of Sciences* 89(15):6896-6900.
42. Tigges U, Hyer EG, Scharf J, & Stallcup WB (2008) FGF2-dependent neovascularization of subcutaneous Matrigel plugs is initiated by bone marrow-derived pericytes and macrophages. *Development* 135(3):523-532.

43. Vitorino P & Meyer T (2008) Modular control of endothelial sheet migration. *Genes & Development* 22(23):3268-3281.
44. Kinsella MG, Irvin C, Reidy MA, & Wight TN (2004) Removal of heparan sulfate by heparinase treatment inhibits FGF2-dependent smooth muscle cell proliferation in injured rat carotid arteries. *Atherosclerosis* 175(1):51-57.
45. Sahni A & Francis CW (2004) Stimulation of endothelial cell proliferation by FGF2 in the presence of fibrinogen requires  $\alpha v \beta 3$ . *Blood* 104(12):3635-3641.
46. Murakami M, et al. (2008) The FGF system has a key role in regulating vascular integrity. *The Journal of Clinical Investigation* 118(10):3355-3366.
47. Murakami M, et al. (2011) FGF-dependent regulation of VEGF receptor 2 expression in mice. *The Journal of Clinical Investigation* 121(7):2668-2678.
48. Hosaka A, et al. (2004) Gelatin hydrogel microspheres enable pinpoint delivery of basic fibroblast growth factor for the development of functional collateral vessels. *Circulation* 110(21):3322-3328.
49. Takehara N, et al. (2008) Controlled delivery of basic fibroblast growth factor promotes human cardiosphere-derived cell engraftment to enhance cardiac repair for chronic myocardial infarction. *J Am Coll Cardiol* 52(23):1858-1865.
50. Laham RJ, et al. (2000) Intracoronary basic fibroblast growth factor (FGF2) in patients with severe ischemic heart disease: results of a Phase I open-label dose escalation study. *J Am Coll Cardiol* 36(7):2132-2139.
51. Bush M, et al. (2001) Pharmacokinetics and pharmacodynamics of recombinant FGF2 in a phase I trial in coronary artery disease. *The Journal of Clinical Pharmacology* 41(4):378-385.
52. Simons M, et al. (2002) Pharmacological treatment of coronary artery disease with recombinant fibroblast growth factor-2. *Circulation* 105(7):788-793.
53. Aviles RJ, Annex BH, & Lederman RJ (2003) Testing clinical therapeutic angiogenesis using basic fibroblast growth factor (FGF2). *British Journal of Pharmacology* 140(4):637-646.
54. Lynch P, Lee T-C, Fallavollita JA, Canty JM, & Suzuki G (2007) Intracoronary administration of AdvFGF-5 (Fibroblast Growth Factor-5) ameliorates left ventricular dysfunction and prevents myocyte loss in swine with developing collaterals and ischemic cardiomyopathy. *Circulation* 116(11 suppl):I-71-I-76.
55. Henry TD, et al. (2007) Effects of Ad5FGF-4 in patients with angina: an analysis of pooled data from the AGENT-3 and AGENT-4 trials. *Journal of the American College of Cardiology* 50(11):1038-1046.
56. White AC, Lavine KJ, & Ornitz DM (2007) FGF9 and SHH regulate mesenchymal vegfa expression and development of the pulmonary capillary network. *Development* 134(20):3743-3752.

57. Frontini MJ, et al. (2011) Fibroblast growth factor 9 delivery during angiogenesis produces durable, vasoresponsive microvessels wrapped by smooth muscle cells. *Nat Biotech* 29(5):421-427.
58. Shyu K-G, Manor O, Magner M, Yancopoulos GD, & Isner JM (1998) Direct intramuscular injection of plasmid DNA encoding angiopoietin-1 but not angiopoietin-2 augments revascularization in the rabbit ischemic hindlimb. *Circulation* 98(19):2081-2087.
59. Tao Z, et al. (2011) Coexpression of VEGF and angiopoietin-1 promotes angiogenesis and cardiomyocyte proliferation reduces apoptosis in porcine myocardial infarction (MI) heart. *Proceedings of the National Academy of Sciences* 108(5):2064-2069.
60. Van Belle E, et al. (1998) Potentiated angiogenic effect of scatter factor/hepatocyte growth factor via Induction of vascular endothelial growth factor : the case for paracrine amplification of angiogenesis. *Circulation* 97(4):381-390.
61. Tomita N, et al. (2003) Angiogenic property of hepatocyte growth factor is dependent on upregulation of essential transcription factor for angiogenesis, ets-1. *Circulation* 107(10):1411-1417.
62. Ince H, et al. (2005) Prevention of left ventricular remodeling with granulocyte colony-stimulating factor after acute myocardial infarction. *Circulation* 112(9 suppl):I-73-I-80.
63. Hill JM & Bartunek J (2006) The end of granulocyte colony-stimulating factor in acute myocardial infarction? *Circulation* 113(16):1926-1928.
64. Beohar N, Rapp J, Pandya S, & Losordo DW (2010) Rebuilding the damaged heart: the potential of cytokines and growth factors in the treatment of ischemic heart disease. *J Am Coll Cardiol* 56(16):1287-1297.
65. Pola R, et al. (2001) The morphogen Sonic hedgehog is an indirect angiogenic agent upregulating two families of angiogenic growth factors. *Nat Med* 7(6):706-711.
66. Jakobsson L, et al. (2010) Endothelial cells dynamically compete for the tip cell position during angiogenic sprouting. *Nat Cell Biol* 12(10):943-953.
67. Gore AV, et al. (2011) Rspo1/Wnt signaling promotes angiogenesis via Vegfc/Vegfr3. *Development*.
68. Pellegrini L (2001) Role of heparan sulfate in fibroblast growth factor signalling: a structural view. *Current Opinion in Structural Biology* 11(5):629-634.
69. Decher G (1997) Fuzzy nanoassemblies: toward layered polymeric multicomposites. *Science* 277(5330):1232-1237.
70. Picart C, et al. (2002) Molecular basis for the explanation of the exponential growth of polyelectrolyte multilayers. *Proc. Natl. Acad. Sci. U. S. A.* 99(20):12531-12535.

71. Capito RM, Azevedo HS, Velichko YS, Mata A, & Stupp SI (2008) Self-assembly of large and small molecules into hierarchically ordered sacs and membranes. *Science* 319(5871):1812-1816.
72. Pack DW, Hoffman AS, Pun S, & Stayton PS (2005) Design and development of polymers for gene delivery. *Nat Rev Drug Discov* 4(7):581-593.
73. Jessel N, *et al.* (2006) Multiple and time-scheduled in situ DNA delivery mediated by  $\beta$ -cyclodextrin embedded in a polyelectrolyte multilayer. *Proceedings of the National Academy of Sciences* 103(23):8618-8621.
74. Wood KC, Chuang HF, Batten RD, Lynn DM, & Hammond PT (2006) Controlling interlayer diffusion to achieve sustained, multiagent delivery from layer-by-layer thin films. *Proceedings of the National Academy of Sciences* 103(27):10207-10212.
75. Ono SS & Decher G (2006) Preparation of ultrathin self-standing polyelectrolyte multilayer membranes at physiological conditions using pH-responsive film segments as sacrificial layers. *Nano Lett.* 6(4):592-598.
76. Dimitrova M, *et al.* (2008) Sustained delivery of siRNAs targeting viral infection by cell-degradable multilayered polyelectrolyte films. *Proceedings of the National Academy of Sciences* 105(42):16320-16325.
77. Mazia D, Schatten G, & Sale W (1975) Adhesion of cells to surfaces coated with polylysine. Applications to electron microscopy. *J. Cell Biol.* 66(1):198-200.
78. Jacobson BS & Branton D (1977) Plasma membrane: rapid isolation and exposure of the cytoplasmic surface by use of positively charged beads. *Science* 195(4275):302-304.
79. Kinoshita T, Nachman RL, & Minick R (1979) Isolation of human platelet plasma membranes with polylysine beads. *J. Cell Biol.* 82(3):688-696.
80. Yazynina EV, *et al.* (1999) Immunoassay Techniques for Detection of the Herbicide Simazine Based on Use of Oppositely Charged Water-Soluble Polyelectrolytes. *Analytical Chemistry* 71(16):3538-3543.
81. Zeya HI & Spitznagel JK (1968) Arginine-rich proteins of polymorphonuclear leukocyte lysosomes: antimicrobial specificity and biochemical heterogeneity. *J. Exp. Med.* 127(5):927-941.
82. Peterson PK, Gekker G, Shapiro R, Freiberg M, & Keane WF (1984) Polyamino acid enhancement of bacterial phagocytosis by human polymorphonuclear leukocytes and peritoneal macrophages. *Infect. Immun.* 43(2):561-566.
83. Helander IM, Alakomi HL, LatvaKala K, & Koski P (1997) Polyethyleneimine is an effective permeabilizer of Gram-negative bacteria. *Microbiology-Uk* 143:3193-3199.
84. Elferink JGR (1985) Cytolytic effect of polylysine on rabbit polymorphonuclear leukocytes. *Inflammation* 9(3):321-331.

85. Elferink J & Deierkauf M (1989) Permeabilization and calcium-dependent activation of rabbit polymorphonuclear leukocytes by poly-L -arginine. *Inflammation* 13(3):285-294.
86. Moghimi SM, *et al.* (2005) A two-stage poly(ethylenimine)-mediated cytotoxicity: implications for gene transfer/therapy. *Mol Ther* 11(6):990-995.
87. Hunter AC (2006) Molecular hurdles in polyfectin design and mechanistic background to polycation induced cytotoxicity. *Advanced Drug Delivery Reviews* 58(14):1523-1531.
88. Choksakulnimitr S, Masuda S, Tokuda H, Takakura Y, & Hashida M (1995) In vitro cytotoxicity of macromolecules in different cell culture systems. *Journal of Controlled Release* 34(3):233-241.
89. Moreau E, Domurado M, Chapon P, Vert M, & Domurado D (2002) Biocompatibility of polycations: In vitro agglutination and lysis of red blood cells and in vivo toxicity. *Journal of Drug Targeting* 10(2):161-173.
90. Fischer D, Li YX, Ahlemeyer B, Krieglstein J, & Kissel T (2003) In vitro cytotoxicity testing of polycations: influence of polymer structure on cell viability and hemolysis. *Biomaterials* 24(7):1121-1131.
91. Breunig M, Lungwitz U, Liebl R, & Goepferich A (2007) Breaking up the correlation between efficacy and toxicity for nonviral gene delivery. *Proc. Natl. Acad. Sci. U. S. A.* 104(36):14454-14459.
92. De Koker S, *et al.* (2007) In vivo cellular uptake, degradation, and biocompatibility of polyelectrolyte microcapsules. (Translated from English) *Advanced Functional Materials* 17(18):3754-3763.
93. Xiong MP, *et al.* (2007) PH-Responsive multi-PEGylated dual cationic nanoparticles enable charge modulations for safe gene delivery. *Chemmedchem* 2(9):1321-1327.
94. Xiong MP, *et al.* (2007) Poly(aspartate-g-PEI800), a polyethylenimine analogue of low toxicity and high transfection efficiency for gene delivery. *Biomaterials* 28(32):4889-4900.
95. Zern BJ, Chu H, Osunkoya AO, Gao J, & Wang Y (2011) A biocompatible arginine-based polycation. *Advanced Functional Materials* 21(3):434-440.
96. Zern BJ, Chu H, & Wang Y (2010) Control growth factor release using a self-assembled [polycation:heparin] complex. *PLoS ONE* 5(6):e11017.
97. Rick DL, Davis JW, Kram SL, Mang MN, & Lickly TD (1998) Biodegradation of an epoxy-based thermoplastic polyester, poly(hydroxy ester ether) in a laboratory-scale compost system. *Journal of Environmental Polymer Degradation* 6(3):143-157.
98. Ito N, Tonosaki S, Kudo H, Kameyama A, & Nishikubo T (2002) Synthesis and characterization of fluoropolymers by the polyaddition of bis(epoxide)s with dicarboxylic acids and diols. *Journal of Polymer Science Part a-Polymer Chemistry* 40(10):1395-1404.

99. You Z, *et al.* (2010) A functionalizable polyester with free hydroxyl groups and tunable physiochemical and biological properties. *Biomaterials* 31(12):3129-3138.
100. Gao J, *et al.* (2006) A neuroinductive biomaterial based on dopamine. *Proceedings of the National Academy of Sciences* 103(45):16681-16686.
101. Boussif O, *et al.* (1995) A versatile vector for gene and oligonucleotide transfer into cells in culture and in vivo: polyethylenimine. *Proceedings of the National Academy of Sciences* 92(16):7297-7301.
102. Chu H, Gao J, Chen C-W, Huard J, & Wang Y (2011) Injectable fibroblast growth factor-2 coacervate for persistent angiogenesis. *Proceedings of the National Academy of Sciences* 108(33):13444-13449.
103. Taipale, J. and J. KeskiOja (1997). "Growth factors in the extracellular matrix." *Faseb Journal* 11(1): 51-59.
104. Macri, L., D. Silverstein, *et al.* (2007). "Growth factor binding to the pericellular matrix and its importance in tissue engineering." *Advanced Drug Delivery Reviews* 59(13): 1366-1381.
105. Uebersax, L., H. P. Merkle, *et al.* (2009). "Biopolymer-Based Growth Factor Delivery for Tissue Repair: From Natural Concepts to Engineered Systems." *Tissue Engineering Part B-Reviews* 15(3): 263-289.
106. Whitelock, J. M., A. D. Murdoch, *et al.* (1996). "The degradation of human endothelial cell-derived perlecan and release of bound basic fibroblast growth factor by stromelysin, collagenase, plasmin, and heparanases." *Journal of Biological Chemistry* 271(17): 10079-10086.
107. Raman, R., V. Sasisekharan, *et al.* (2005). "Structural insights into biological roles of protein-glycosaminoglycan interactions." *Chemistry & Biology* 12(3): 267-277.
108. Gallagher, J. T. and J. E. Turnbull (1992). "Heparin-sulfate in the binding and activation of basic fibroblast growth-factor." *Glycobiology* 2(6): 523-528.
109. Whitelock, J. M., J. Melrose, *et al.* (2008). "Diverse Cell Signaling Events Modulated by Perlecan." *Biochemistry* 47(43): 11174-11183.
110. Saksela, O., D. Moscatelli, *et al.* (1988). "Endothelial cell-derived heparan sulfate binds basic fibroblast growth factor and protects it from proteolytic degradation." *Journal of Cell Biology* 107(2): 743-751.
111. Kreuger, J., D. Spillmann, *et al.* (2006). "Interactions between heparan sulfate and proteins: the concept of specificity." *Journal of Cell Biology* 174(3): 323-327.
112. Gorski, B. and S. E. Stringer (2007). "Tinkering with heparan sulfate sulfation to steer development." *Trends in Cell Biology* 17(4): 173-177.

113. Capila, I. and R. J. Linhardt (2002). "Heparin - Protein interactions." *Angewandte Chemie-International Edition* **41**(3): 391-412.
114. de Jong, J. G., R. A. Wevers, et al. (1989). "Dimethylmethylene blue-based spectrophotometry of glycosaminoglycans in untreated urine: a rapid screening procedure for mucopolysaccharidoses." *Clinical Chemistry* **35**(7): 1472-1477.
115. DeBlois, C., M.-F. Côté, et al. (1994). "Heparin-fibroblast growth factor/fibrin complex: in vitro and in vivo applications to collagen-based materials." *Biomaterials* **15**(9): 665-672.
116. Drogoz, A., L. David, et al. (2007). "Polyelectrolyte Complexes from Polysaccharides: Formation and Stoichiometry Monitoring." *Langmuir* **23**(22): 10950-10958.
117. Chen P-R, Chen M-H, Lin F-H, & Su W-Y (2005) Release characteristics and bioactivity of gelatin-tricalcium phosphate membranes covalently immobilized with nerve growth factors. *Biomaterials* **26**(33):6579-6587.
118. Lee MK & Lander AD (1991) Analysis of affinity and structural selectivity in the binding of proteins to glycosaminoglycans: development of a sensitive electrophoretic approach. *Proceedings of the National Academy of Sciences of the United States of America* **88**(7):2768-2772.
119. Silva EA & Mooney DJ (2010) Effects of VEGF temporal and spatial presentation on angiogenesis. *Biomaterials* **31**(6):1235-1241.
120. Wenk E, et al. (2010) The use of sulfonated silk fibroin derivatives to control binding, delivery and potency of FGF2 in tissue regeneration. *Biomaterials* **31**(6):1403-1413.
- 121 Wood MD, Borschel GH, & Sakiyama-Elbert SE (2009) Controlled release of glial-derived neurotrophic factor from fibrin matrices containing an affinity-based delivery system. (Translated from English) *J. Biomed. Mater. Res. Part A* **89A**(4):909-918 (in English).
- 122 Kang CE, Tator CH, & Shoichet MS (2010) Poly(ethylene glycol) modification enhances penetration of fibroblast growth factor 2 to injured spinal cord tissue from an intrathecal delivery system. (Translated from English) *J Control Release* **144**(1):25-31 (in English).
- 123 Wang XQ, et al. (2009) Growth factor gradients via microsphere delivery in biopolymer scaffolds for osteochondral tissue engineering. (Translated from English) *J. Control. Release* **134**(2):81-90 (in English).
- 124 Solorio LD, Fu AS, Hernandez-Irizarry R, & Alsberg E (2010) Chondrogenic differentiation of human mesenchymal stem cell aggregates via controlled release of TGF-beta 1 from incorporated polymer microspheres. *J. Biomed. Mater. Res. Part A* **92A**(3):1139-1144.
- 125 Wenk E, et al. (2010) The use of sulfonated silk fibroin derivatives to control binding, delivery and potency of FGF2 in tissue regeneration. *Biomaterials* **31**(6):1403-1413.

- 126 Tae G, Scatena M, Stayton PS, & Hoffman AS (2006) PEG-cross-linked heparin is an affinity hydrogel for sustained release of vascular endothelial growth factor. *Journal of Biomaterials Science, Polymer Edition* 17:187-197.
- 127 Nilasaroya A, Poole-Warren LA, Whitelock JM, & Jo Martens P (2008) Structural and functional characterisation of poly(vinyl alcohol) and heparin hydrogels. *Biomaterials* 29(35):4658-4664.
- 128 Seal BL & Panitch A (2003) Physical Polymer Matrices Based on Affinity Interactions between Peptides and Polysaccharides. *Biomacromolecules* 4(6):1572-1582.
- 129 Rajangam K, *et al.* (2006) Heparin Binding Nanostructures to Promote Growth of Blood Vessels. *Nano Letters* 6(9):2086-2090.
- 130 Johnson PJ, Parker SR, & Sakiyama-Elbert SE (2009) Controlled release of neurotrophin-3 from fibrin-based tissue engineering scaffolds enhances neural fiber sprouting following subacute spinal cord injury. *Biotechnology and Bioengineering* 104(6):1207-1214.
131. Ingber DE (2002) Mechanical signalling and the cellular response to extracellular matrix in angiogenesis and cardiovascular physiology. *Circ Res* 91(10):877-887.
132. Jain RK (2003) Molecular regulation of vessel maturation. *Nat Med* 9(6):685-693
133. Gupta R, Tongers J, & Losordo DW (2009) Human studies of angiogenic gene therapy. *Circ Res* 105(8):724-736.
134. Sarkar K, Fox-Talbot K, Steenbergen C, Bosch-Marce M, & Semenza GL (2009) Adenoviral transfer of HIF-1 alpha enhances vascular responses to critical limb ischemia in diabetic mice. *Proc Natl Acad Sci USA* 106(44):18769-18774.
135. van Royen N, Piek JJ, Schaper W, & Fulton WF (2009) A critical review of clinical arteriogenesis research. *J Am Coll Cardiol* 55(1):17-25.
136. Dityatev A, Seidenbecher CI, & Schachner M (2010) Compartmentalization from the outside: the extracellular matrix and functional microdomains in the brain. *Trends Neurosci* 33(11):503-512.
137. Klim JR, Li L, Wrighton PJ, Piekarczyk MS, & Kiessling LL (2010) A defined glycosaminoglycan-binding substratum for human pluripotent stem cells. *Nat Meth* 7(12):989-994.
138. Hacker U, Nybakken K, & Perrimon N (2005) Heparan sulphate proteoglycans: The sweet side of development. *Nat Rev Mol Cell Biol* 6(7):530-541.
139. Sirko S, von Holst A, Wizenmann A, Götz M, & Faissner A (2007) Chondroitin sulfate glycosaminoglycans control proliferation, radial glia cell differentiation and neurogenesis in neural stem/progenitor cells. *Development* 134(15):2727-2738.

140. Toole BP (2004) Hyaluronan: from extracellular glue to pericellular cue. *Nat Rev Cancer* 4(7):528-539.
141. Gotte M & Yip GW (2006) Heparanase, hyaluronan, and CD44 in cancers: a breast carcinoma perspective. *Cancer Res* 66(21):10233-10237.
142. Casu B, Naggi A, & Torri G (2010) Heparin-derived heparan sulfate mimics to modulate heparan sulfate-protein interaction in inflammation and cancer. *Matrix Biology* 29(6):442-452.
143. Aviezer D, *et al.* (1994) Differential structural requirements of heparin and heparan-sulfate proteoglycans that promote binding of basic fibroblast growth-factor to its receptor. *J Biol Chem* 269(1):114-121.
144. Moy FJ, *et al.* (1997) Properly oriented heparin-decasaccharide-induced dimers are the biologically active form of basic fibroblast growth factor. *Biochemistry* 36(16):4782-4791.
145. Saksela O, Moscatelli D, Sommer A, & Rifkin DB (1988) Endothelial cell-derived heparan-sulfate binds basic fibroblast growth-factor and protect it from proteolytic degradation. *J Cell Biol* 107(2):743-751.
146. Park JE, Keller GA, & Ferrara N (1993) Vascular endothelial growth-factor (VEGF) isoforms - differential deposition into the subepithelial extracellular-matrix and bioactivity of extracellular matrix-bound. *Mol Biol Cell* 4(12):1317-1326.
147. Sellke FW, Laham RJ, Edelman ER, Pearlman JD, & Simons M (1998) Therapeutic angiogenesis with basic fibroblast growth factor: technique and early results. *Ann Thorac Surg* 65(6):1540-1544.
148. Sakiyama-Elbert SE & Hubbell JA (2000) Controlled release of nerve growth factor from a heparin-containing fibrin-based cell ingrowth matrix. *J Control Release* 69(1):149-158.
149. Pellegrini L (2001) Role of heparan sulfate in fibroblast growth factor signalling: a structural view. *Curr Opin Struct Biol* 11(5):629-634.
150. Zern BJ, Chu H, & Wang Y (2010) Control growth factor release using a self-assembled [polycation:heparin] complex. *PLoS ONE* 5(6):e11017.
151. Chu H, Johnson NR, Mason NS, & Wang Y (2011) A [polycation:heparin] complex releases growth factors with enhanced bioactivity. *J Control Release* 150(2):157-163.
152. Rusnati M, *et al.* (1999) Interaction of Fibroblast Growth Factor-2 (FGF2) with Free Gangliosides: Biochemical Characterization and Biological Consequences in Endothelial Cell Cultures. *Mol. Biol. Cell* 10(2):313-327.
153. Crisan M, *et al.* (2008) A perivascular origin for mesenchymal stem cells in multiple human organs. *Cell Stem Cell* 3(3):301-313.
154. Hanson EK & Ballantyne J (2010) A blue spectral shift of the hemoglobin Soret band correlates with the age (time since deposition) of dried bloodstains. *PLoS ONE* 5(9):e12830.

155. Zheng B, *et al.* (2007) Prospective identification of myogenic endothelial cells in human skeletal muscle. *Nat Biotech* 25(9):1025-1034.
156. Lafleur MA, Handsley MM, Knauper V, Murphy G, & Edwards DR (2002) Endothelial tubulogenesis within fibrin gels specifically requires the activity of membrane-type-matrix metalloproteinases (MT-MMPs). *J Cell Sci* 115(17):3427-3438.
157. Hosseinkhani H, Hosseinkhani M, Khademhosseini A, Kobayashi H, & Tabata Y (2006) Enhanced angiogenesis through controlled release of basic fibroblast growth factor from peptide amphiphile for tissue regeneration. *Biomaterials* 27(34):5836-5844.
158. Richardson TP, Peters MC, Ennett AB, & Mooney DJ (2001) Polymeric system for dual growth factor delivery. *Nat Biotech* 19(11):1029-1034.
159. Lindahl P, Johansson BR, Levéen P, & Betsholtz C (1997) Pericyte loss and microaneurysm formation in PDGF-B-deficient mice. *Science* 277(5323):242-245.
160. Nehls V & Drenckhahn D (1991) Heterogeneity of microvascular pericytes for smooth muscle type alpha-actin. *J Cell Biol* 113(1):147-154.
161. Laham RJ, *et al.* (1999) Local perivascular delivery of basic fibroblast growth factor in patients undergoing coronary bypass surgery : results of a phase I randomized, double-blind, placebo-controlled trial. *Circulation* 100(18):1865-1871.
162. Sellke FW & Ruel M (2003) Vascular growth factors and angiogenesis in cardiac surgery. *Ann Thorac Surg* 75(2):S685-690.
163. Simons M, *et al.* (2002) Pharmacological treatment of coronary artery disease with recombinant fibroblast growth factor-2: double-blind, randomized, controlled clinical trial. *Circulation* 105(7):788-793.
164. Cao R, *et al.* (2003) Angiogenic synergism, vascular stability and improvement of hind-limb ischemia by a combination of PDGF-BB and FGF2. *Nat Med* 9(5):604-613.
165. Saif J, *et al.* (2010) Combination of injectable multiple growth factor-releasing scaffolds and cell therapy as an advanced modality to enhance tissue neovascularization. *Arterioscler Thromb Vasc Biol* 30(10):1897-1904.
166. ten Dijke P & Iwata KK (1989) Growth Factors For Wound Healing. *Nat Biotech* 7(8):793-798.
167. Gerard C. Blobe WPS (2000) Role of transforming growth factor  $\beta$  in human disease. *New Engl J Med* 342(18):1350-1358.
168. Lemmon MA & Schlessinger J (2010) Cell signaling by receptor tyrosine kinases. *Cell* 141(7):1117-1134.
169. Cross MJ & Claesson-Welsh L (2001) FGF and VEGF function in angiogenesis: signalling pathways, biological responses and therapeutic inhibition. *Trends Pharmacol Sci* 22(4):201-207.

170. Seghezzi G, *et al.* (1998) Fibroblast growth factor-2 (FGF2) induces vascular endothelial growth factor (VEGF) expression in the endothelial cells of forming capillaries: an autocrine mechanism contributing to angiogenesis. *J Cell Biol* 141(7):1659-1673.
171. Zhang J, *et al.* (2009) Differential roles of PDGFR- $\alpha$  and PDGFR- $\beta$  in angiogenesis and vessel stability. *FASEB J* 23(1):153-163.
172. Millette E, *et al.* (2005) Platelet-derived growth factor-BB-induced human smooth muscle cell proliferation depends on basic FGF release and FGFR-1 activation. *Circ Res* 96(2):172-179.
- 173 Payne TR, *et al.* (2007) A relationship between vascular endothelial growth factor, angiogenesis, and cardiac repair after muscle stem cell transplantation Into Ischemic Hearts. *J Am Coll Cardiol* 50(17):1677-1684.